



United States  
Department of  
Agriculture

Natural  
Resources  
Conservation  
Service

Title 190  
Handbook  
Number 647

# Rangeland Hydrology and Erosion Handbook The RHEM Guide



The U.S. Department of Agriculture (USDA) prohibits discrimination in its programs on the basis of race, color, national origin, sex, religion, age disabilities, political beliefs, and marital and family status. Mention of a trade name in this publication is solely to provide specific information and does not imply recommendation or endorsement by the U.S. Department of Agriculture over others not mentioned.

## Part 647 – The RHEM Guide

Rangeland Hydrology and Soil Erosion Processes Handbook 647: A guide for Conservation Planning with the Rangeland Hydrology and Erosion Model (RHEM)

**Figure i.** Thunderstorm over central Nevada



**Editors: Mark Weltz and Gary Frasier**

### Contributors

Mark A. Weltz, Research Leader, Rangeland Hydrologist; USDA-ARS, Reno, NV  
Mariano Hernandez, Hydrologist, University of Arizona, Tucson, AZ  
Mark A. Nearing, Research Agricultural Engineer, USDA-ARS, Tucson, AZ  
Ken E. Spaeth, Rangeland Management Specialist, USDA-NRCS, Fort Worth, TX  
Fred B. Pierson, Research Leader, USDA-ARS, Boise, ID  
C. Jason Williams, Research Hydrologist, USDA-ARS, Tucson, AZ  
Osama Z. Al-Hamdan, Assistant Professor, Texas A&M Kingsville, Kingsville, TX  
S. Kossi, Nouwakpo, Soil Scientist, USDA-ARS, Kimberly, ID  
Gerardo Armendariz, IT Specialist, USDA-ARS, Tucson, AZ  
Haiyan Wei, Hydrologist, University of Arizona, Tucson, AZ  
Dave C. Goodrich, Research Hydraulic Engineer, USDA-ARS, Tucson, AZ  
Phillip Guertin, Hydrologist, University of Arizona, Tucson, AZ  
Carl Unkrich, Hydrologist, USDA-ARS, Tucson, AZ  
Viktor Polyakov, Soil Scientist, USDA-ARS, Tucson, AZ  
Kenneth McGwire, Physical Scientist, Desert Research Institute, Reno, NV.  
Jason Nesbit, IT Specialist, USDA-ARS, Reno, NV  
Gary Frasier, retired USDA-ARS, Loveland, CO  
Leonard Jolley, retired NRCS, Napa, CA  
Jeff Stone, retired ARS, Tucson, AZ

## Citation

Weltz, M.A., Hernandez, M., M. A. Nearing, K. E. Spaeth, F. B. Pierson, C. J. Williams, O. Z. Al-Hamdan, S. K. Nouwakpo, G. Armendariz, Haiyan Wei, Dave C. Goodrich, Phillip Guertin, Carl Unkrich, Viktor Polyakov, K. McGwire, J. Nesbit, G. Frazier, L Jolley, J Stone (2021). Rangeland Hydrology and Soil Erosion Processes: A guide for Conservation Planning with the Rangeland Hydrology and Erosion Model (RHEM). United States Department of Agriculture, Natural Resources Conservation Service, Handbook No. 647, 80 pg.

**Abstract:** Soil loss rates on rangelands are considered one of the few quantitative indicators for assessing rangeland health and conservation practice effectiveness. An erosion model to predict soil loss specific for rangeland applications is needed because existing erosion models were developed from croplands. Hydrologic and erosion processes are different on rangelands than croplands due to much higher levels of heterogeneity in soil and plant properties and the consolidated nature of the soils. The purpose of this Handbook is to improve the understanding of hydrologic processes and sources and transport mechanisms of sediment in rangeland catchments at the scale of the hillslope. The first Handbook, Part 646 Rangeland Hydrology and Soil Erosion Processes, provides a review of relevant rangeland hydrology literature on what is known about the impact of range management practices and field experiments conducted across the western United States. This Handbook, Part 647–The RHEM Guide, provides the background for understanding how to use the Rangeland Hydrology and Erosion Model (RHEM) and understand its output for making informed decisions before implementing new management actions. The RHEM model is a newly conceptualized, process-based erosion prediction tool specific for rangeland application, based on fundamentals of infiltration, hydrology, plant science, hydraulics, and erosion mechanics. The model is event-based and was developed specifically from rangeland data. The erosion prediction tool estimates runoff, erosion, and sediment delivery rates and volumes at the spatial scale of the hillslope and the temporal scale of a single rainfall event. The data drawn on to develop and validate the RHEM series of tools contains over 2,000 rainfall simulation plots and 100 plant communities collected over the last 40 years across the western United States by the Agricultural Research Service and the Natural Resources Conservation Service. These data can be used to understand ecological processes when combined with the RHEM tools to provide sound science when making critical land management decisions. The RHEM assessment tool provides information that can be combined with state and transition models and enhance Ecological Site Descriptions. The RHEM assessment tool has been incorporated into the Automated Geospatial Watershed Assessment (AGWA) tool for understanding and predicting hydrologic and soil erosion processes at the watershed scale.

**Figure ii.** Overland flow channel in bare interspace between Pinyon and Juniper trees, central Nevada.



**Figure iii.** Gully and rill erosion following wildfire near Minden, Nevada.



**Figure iv.** Salt and biological soil crusts with intervening concentrated flow erosion.



**Keywords:** soil erosion; rangelands; rill erosion; concentrated flow; interrill erosion; soil erodibility; slope length, steepness, and shape; runoff; infiltration; risk assessment; foliar and ground cover; soil texture; precipitation intensity; duration and frequency; Ecological Site Description; conservation practice; grazing management; brush management; and fire.

## **RHEM Guides for Specific Ecological Sites**

RHEM Guide Sheets for specific Ecological Sites, State-and-Transition models, and disturbances have been developed separately to quantify how changes in state within an ecological site influences hydrologic and soil erosion process at the scale of a hillslope. Guide Sheets are included as Appendices and provide documented case studies that discuss how to define sustainability in the context of risk of soil erosion. The Guides discuss when sites may cross an ecological/environmental threshold where restoration may not be physically possible. By altering model inputs for vegetation community attributes, the RHEM tools allow for evaluation of hydrologic and soil loss response in relation to defined user management actions (e.g., percent increase in bunchgrass and decrease in bare soil derived from a seeding practice). This allows quantification of conservation benefits. By comparing runoff from various states within an ecological site, one can enhance ecological site descriptions by incorporating this information, how hydrologic properties change as plant communities change, into ecological site descriptions.



## Part 647 – The RHEM Guide, Handbook 647

### Contents

Editors: Mark Weltz and Gary Frasier.....	i.2
Contributors.....	i.2
Citation .....	i.3
RHEM Guides for Specific Ecological Sites.....	i.4
List of Figures.....	i.6
List of Tables.....	i.8

### Subpart A – Rangeland Hydrology and Erosion Model (RHEM) Technical Documentation..

647.01 Introduction .....	A.2
647.02 Model Description .....	A.3
647.03 Fundamental hydrologic and erosion equations: Overland flow model.....	A.3
647.04 Fundamental hydrologic and erosion equations: Overland soil erosion, deposition, and transport.....	A.4
647.05 RHEM Model Parameter Estimation Equations .....	A.6
647.06 Effective saturated hydraulic conductivity .....	A.6
647.07 Hydraulic roughness coefficient .....	A.7
647.08 Splash and sheet erodibility factor.....	A.8
647.09 Concentrated flow erodibility coefficients for hillslope micro-channels.....	A.9

647.10	PEST model parameterization .....	A.9
647.11	Statistical analysis.....	A.9
647.12	Study Area and NRI database – Model performance and capabilities, Lucky Hills 106 watershed.....	A.10
647.13	Model performance with RHEM parameter estimation equations.....	A.14
647.14	Model calibration.....	A.16
647.15	Performance improvement from RHEM V1.0 to RHEM V2.3 .....	A.16
647.16	Model application using NRI data .....	A.17
647.17	Parameter estimation equations for saline and sodic soils .....	A.22
647.18	Performance evaluation for salinity adjustments .....	A.24
647.19	Results of salinity adjustments .....	A.25
647.20	Conclusions .....	A.29

**Subpart B – Rangeland Hydrology and Erosion Model Tutorial Guide ..... B.1**

647.21	Introduction .....	B.3
647.22	Description of the Ecological Site .....	B.5
647.23	Soil.....	B.6
647.24	Plant Communities.....	B.8

**Subpart C – Part I: Developing and Analyzing RHEM Scenarios ..... C.1**

647.31	Data Available for Analysis.....	C.1
647.32	Modeling Results .....	C.6
647.33	Discussion.....	C.9

**Subpart D – Part II: Developing and Analyzing a Risk Assessment ..... D.1**

647.41	Example.....	D.1
647.42	Risk Assessment Modeling Results.....	D.3
647.43	Risk Assessment Discussion.....	D.4
647.44	Summary.....	D.5

**Subpart E – References..... E.1**

647.51	Conversion Factors .....	E.1
647.52	Vegetation and ground cover definitions and photographs.....	E.1
647.53	Hydrologic Terms.....	E.5
647.54	References .....	E.5

**Appendices: RHEM Guide Sheets (See Title 190, Part 647 in eDirectives to access Appendices) ..... E.11**

**List of Figures**

Figure i.	Thunderstorm over central Nevada .....	i.2
Figure ii.	Overland flow channel in bare interspace between Pinyon and Juniper trees, central Nevada.....	i.3
Figure iii.	Gully and rill erosion following wildfire near Minden, Nevada. ....	i.4
Figure iv.	Salt and biological soil crusts with intervening concentrated flow erosion. ....	i.4
Figure v.	Accelerated rill erosion, Badger Wash, Colorado. ....	i.9

**Subpart A – Rangeland Hydrology and Erosion Model (RHEM) Technical Documentation**

Figure A-1.	Location of the Lucky Hills subwatershed study area within the Walnut Gulch Experimental Watershed. ....	A.10
Figure A-2.	Lucky Hills 106 and its representation as overland flow plane in the RHEM model. ....	A.11
Figure A-3.	Distributions of ground surface cover grouped by the five weather stations. (a) litter cover, (b) cryptogams, (c) basal area, and (d) rock cover. ....	A.12
Figure A-4.	Distributions of foliar cover grouped by the five weather stations: (a) Bunchgrass, (b) Forbs/Annual grasses, (c) Shrub, and (d) Sod grasses. ....	A.13

Figure A-5. Distributions of total ground surface cover and foliar cover, grouped by the five weather stations and slope gradient for each NRI point classified based on the weather station’s radius of influence. .... A.13

Figure A-6. Comparison between observed and simulated results for each rainfall-runoff event at Lucky Hills 106: (a) Runoff volume, (b) Peak runoff and (c) Sediment yield. The parameters for these simulations were based on the RHEM V2.3 parameter estimation equations. .... A.15

Figure A-7. Performance improvement on the 23 LH106 sediment yield events by both RHEM V2.3 and RHEM V1.0 models according to the NSE criterion. .... A.17

Figure A-8. The association between ground cover and total friction factor ( $f_t$ ), effective saturated hydraulic conductivity ( $K_e$ ), and splash and sheet erodibility coefficient ( $K_{ss}$ ): (a) strong positive linear correlation between ground cover and  $\log_{10}(f_t)$ , (b) moderate linear correlation between ground cover and  $K_e$ , and (c) strong Spearman rank correlation coefficient between ground cover and  $K_{ss}$ . .... A.18

Figure A-9. Runoff as a percent of precipitation showing the negative relationship with (a) litter cover percent and (b) basal cover percent. .... A.19

Figure A-10. Relationship between average annual sediment yield and slope gradient for the 124 NRI points affected by five precipitation regimes. .... A.19

Figure A-11. Association between predicted average sediment yield and foliar cover and ground cover for the five precipitation regimes. .... A.20

Figure A-12. Research sites near Farmington, New Mexico (left) and Moab, Utah (right) showing naturally occurring erosive conditions due to geologic formation and parent materials, steep slopes, and minimal vegetation that facilitate high salt load transport capacities. No known vegetation management practices are available to reduce soil erosion and salt transport under these naturally occurring conditions. Salt loads can be exacerbated if sites are disturbed through off road activities such as from vehicles and bikes. .... A.23

Figure A-13. Flowchart diagram of the experimental data utilized for the development and validation of new parameter-estimation equations on saline sites. .... A.25

Figure A-14. Observed vs. predicted runoff on 36 rainfall simulation calibration plots using current RHEM parameter estimation equations. .... A.26

Figure A-15. Observed vs. predicted soil loss on 36 rainfall simulation calibration plots using current RHEM parameter estimation equations. .... A.26

Figure A-16. Observed vs. predicted runoff on the 36 validation data points using the current and the newly developed estimation equation for the hydraulic conductivity  $K_e$ . .... A.27

Figure A-17. Observed vs. predicted soil loss on the 36 validation data points using the current and the newly developed estimation equation for the sheet and splash erodibility  $K_{ss}$ . .... A.27

Figure A-18. Relationship between cumulative soil loss and cumulative dissolved solids measured in runoff. ... A.28

Figure A-19. Observed vs. predicted total dissolved solids (TDS) on the 36 calibration (a) and 36 validation (b) data points using the current and the newly developed estimation equations for  $K_e$  and  $K_{ss}$ . .... A.29

Figure A-20. Rill erosion in western Nevada where the site has been burned, and the annual invasive grass has revegetated the site. .... A.31

**Subpart B – Rangeland Hydrology and Erosion Model Tutorial Guide ..... B.1**

Figure B-1. Rill erosion western Colorado ..... B.1

Figure B-2. Gully erosion central Utah ..... B.1

Figure B-3. Sagebrush plant community in Central Nevada near reference condition. .... B.2

Figure B-4. Mixed grass prairie in North Dakota near reference conditions. .... B.2

Figure B-5. Map of rainfall simulation experiments sites from which RHEM was developed shown on Omernik Level IV Ecoregions. .... B.4

Figure B-6. Limy Slopes 12–16” PZ Ecological Site within the Walnut Gulch Experimental Watershed in Tombstone, Arizona. .... B.6

Figure B-7. Web Soil Survey area of interest with map unit legend. .... B.7

Figure B-8. Historic Plant Community (HPC). .... B.8

Figure B-9. The State and Transition Model diagram for the Limy Slopes 12–16” PZ Ecological Site. Site Type: Rangeland; Site Id: R041XC308AZ; Major Land Resource Area (MLRA) 041- Southern Arizona Basin and Range. CAER = false mesquite (*Calliandra conferta*); KRER = ratany (*Krameria erecta*); BOER = black grama (*Bouteloua eriopoda*); BOSCU = sideoats grama (*Bouteloua curtipendula*). .... B.10

Figure B-10. Exotic perennial grass. .... B.10

Figure B-11. Shrub Invaded State. .... B.11

Figure B-12. Eroded rangeland. .... B.11

**Subpart C – Part I: Developing and Analyzing RHEM Scenarios ..... C.1**

Figure C-1. RHEM initial screen Web-based system .....C-2  
 Figure C-2. Define scenario for RHEM analysis ..... C.3  
 Figure C-3. Define units for analysis ..... C.3  
 Figure C-4. Define climate station for analysis. .... C.2  
 Figure C-5. Define soil texture of the site. .... C.3  
 Figure C-6. Define slope of the site. .... C.4  
 Figure C-7. Define vegetation type, canopy cover and ground cover. .... C.5  
 Figure C-8. Diagram of ground surface cover classes as used by RHEM. .... C.5  
 Figure C-9. Run the scenario ..... C.5  
 Figure C-10. Select scenario to review output. .... C.6  
 Figure C-11. Average annual results for rain, runoff, sediment yield, and soil loss. .... C.6  
 Figure C-12. Annual averages for precipitation, runoff, sediment yield, and soil loss for scenarios. .... C.7  
 Figure C-13. Return frequency graphs for rain, runoff, sediment yield, and soil loss based on yearly summation values. .... C.7

**Subpart D – Part II: Developing and Analyzing a Risk Assessment ..... D.1**

Figure D-1. Select scenario for risk assessment from completed model runs. ....D.1  
 Figure D-2. Select Account button. ....D.1  
 Figure D-3. Screenshot illustrating how to enable the detailed output option. ....D.2  
 Figure D-4. Screenshot illustrating scenarios with detailed output previously generated in Part I. The green button indicates the baseline scenario. ....D.3  
 Figure D-5. Probability of occurrence for yearly soil loss for all scenarios. ....D.4  
 Figure D-6. Rotating boom simulator used to collect data for development of the Rangeland Hydrology and Erosion Model (RHEM). Plots were 3 m (10 ft.) wide by 10.7 m (35 ft.) long. ....D.6  
 Figure D-7. Walnut Gulch rainfall simulator used to collect data near Moab, Utah for development of the Rangeland Hydrology and Erosion Model (RHEM). Plots were 2m (6ft) wide by 6m (20ft) long. ....D.7

**List of Tables**

**Subpart A – Rangeland Hydrology and Erosion Model (RHEM) Technical Documentation 1**

Table A-1. Estimation guides for soil hydraulic properties based on sample data (Rawls et al., 1998). The geometric mean of the  $K_s$  sorted according to soil texture and bulk density classes along with the 25<sup>th</sup> and 75<sup>th</sup> percentile. ....A.7  
 Table A-2. Summary of the ground surface and foliar cover for THE Lucky Hills 106 subwatershed.....A.11  
 Table A-3. Summary descriptive statistics of the 23 events at Lucky Hills 106. ....A.12  
 Table A-4. RHEM parameter values estimated using the empirical equations.....A.14  
 Table A-5. Model performance statistics for Lucky Hills 106. ....A.14  
 Table A-6. Minimum, maximum, and average values for the calibrated parameters. ....A.16  
 Table A-7. Variation of mean and CV (Coefficient of Variation) in slope steepness, litter, rock and annual sediment yield for the 124 NRI points.....A.20

**Subpart B – Rangeland Hydrology and Erosion Model Tutorial Guide ..... B.1**

Table B-1. Description of community transitions..... B.8  
 Table B-2. Summary of input parameters for various represented states. .... B.9

**Subpart C – Part I: Developing and Analyzing RHEM Scenarios ..... C.1**

Table C-1. Estimated rain, runoff, sediment yield, and soil loss for the 5-year return frequency year..... C.8  
 Table C-2. Estimated rain, runoff, sediment yield, and soil loss for the 25-year return frequency year..... C.8  
 Table C-3. Estimated rain, runoff, sediment yield, and soil loss for the 50-year return frequency year..... C.8  
 Table C-4. Estimated rain, runoff, sediment yield, and soil loss for the 100-year return frequency year..... C.8

**Subpart D – Part II: Developing and Analyzing a Risk Assessment ..... D.1**

Table D-1. Percent probability of occurrence of yearly soil losses and soil loss severity. ....D.3

**Figure v.** Accelerated rill erosion, Badger Wash, Colorado.



## Subpart A – Rangeland Hydrology and Erosion Model (RHEM) Technical Documentation

### Contents

647.01	Introduction .....	A.1
647.02	Model Description .....	A.3
647.03	Fundamental hydrologic and erosion equations: Overland flow model.....	A.3
647.04	Fundamental hydrologic and erosion equations: Overland soil erosion, deposition, and transport .....	A.4
647.05	RHEM Model Parameter Estimation Equations .....	A.6
647.06	Effective saturated hydraulic conductivity .....	A.6
647.07	Hydraulic roughness coefficient .....	A.7
647.08	Splash and sheet erodibility factor.....	A.8
647.09	Concentrated flow erodibility coefficients for hillslope micro-channels.....	A.9
647.10	PEST model parameterization .....	A.9
647.11	Statistical analysis.....	A.9
647.12	Study Area and NRI database – Model performance and capabilities, Lucky Hills 106 watershed.....	A.10
647.13	Model performance with RHEM parameter estimation equations.....	A.14
647.14	Model calibration.....	A.16
647.15	Performance improvement from RHEM V1.0 to RHEM V2.3 .....	A.16
647.16	Model application using NRI data .....	A.17
647.17	Parameter estimation equations for saline and sodic soils .....	A.22
647.18	Performance evaluation for salinity adjustments .....	A.24
647.19	Results of salinity adjustments .....	A.25
647.20	Conclusions .....	A.29

### List of Figures

Figure A-1.	Location of the Lucky Hills subwatershed study area within the Walnut Gulch Experimental Watershed.....	A.10
Figure A-2.	Lucky Hills 106 and its representation as overland flow plane in the RHEM model. ....	A.11
Figure A-3.	Distributions of ground surface cover grouped by the five weather stations. (a) litter cover, (b) cryptogams, (c) basal area, and (d) rock cover.....	A.12
Figure A-4.	Distributions of foliar cover grouped by the five weather stations: (a) Bunchgrass, (b) Forbs/Annual grasses, (c) Shrub, and (d) Sod grasses. ....	A.13
Figure A-5.	Distributions of total ground surface cover and foliar cover, grouped by the five weather stations and slope gradient for each NRI point classified based on the weather station’s radius of influence.....	A.13
Figure A-6.	Comparison between observed and simulated results for each rainfall-runoff event at Lucky Hills 106: (a) Runoff volume, (b) Peak runoff and (c) Sediment yield. The parameters for these simulations were based on the RHEM V2.3 parameter estimation equations.....	A.15
Figure A-7.	Performance improvement on the 23 LH106 sediment yield events by both RHEM V2.3 and RHEM V1.0 models according to the NSE criterion.....	A.17
Figure A-8.	The association between ground cover and total friction factor ( $f_t$ ), effective saturated hydraulic conductivity ( $K_e$ ), and splash and sheet erodibility coefficient ( $K_{ss}$ ): (a) strong positive linear correlation between ground cover and $\log_{10}(f_t)$ , (b) moderate linear correlation between ground cover and $K_e$ , and (c) strong Spearman rank correlation coefficient between ground cover and $K_{ss}$ .....	A.18
Figure A-9.	Runoff as a percent of precipitation showing the negative relationship with (a) litter cover percent and (b) basal cover percent. ....	A.19
Figure A-10.	Relationship between average annual sediment yield and slope gradient for the 124 NRI points affected by five precipitation regimes. ....	A.19
Figure A-11.	Association between predicted average sediment yield and foliar cover and ground cover for the five precipitation regimes. ....	A.20
Figure A-12.	Research sites near Farmington, New Mexico (left) and Moab, Utah (right) showing naturally occurring erosive conditions due to geologic formation and parent materials, steep slopes, and minimal vegetation that facilitate high salt load transport capacities. No known vegetation management practices are	

available to reduce soil erosion and salt transport under these naturally occurring conditions. Salt loads can be exacerbated if sites are disturbed through off road activities such as from vehicles and bikes. .... A.23

Figure A-13. Flowchart diagram of the experimental data utilized for the development and validation of new parameter-estimation equations on saline sites..... A.25

Figure A-14. Observed vs. predicted runoff on 36 rainfall simulation calibration plots using current RHEM parameter estimation equations. .... A.26

Figure A-15. Observed vs. predicted soil loss on 36 rainfall simulation calibration plots using current RHEM parameter estimation equations. .... A.26

Figure A-16. Observed vs. predicted runoff on the 36 validation data points using the current and the newly developed estimation equation for the hydraulic conductivity  $K_e$ . .... A.27

Figure A-17. Observed vs. predicted soil loss on the 36 validation data points using the current and the newly developed estimation equation for the sheet and splash erodibility  $K_{ss}$ . .... A.27

Figure A-18. Relationship between cumulative soil loss and cumulative dissolved solids measured in runoff. .... A.28

Figure A-19. Observed vs. predicted total dissolved solids (TDS) on the 36 calibration (a) and 36 validation (b) data points using the current and the newly developed estimation equations for  $K_e$  and  $K_{ss}$ . .... A.29

Figure A-20. Rill erosion in western Nevada where the site has been burned, and the annual invasive grass has revegetated the site. .... A.31

**List of Tables**

Table A-1. Estimation guides for soil hydraulic properties based on sample data (Rawls et al., 1998). The geometric mean of the  $K_s$  sorted according to soil texture and bulk density classes along with the 25<sup>th</sup> and 75<sup>th</sup> percentile. .... A.7

Table A-2. Summary of the ground surface and foliar cover for THE Lucky Hills 106 subwatershed. .... A.11

Table A-3. Summary descriptive statistics of the 23 events at Lucky Hills 106. .... A.12

Table A-4. RHEM parameter values estimated using the empirical equations..... A.14

Table A-5. Model performance statistics for Lucky Hills 106. .... A.14

Table A-6. Minimum, maximum, and average values for the calibrated parameters. .... A.16

Table A-7. Variation of mean and CV (Coefficient of Variation) in slope steepness, litter, rock and annual sediment yield for the 124 NRI points. .... A.20

**647.01 Introduction**

A. The complex interactions of variable climate, vegetation, surface soil dynamics, and human activities have major impacts on runoff and soil erosion processes on rangeland ecosystems. These processes and activities affect ecosystem functions over a wide range of spatial and temporal scales (Williams et al., 2016). Nearing et al. (2004) suggested that climatic variability will increase erosion in the future in many environments. That is, future climates are expected to lead to a more vigorous hydrological cycle, including total rainfall amount and variability, and more frequent high-intensity rainfall events that drive the water erosion process (Nearing et al., 2004; Nearing et al., 2015). The consequence is often rangeland degradation—a decrease in vegetation cover or a change of vegetation composition, with a subsequent loss of the system’s productivity (UNCCD 1994). Decades of research have shown that rangelands can sustainably produce a variety of goods and services if managers respond quickly and appropriately to changes, even in the face of extreme climatic events (Havstad et al., 2009). While land managers may not be able to alter variability in climate, they may be able to adapt to changes in precipitation intensity, duration, and frequency and devise management practices that are more resilient and resistant to climatic impacts. Soil erosion is among the climate-related impacts that concern rangeland managers, since conservation of topsoil is critical to sustained productivity in rangeland ecosystems. Soil loss rates on rangelands are regarded as one of the few quantitative indicators for assessing rangeland health and conservation practice effectiveness (Nearing et al., 2011 and Weltz et al., 2014).

B. The Rangeland component of the Conservation Effects Assessment Project (CEAP) was formally initiated in 2006 to evaluate conservation effectiveness on rangelands, pastures, and grazed forests that together comprise 188 million hectares of USA nonfederal land, as well as large areas of federal land in the western United States. Broad-scale assessments of this type need reliable modeling capabilities. Erosion prediction technology must be capable of simulating the complex interactions between vegetation characteristics, surface soil properties, and hydrologic and erosion processes on rangelands (Nearing and Hairsine 2011). Al-Hamdan et al. (2012b) pointed out that better representation of the temporal dynamics of soil erodibility related to disturbed rangeland conditions (e.g., fire) is also needed to accurately estimate soil erosion on rangelands.

C. The goals of this Handbook are to provide an exact description of the Rangeland Hydrology and Erosion Model (RHEM) V2.3 by providing a detailed layout of the mathematical model structure and to present the results of model applications and potential uses. This Handbook also demonstrates the gains in model performance and reliability over the former model version RHEM V1.0. The Handbook has the following sections: (1) to present the driving equations for RHEM V2.3 model; (2) to calibrate the RHEM V2.3 model using 23 rainfall-runoff-sediment yield events on a small semiarid sub-watershed within the Walnut Gulch Experimental Watershed in Arizona, and compare them against parameters estimated by the RHEM V2.3 parameter estimation equations; (3) to examine the performances improvement from RHEM V1.0 to RHEM V2.3; (4) to provide a User Guide for implementing the model; (5) to present a case study for application and interpretation of the model for planning conservation; and (6) to document where data were derived to develop and validate the model.

## 647.02 Model Description

This section is divided into four main parts: (1) presentation of fundamental hydrologic and erosion equations in RHEM V2.3, (2) an overview of the RHEM V2.3 parameter estimation equations, (3) model calibration with the Model-Independent Parameter ESTimation (PEST) program, and (4) statistical analysis and results.

## 647.03 Fundamental hydrologic and erosion equations: Overland flow model

A. The hydrology component of the enhanced RHEM V2.3 model is based on the KINEROS2 model (Smith et al., 1995). The model was implemented to simulate one-dimensional overland flow within an equivalent plane representing a hillslope with uniform or curvilinear slope profiles. The flow per unit width across a plane surface, as a result of rainfall, can be described by the one-dimensional continuity equation (Woolhiser et al., 1990).

$$\frac{\partial h}{\partial t} + \frac{\partial q}{\partial x} = \sigma(x, t) \quad (1)$$

where  $h$  is the flow depth at time  $t$ , and the position  $x$  is the space coordinate along the direction of flow;  $q$  is the volumetric water flux per unit plane width ( $\text{m}^2 \text{s}^{-1}$ ); and  $\sigma(x, t)$  is the rainfall excess ( $\text{m s}^{-1}$ ).

$$\sigma(x, t) = r - f \quad (2)$$

where  $r$  is the rainfall rate ( $\text{m s}^{-1}$ ), and  $f$  is the infiltration rate ( $\text{m s}^{-1}$ ). The following equation represents the relationship between  $q$  and  $h$ :

$$q = \left( \frac{8gS}{f_t} \right)^{1/2} h^{3/2} \quad (3)$$

where  $g$  is the gravity acceleration ( $\text{m s}^{-2}$ ),  $S$  is the slope gradient ( $\text{m m}^{-1}$ ), and  $f_t$  is the total Darcy-Weisbach friction factor estimated using equation 18 developed by Al-Hamdan et al., 2013. Substituting Equations (2) and (3) in Equation (1) results in the hydrology routing equation:

$$\frac{\partial h}{\partial t} + \frac{3}{2} \left( \frac{8gS}{f_t} \right)^{1/2} h^{1/2} \frac{\partial h}{\partial x} = r - f \quad (4)$$

B. In RHEM, for a single plane, the upstream boundary is assumed to be at zero depth, and the downstream boundary is a continuing plane (along the direction of flow).

$$h(0, t) = 0 \quad (5)$$

C. The infiltration rate is computed in KINEROS2 using the three-parameter infiltration equation (Parlange et al., 1982), in which the models of Green and Ampt (1911) and Smith and Parlange (1978) are included as two limiting cases.

$$f = K_e \left[ 1 + \frac{\alpha}{\exp\left(\frac{\alpha I}{C_d \Delta \theta_i}\right) - 1} \right] \quad (6)$$

where  $I$  is the cumulative depth of the water infiltrated into the soil (m),  $K_e$  is the surface effective saturated hydraulic conductivity ( $m\ s^{-1}$ ),  $C_d$  (m) accounts for the effect of capillary forces on moisture absorption during infiltration, and  $\alpha$  is a scaling parameter. When  $\alpha = 0$ , Equation 6 is reduced to the simple Green and Ampt infiltration model, and when  $\alpha = 1$ , the equation simplifies to the Parlange model. Most soils exhibit infiltrability behavior intermediate to these two models, and KINEROS2 uses a weighting value ( $\alpha$ ) of 0.85 (Smith et al., 1993). The stated variable for infiltrability is the initial water content, in the form of the soil saturation deficit,  $B = C_d(\theta_s - \theta_i)$ , defined as the saturated moisture content minus the initial moisture content. The saturation deficit ( $\theta_s - \theta_i$ ) is one parameter because  $\theta_s$  is fixed from storm to storm. For ease of estimation, the KINEROS2 input parameter for soil water is a scaled moisture content,  $S = \theta/\phi$  ( $\phi$  is the soil porosity), which varies from 0 to 1. Thus, initial soil conditions are represented by the variable  $S_i$  ( $S_i = \theta_i/\phi$ ). Two parameters,  $K_e$  and  $C_d$ , characterize the soil, and the variable  $S_i$  characterizes the initial condition

#### 647.04 Fundamental hydrologic and erosion equations: Overland soil erosion, deposition, and transport

A. The RHEM erosion model uses a dynamic sediment continuity equation to describe the movement of suspended sediment in a concentrated flow area (Bennett, 1974):

$$\frac{\partial(Ch)}{\partial t} + \frac{\partial(Cq_r)}{\partial x} = D_{ss} + D_{cf} \quad (7)$$

where  $C$  is the measured sediment concentration ( $kg\ m^{-3}$ ),  $q_r$  is the flow discharge of concentrated flow per unit width ( $m^2\ s^{-1}$ ),  $D_{ss}$  is the splash and sheet detachment rate ( $kg\ s^{-1}\ m^{-2}$ ), and  $D_{cf}$  is the concentrated flow detachment rate ( $kg\ s^{-1}\ m^{-2}$ ). For a unit wide plane, when overland flow accumulates into a concentrated flow path, the following equation calculates the concentrated flow discharge per unit width ( $q_r$ ):

$$q_r = \frac{q}{w} \quad (8)$$

where  $w$  is the concentrated flow width (m) calculated by Al-Hamdan et al. (2012a).

$$w = \frac{2.46 Q^{0.39}}{S^{0.4}} \quad (9)$$

B. The splash and sheet detachment rate ( $D_{ss}$ ) is calculated by the following equation (Wei et al., 2009):

$$D_{ss} = K_{ss} r^{1.052} \sigma^{0.592} \quad (10)$$

where  $K_{ss}$  is the splash and sheet erodibility,  $r$  ( $m\ s^{-1}$ ) is the rainfall intensity, and  $\sigma$  is rainfall excess ( $m\ s^{-1}$ ).

C. RHEM is a hillslope scale model. As such, it does not address flow in channels. It does have the capability to estimate transport and erosion in ephemeral (rills) or semi-permanent micro-channels on the hillslopes of up to a few cm in width and depth. Concentrated flow detachment rate ( $D_{cf}$ ) is calculated as the net detachment and deposition rate (Foster, 1982):

$$D_{cf} = \begin{cases} D_c \left(1 - \frac{CQ}{T_c}\right), & CQ \leq T_c \\ \frac{0.5 V_f}{Q} (T_c - CQ), & CQ \geq T_c \end{cases} \quad (11)$$

where  $D_c$  is the concentrated flow detachment capacity ( $\text{kg s}^{-1} \text{m}^{-2}$ ),  $Q$  is the flow discharge ( $\text{m}^3 \text{s}^{-1}$ ),  $T_c$  is the sediment transport capacity ( $\text{kg s}^{-1}$ ), and  $V_f$  is the soil particle fall velocity ( $\text{m s}^{-1}$ ) that is calculated as a function of particle density and size (Fair and Geyer, 1954).

D. Sediment detachment rates from the concentrated flow is calculated by employing soil erodibility characteristics of the site and hydraulic parameters of the flow, such as flow width and stream power. Soil detachment is assumed to start when concentrated flow starts (i.e., no threshold concept for initiating detachment is used) (Al-Hamdan et al., 2012b).

To calculate  $D_c$ , the equation developed by Al-Hamdan et al. (2012b) is used:

$$D_c = K_\omega(\omega) \quad (12)$$

where  $K_\omega$  is the stream power erodibility factor ( $\text{s}^2 \text{m}^{-2}$ ), and  $\omega$  is the stream power ( $\text{kg s}^{-3}$ ). We implemented the empirical equation developed by Nearing et al. (1997) to calculate the transport capacity ( $T_c$ ).

$$\text{Log}_{10} \left( \frac{10T_c}{w} \right) = -34.47 + 38.61 * \frac{\exp[0.845+0.412 \log(1000\omega)]}{1+\exp[0.845+0.412 \log(1000\omega)]} \quad (13)$$

E. Soil detachment is not considered a selective process, so the sediment particle size distribution generated from actively eroding areas is assumed to be a function of the fraction of total sediment load represented by five particle classes, based on soil texture. The transport capacity equation of Nearing et al. (1997) does not account for particle sorting. Consequently, routing of sediment by size particle is not carried out.

F. Several studies have documented increases in peak flows and erosion occurring on systems that have been altered by some disturbance. For example, at the plot or hillslope scale, increases in sediment delivery between 2- and 1000-fold have been reported (Morris and Moses, 1987; Scott and Van Wyk, 1992; Shakesby et al., 1993; Cerdà, 1998; Pierson et al., 2002). Results from rainfall simulator experiments suggest that erosion rates are much higher on forest roads and burned rangeland in the early part of a runoff event than in the latter part of the event (Foltz et al., 2008) (Pierson et al., 2008). These rapid changes in the concentrated flow erosion rate on disturbed soils may be caused by the winnowing of fine or easily detached soil particles during the early stages of erosive runoff, thus leaving larger or more embedded particles and aggregates, which require greater stream power for detachment (Robichaud et al., 200).

G. Because RHEM V2.3 is a dynamic model, it also has the capacity, as an option, to use equations developed by Al-Hamdan et al. (2012b) for characterizing events on recently disturbed rangelands with high concentrated flow erodibility at the onset of the event, and with exponentially decreasing erodibility throughout the event, due to reduction in sediment availability (winnowing of readily available sediment).

$$D_c = K_{\omega(\text{Max})\text{adj}} \exp(\beta q_c) \omega \quad (14)$$

$$q_c = \int q_r dt \quad (15)$$

$$\omega = \gamma S q_r \quad (16)$$

where  $K_{\omega(\text{Max})\text{adj}}$  is the maximum stream power erodibility ( $\text{s}^2 \text{m}^{-2}$ ) corresponding to the decay factor  $\beta = -5.53 \text{ (m}^{-2}\text{)}$ ,  $\beta$  is a decay coefficient representing erodibility change during an event ( $\text{m}^{-2}$ ),  $\omega$  is the stream power ( $\text{kg s}^{-3}$ ),  $q_c$  is the cumulative flow discharge of concentrated flow per unit width ( $\text{m}^2$ ),  $\gamma$  is the water specific weight ( $\text{kg m}^{-2} \text{s}^{-2}$ ), and  $S$  is the slope gradient ( $\text{m m}^{-1}$ ).

## 647.05 RHEM Model Parameter Estimation Equations

An important aspect of RHEM for application by rangeland managers is that the model is parameterized based on plant growth form types using data commonly collected in rangeland inventory and assessment efforts (e.g., rangeland health or NRI assessments).

## 647.06 Effective saturated hydraulic conductivity

A. Research has indicated that infiltration, runoff, and erosion dynamics are correlated with the presence or absence and composition of specific plant taxa and growth attributes (Davenport et al., 1998; Wainwright et al., 2000; Ludwig et al., 2005; Peters et al., 2007; Turnbull et al., 2008; Turnbull et al., 2012; Petersen et al., 2009; Pierson et al., 2010; Pierson et al., 2013; Wilcox et al., 2012; and Williams et al., 2014). Numerous studies have documented that infiltration of rainfall increases with increasing vegetative surface cover (Ludwig et al., 2005). For example, Tromble et al. (1974) evaluated infiltrability on three range sites in Arizona and found that infiltrability was positively related to vegetal cover and litter biomass and negatively related to gravel cover. Meeuwig (1970) and Dortignac and Love (1961) also found infiltrability and litter cover to be positively related. Work by Spaeth et al. (1996) using data from across the western U.S. concluded that inclusion of plant species and ground cover variables in prediction equations significantly improved infiltration estimation with respect to purely physically-based prediction equations. Thompson et al. (2010) provides a detailed review of research findings on vegetation-infiltration relationships across climate and soil type gradients.

B. Soil texture may be used as the first estimator of  $K_e$  because texture affects the pore space available for water movement. Also, soil texture is easy to measure and often available for an area of interest. Rawls et al. (1982) developed a look-up table of  $K_s$  values for the 11 USDA soil textural classes. Bulk density is another basic soil property that is related to pore space and water movement. Rawls et al. (1998) revised the texture-based look-up table to include two porosity classes within each textural class—the geometric means of the  $K_s$  along with the 25<sup>th</sup> and 75<sup>th</sup> percentile values. The texture or porosity estimates ( $K_s$ ) were based on a national database of measured  $K_s$  values and soil properties at 953 locations. These estimates indicate that  $K_s$  is highest for coarse-textured soils, and soils with greater porosity (lower bulk density) have higher  $K_s$  values within a textural class.

C. The geometric mean of  $K_s$ , sorted according to the soil texture and bulk density classes along with the 25<sup>th</sup> and 75<sup>th</sup> percentile values, are presented in table A-1. Also reported in table A-1 is the corresponding arithmetic mean porosity  $\phi$  ( $m^3 m^{-3}$ ) and mean capillary drive  $C_d$  (mm).

D. Saturated hydraulic conductivity has been characterized as being lognormally distributed in space (Nielsen et al., 1973; Smith and Goodrich, 2000), with variations of an order of magnitude or more across relatively short distances. It is clear that this approach of representing a landscape using various values of saturated conductivity distributed across space with a lognormal distribution is more realistic than a single uniformly applied mean value. The RHEM model defines a range of hydraulic conductivity values based on the 25<sup>th</sup> and 75<sup>th</sup> percentile values for each soil textural class reported in table A-2 (Rawls et al., 1998). Then we adjusted them to account for the effects of litter and basal cover based on the exponential model developed by Stone et al. (1992). Stone et al. (1992) developed an exponential model to adjust the baseline saturated hydraulic conductivity (Rawls et al., 1982) as a function of surface cover and foliar cover, based on an unpublished analysis of rainfall simulator data on desert brush dominated sites in Arizona and Nevada. Moreover, they divided the baseline saturated hydraulic conductivity by two to account for the effects of crusting on the effective saturated hydraulic conductivity. However, Stone et al. (1992) did not report criteria to assess the goodness of fit of the model and the range of values of the predictor variables. In the model developed by Stone et al. (1992), the effective saturated hydraulic conductivity increases exponentially as ground cover and

foliar cover increase, which is consistent with the trend shown in croplands reported by Rawls et al. (1990) and Zhang et al. (1995). Moreover, as pointed out by Zhang et al. (1995), the impact of canopy height must also be considered for accurate simulation of the effects of foliar cover on infiltration and runoff.

**Table A-1.** Estimation guides for soil hydraulic properties based on sample data (Rawls et al., 1998). The geometric mean of the  $K_s$  sorted according to soil texture and bulk density classes along with the 25<sup>th</sup> and 75<sup>th</sup> percentile.

USDA Soil Class Texture	Sand (%)	Clay (%)	Porosity (m <sup>3</sup> m <sup>-3</sup> )	Geometric Mean $K_s$ (mm h <sup>-1</sup> )	$K_s$ 25% percentile (mm h <sup>-1</sup> )	$K_s$ 75% Percentile (mm h <sup>-1</sup> )	Mean capillary drive $C_a$ (mm)	Sample Size
Sand	92	4	0.44	181.9	96.5	266.8	50	39
	91	4	0.39	91.4	64.0	218.5		30
Loamy Sand	82	6	0.45	123.0	83.8	195.5	70	19
	82	7	0.37	41.4	30.5	77.6		28
Sandy Loam	65	11	0.47	55.8	30.5	129.6	130	75
	68	13	0.37	12.8	5.1	31.3		112
Loam	38	23	0.47	3.9	1.6	28.4	110	44
	43	22	0.39	6.2	2.8	16.5		65
Silt Loam	18	19	0.49	14.4	7.6	37.1	200	61
	21	20	0.39	3.4	1.0	9.9		46
Sandy Clay Loam	56	26	0.44	7.7	2.0	50.5	260	20
	58	26	0.37	2.8	1.0	10.9		53
Clay Loam	29	35	0.48	4.2	2.2	13.1	260	20
	35	35	0.40	0.7	0.2	3.8		53
Silty Clay Loam	10	34	0.50	3.7	2.3	10.4	350	26
	10	32	0.43	4.9	2.3	14.0		33
Sandy Clay	51	36	0.39	0.9	0.3	2.5	300	14
Silty Clay	4	49	0.53	1.8	0.5	7.5	380	10
Clay	18	53	0.48	2.0	0.9	6.0	410	20
	26	50	0.40	1.8	0.3	6.9		21

E. RHEM estimates of effective saturated hydraulic conductivity are computed as follows:

$$K_{ei} = K_{bi} e^{[p_i(\text{litter}+\text{basal})]} \quad (17)$$

In this equation,  $K_{bi}$  is the 25<sup>th</sup> percentile saturated hydraulic conductivity for each soil textural class,  $i$ , listed in table A-1;  $p$  is defined as the natural log of the ratio of the 75<sup>th</sup> to the 25<sup>th</sup> percentile values of saturated hydraulic conductivity; litter is litter cover (percent); and basal is basal area cover (percent).

### 647.07 Hydraulic roughness coefficient

A. Al-Hamdan et al. (2013) developed empirical equations that predict the total measured friction factor ( $f_i$ ) by regressing the total measured friction against the measured vegetation and rock cover, slope, and flow rate. The data used in their study were obtained from rangeland overland flow experiments conducted by the USDA-ARS Northwest Watershed Research Center in Boise, Idaho. Overland flow was simulated by releasing water from a flow regulator located upstream of each plot.

B. The data were collected from rangeland sites within the U.S. Great Basin Region, with a broad range of slope gradients (5.6 percent to 65.8 percent), soil types, and vegetation cover. Many of these sites show some degree of disturbance or treatment, such as tree encroachment, prescribed fire,

wildfire, tree mastication, or tree cutting. Average slope, foliar and ground cover, and micro-topography were measured for each plot (Pierson et al., 2007, 2009, 2010).

C. According to Al-Hamdan et al. (2013), total hydraulic friction was negatively correlated with flow discharge and the percentage of bare ground, and it was positively correlated with the presence of vegetation cover and slope. Equations that were developed from concentrated flow data have significantly different coefficient values compared to those developed from sheet flow data. The flow discharge and slope in the total friction equation improved the prediction of the total friction, and consequently improved the estimation of the proportion of the assumed soil friction to total friction. All equations derived by Al-Hamdan et al. (2013) showed that basal plant cover exerted the most influence and was the most important effect on total friction among other measured cover attributes. RHEM computes the total Darcy-Weisbach friction ( $f_t$ ) factor estimated by Al-Hamdan et al. (2013) as follows:

$$\log(f_t) = -0.109 + 1.425 \text{ litter} + 0.442 \text{ rock} + 1.764 (\text{basal} + \text{cryptogams}) + 2.068 S \quad (18)$$

where litter is the fraction of area covered by litter to total area ( $\text{m}^2 \text{m}^{-2}$ ), basal + cryptogams is the fraction of area covered by basal plants and cryptogams to total area ( $\text{m}^2 \text{m}^{-2}$ ), rock is the fraction of area covered by rock to total area ( $\text{m}^2 \text{m}^{-2}$ ), and S is the slope gradient ( $\text{m m}^{-1}$ ).

### 647.08 Splash and sheet erodibility factor

A. The RHEM model parameterization represents erosion processes on undisturbed rangelands, as well as rangelands that show disturbances such as fire or woody plant encroachment (Nearing et al., 2011; Hernandez et al., 2013; Al-Hamdan et al., 2017; Williams et al., 2016). In RHEM, soil detachment is predicted as a combination of two erosion processes: rain splash and thin sheet flow detachment (splash and sheet), and concentrated flow detachment.

B. This section presents empirical equations developed by Al-Hamdan et al. (2017) using piecewise regression analysis to predict splash and sheet erodibility across a broad range of soil texture classes, based on vegetation cover and surface slope gradient, where G is the area fraction of ground cover, F is the area fraction of foliar cover, and S is the slope gradient (expressed as a fraction).

(1) Bunchgrass:

$$\text{Log}_{10} K_{SS} = \begin{cases} 4.154 - 2.547 * G - 0.7822 * F + 2.5535 * S & \text{if } G \leq 0.475 \\ 3.1726975 - 0.4811 * G - 0.7822 * F + 2.5535 * S & \text{if } G > 0.475 \end{cases} \quad (19)$$

(2) Sod Grass:

$$\text{Log}_{10} K_{SS} = \begin{cases} 4.2169 - 2.547 * G - 0.7822 * F + 2.5535 * S & \text{if } G \leq 0.475 \\ 3.2355975 - 0.4811 * G - 0.7822 * F + 2.5535 * S & \text{if } G > 0.475 \end{cases} \quad (20)$$

(3) Shrub:

$$\text{Log}_{10} K_{SS} = \begin{cases} 4.2587 - 2.547 * G - 0.7822 * F + 2.5535 * S & \text{if } G \leq 0.475 \\ 3.2773975 - 0.4811 * G - 0.7822 * F + 2.5535 * S & \text{if } G > 0.475 \end{cases} \quad (21)$$

(4) Forbs:

$$\text{Log}_{10} K_{SS} = \begin{cases} 4.1106 - 2.547 * G - 0.7822 * F + 2.5535 * S & \text{if } G \leq 0.475 \\ 3.1292975 - 0.4811 * G - 0.7822 * F + 2.5535 * S & \text{if } G > 0.475 \end{cases} \quad (22)$$

C. Al-Hamdan et al. (2017) reported that RHEM performed well using  $K_{SS}$  alone, if the small concentrated flow paths on the hillslope are the primary transport mechanism for the splash and sheet-generated sediments. It is recommended to use the  $K_{SS}$  equation that represents the dominant vegetation community in the site to be evaluated. However, if the site does not have a dominant vegetation form, or more details are needed, then weight-averaging between equations (19) through (22) based on the percentage of life form can be used.

### 647.09 Concentrated flow erodibility coefficients for hillslope micro-channels

A. The parameterization of  $K_{\omega}$  is needed only in the special case of abrupt disturbance with steep slope gradients ( $> 20$  percent) and soils with high silt content. In RHEM, the default value for  $K_{\omega}$  was set as  $7.7 \times 10^{-6}$  ( $s^2 m^{-2}$ ), based on rainfall simulator studies and model calibration carried out in the Walnut Gulch Experimental Watershed in Tombstone, Arizona. This small value of concentrated flow erodibility is typical for undisturbed rangeland (Al-Hamdan et al., 2017). Moreover, Al-Hamdan et al. (2012b) developed an empirical equation to calculate  $K_{\omega}$  for a broad range of undisturbed rangeland sites and tree-encroached sites.

$$\log_{10}(K_{\omega}) = -4.14 - 1.28\text{litter} - 0.98\text{rock} - 15.16\text{clay} + 7.09\text{silt} \quad (23)$$

B. The model also has the capacity, as an option, to use equations developed by Al-Hamdan et al. (2012b) for predicting maximum erodibility for a wide range of burned rangeland sites, including burned tree-encroached sites.

$$\log_{10}(K_{\omega(\max)\text{adj}}) = -3.28 - 1.77\text{litter} - 1.26\text{rock} - 2.46(\text{basal} + \text{crypto}) + 3.53\text{silt} \quad (24)$$

$$\log_{10}(K_{\omega(\max)\text{adj}}) = -3.64 - 1.97(\text{litter} + \text{basal} + \text{crypto}) - 1.85\text{rock} - 4.99\text{clay} + 6.0\text{silt} \quad (25)$$

where litter, basal, and crypto are the fraction of area covered by litter, basal, and cryptogam to total area ( $m^2 m^{-2}$ ), rock is the fraction of area covered by rock to the total area ( $m^2 m^{-2}$ ), and clay and silt fraction (percent).

### 647.10 PEST model parameterization

This study employs the Model-Independent Parameter ESTimation (PEST) software (Doherty, 1994) to calibrate RHEM parameters and evaluate model performance for the 23 rainfall-runoff-erosion events at Lucky Hills 106 (LH106). The parameter calibration process included two approaches. First, the overland flow related parameters were calibrated (effective saturated hydraulic conductivity, total friction factor, and capillary drive). The slope gradient, coefficient of variation for  $K_e$ , and Interception parameters were held constant during the calibration. A detailed description of the overland flow parameters can be found in Smith et al. (1995). Second, the calibration of the splash-and-sheet soil erodibility coefficient was achieved by keeping the optimized overland flow parameters constant.

### 647.11 Statistical analysis

A. Nash-Sutcliffe Efficiency (NSE) (Nash and Sutcliffe, 1970) between observed and calculated cumulative flows was calculated for each single event at LH106 as follows:

$$NSE = 1 - \frac{\sum_{t=1}^T (O_t - M_t)^2}{\sum_{t=1}^T (O_t - \bar{O})^2} \quad (26)$$

where  $O_t$ ,  $\bar{O}$  and  $M_t$  are observed cumulative flows at time step  $t$ , average cumulative value, and modeled cumulative flows at time step  $t$ , respectively.  $T$  is the total number of time steps in the simulation for each rainfall event.

B. Moreover, percent bias (PBIAS) (Gupta et al., 1999) and the RMSE-observations standard deviation ratio (RSR) (Moriassi et. al., 2007) were calculated to evaluate the overall performance of the model for runoff volume, peak runoff, and sediment yield estimates from the 23 events at LH106.

PBIAS was calculated by

$$PBIAS = \frac{\sum_{i=1}^N (O_i - M_i) * 100}{\sum_{i=1}^N O_i} \quad (27)$$

RSR was calculated by

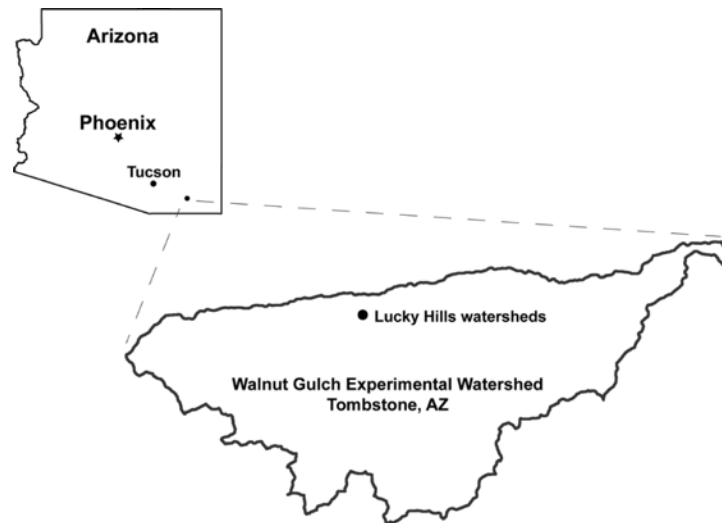
$$RSR = \frac{\sqrt{\sum_{i=1}^N (O_i - M_i)^2}}{\sqrt{\sum_{i=1}^N (O_i - \bar{O})^2}} \quad (28)$$

where  $O_i$  is the observed value of event  $i$ ,  $M_i$  is the model generated value for the corresponding event  $i$ ,  $\bar{O}$  is the average of the observed values, and  $N$  is the total number of events at LH106.

### 647.12 Study Area and NRI database – Model performance and capabilities, Lucky Hills 106 watershed

A. The data used for the calibration and evaluation of the model were obtained from the USDA-ARS Southwest Watershed Research Center's Lucky Hills experimental site, located in the Walnut Gulch Experimental Watershed (WGEW). The semiarid WGEW is located in southeastern Arizona ( $31^{\circ} 43'N$ ,  $110^{\circ} 41'W$ ) and surrounds the town of Tombstone, Arizona (figure A-1). It has a mean annual temperature of  $17.7^{\circ}C$  and a mean annual precipitation of 350 mm, the majority of which is a result of high-intensity convective thunderstorms in the summer monsoon season (Keefer et al., 2015).

**Figure A-1.** Location of the Lucky Hills subwatershed study area within the Walnut Gulch Experimental Watershed.



B. The LH106 subwatershed has an area of 0.367 hectares. The LH106 subwatershed presents an excellent location for this study because of the availability of rainfall, runoff, Time Domain Reflectometry (TDR) sensors placed at each rain gauge for estimating gravimetric soil moisture, and sediment time-series data required for model calibration at the hillslope scale. LH106 also is appropriate because it is not channelized and acts more as a large hillslope rather than a watershed with significant contribution of channel sediment (Nearing et al., 2007; Nichols et al., 2012). The slope length for the subwatershed is 65.3 m. At this scale, rainfall amount and intensity, vegetative foliar cover, ground surface cover, and micro-topography (and their spatial variability) largely determine overland flow and soil erosion processes (Lane et al., 1997). Rainfall is recorded at Rain Gauge 83 with a temporal resolution of 1 min (figure A-2). A 1m x 1m Digital Elevation Model (DEM) was prepared based on a LIDAR survey and was used to relate to micro-topography characteristics.

C. The vegetation is comprised mostly of shrubs on an 8 percent slope gradient. Dominant shrubs include Creosote (*Larrea tridentata* [Sessé and Moc. ex DC.] Coville) and Whitethorn (*Acacia constricta* Benth.). Foliar and ground cover information is given in table A-2. The soil is a Lucky Hills-McNeal sandy loam complex with approximately 52 percent sand, 26 percent silt, and 22

percent clay on a Limy Uplands (12–16” p.z.) ecological site. Rainfall and runoff data have been collected at Lucky Hills since 1963, when rain gauge 83 and weirs LH 104 and 102 were installed (figure A-2). Rain gauge 84 was added in 1964, when an H-flume was installed on LH106 in 1965 (figure A-2) to collect suspended sediment samples, in addition to the coarse load deposited in the flume during each event (Simanton et al., 1993). Since the instrumentation was installed in the early 1960s, rainfall and runoff data have been collected with only short interruptions for upgrading equipment, which occurred during the winter (Renard et al., 1980). Sediment data are prone to periodic sampling errors, so sediment data are not available for many events for which rainfall and runoff data are available (Nearing et al., 2007).

**Figure A-2.** Lucky Hills 106 and its representation as overland flow plane in the RHEM model.

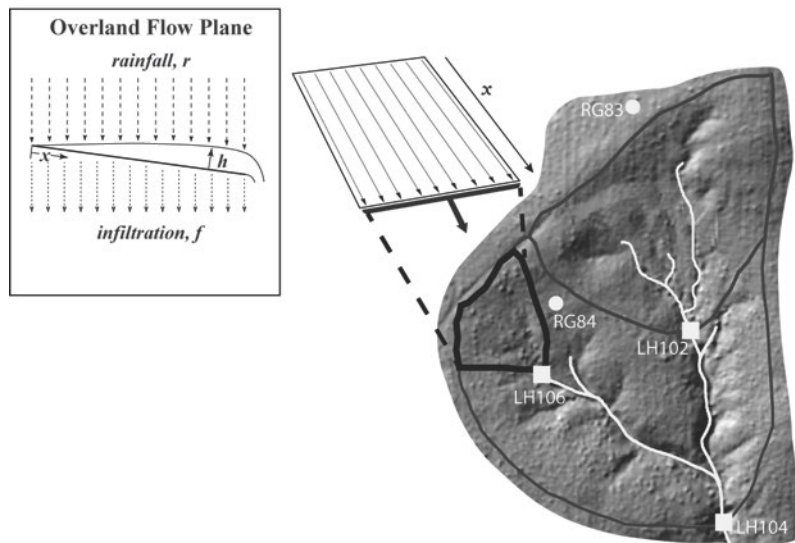


**Table A-2.** Summary of the ground surface and foliar cover for The Lucky Hills 106 subwatershed.

Ground Surface Cover	(%)	Foliar Cover	(%)
Basal	3	Bunchgrass	1
Rock	45	Forbs/Annual Grasses	2
Litter	10	Shrub	35
Cryptogams	0	Sod Grass	0
<b>Total</b>	<b>58</b>	<b>Total</b>	<b>38</b>

D. Twenty-three time-intensity data pairs were collected between 2005 and 2010 from Rain Gauge 83 as an input into the RHEM model to assess the hydrologic and erosion response of LH106 (figure A-2). Summary descriptive statistics of rainfall, observed runoff volume, observed peak runoff, and observed sediment yield are presented in table A-3.

E. Next, ground surface cover, foliar cover, basal area, cryptogams cover, litter cover, rock fragment cover, and slope gradient percent were estimated for the 124 NRI points. Figures A-3, A-4, and A-5 present the distributions for ground surface cover, foliar cover, and slope gradient grouped by annual rainfall amounts. For purposes of RHEM application, ground cover is the cover of the soil surface that essentially is in contact with the soil, as opposed to foliar cover, which is cover above the ground surface and provided by plants. Ground cover may be present in the form of plant litter, rock fragments, cryptogams, and plant bases and stems. A comprehensive review of the NRI inventory sampling strategy is presented in Goebel (1998). A review of new proposed NRI protocols on non-

federal rangelands is presented in the National Resources Inventory Handbook of Instructions for Rangeland Field Study Data Collection (USDA 2018), and a summary of NRI results on rangeland is presented in Herrick et al. (2010) and Weltz et al. (2014a).

**Table A-3.** Summary descriptive statistics of the 23 events at Lucky Hills 106.

Gauge 83	Mean	Min	Max	Std
Rainfall Volume (mm)	21.86	8.64	46.35	12.08
Runoff Volume (mm)	7.63	2.10	22.82	6.06
Peak Runoff Rate (mm h <sup>-1</sup> )	38.34	11.92	106.56	24.01
Sediment Yield (t ha <sup>-1</sup> )	0.23	0.03	0.94	0.23

**Figure A-3.** Distributions of ground surface cover grouped by the five weather stations. (a) litter cover, (b) cryptogams, (c) basal area, and (d) rock cover.

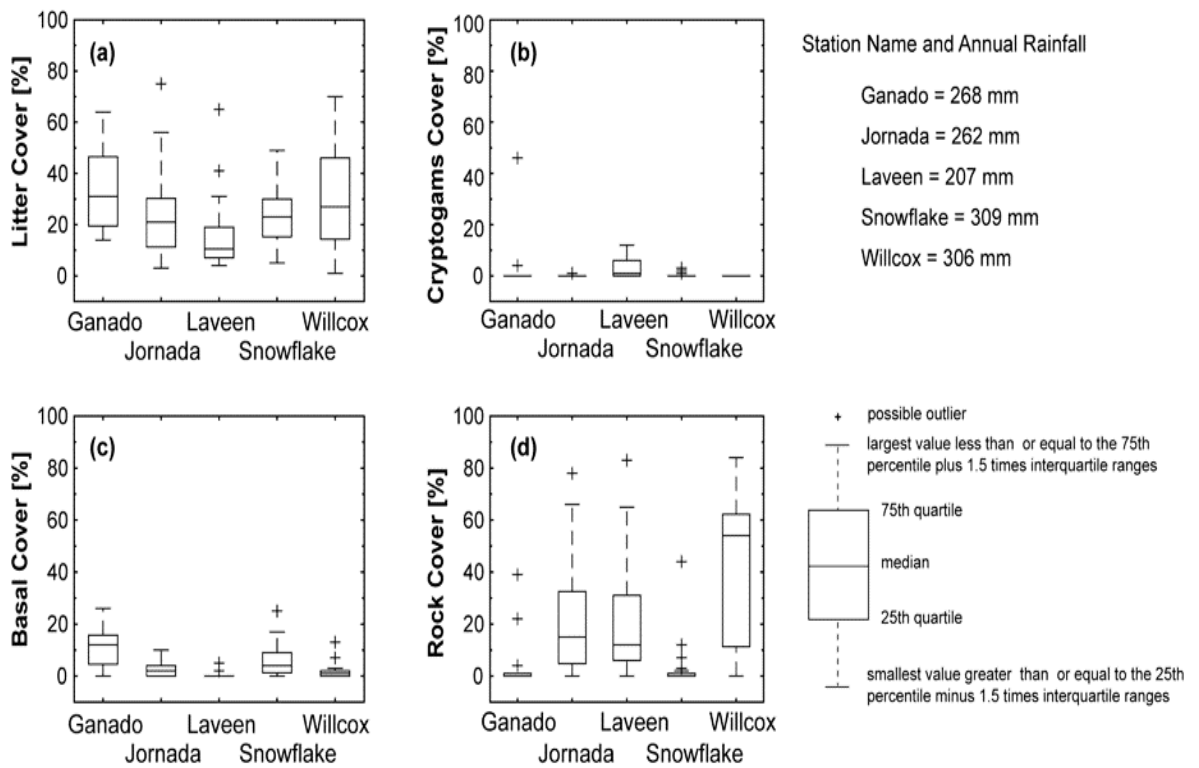


**Figure A-4.** Distributions of foliar cover grouped by the five weather stations: (a) Bunchgrass, (b) Forbs/Annual grasses, (c) Shrub, and (d) Sod grasses.

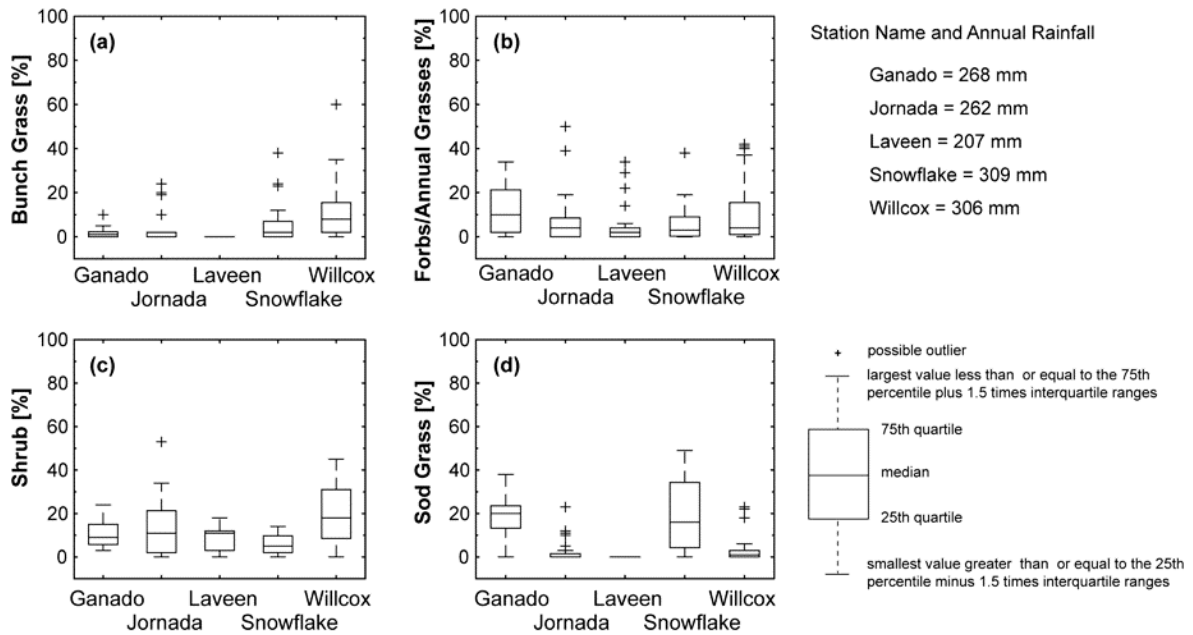
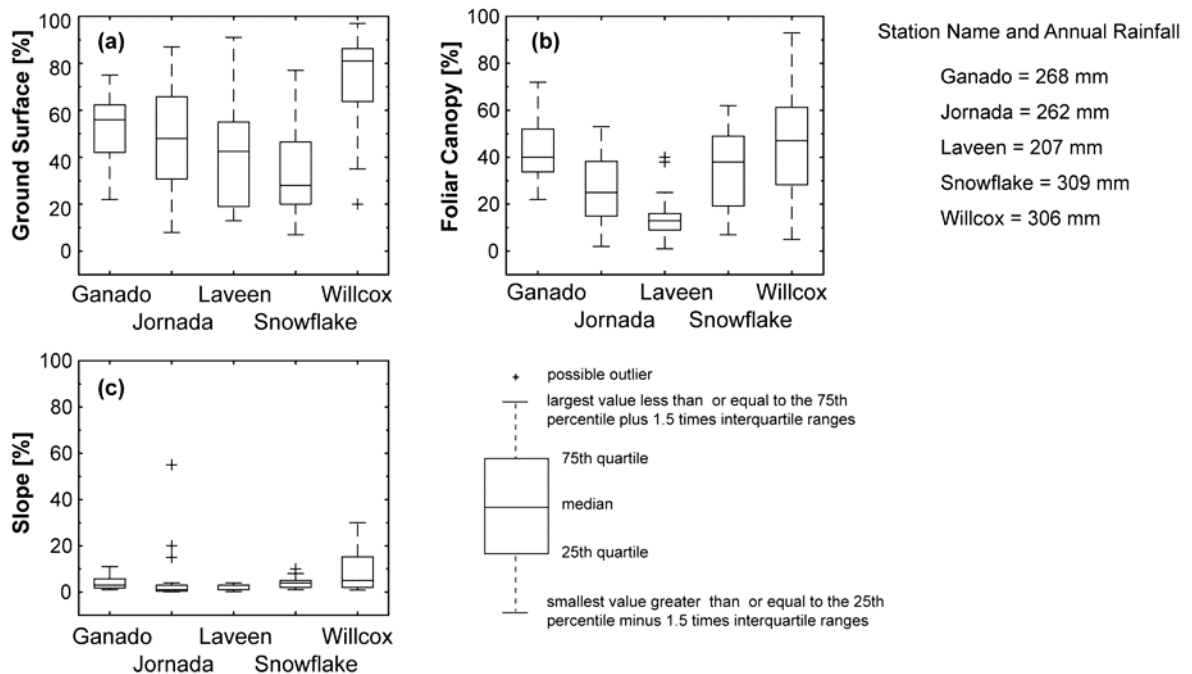


**Figure A-5.** Distributions of total ground surface cover and foliar cover grouped by the five weather stations and slope gradient for each NRI point classified based on the weather station’s radius of influence.



### 647.13 Model performance with RHEM parameter estimation equations

A. Total friction factor ( $f_t$ ), effective saturated hydraulic conductivity ( $K_e$ ), splash and sheet erodibility coefficient ( $K_{ss}$ ), and concentrated flow erodibility coefficient ( $K_o$ ) were estimated with the RHEM V2.3 empirical equations for LH106 (table A-4). We calculated  $K_o$  ( $4.37 \times 10^{-6} \text{ (s}^2 \text{ m}^{-2}\text{)}$ ) and compared to the default value ( $7.74 \times 10^{-6} \text{ (s}^2 \text{ m}^{-2}\text{)}$ ). The values are within the same order of magnitude, and the difference did not affect the output of the simulation results. Consequently, we kept the default value for this study.

B. The model performance based on the PBIAS and RSR goodness of fit criteria for runoff volume, peak runoff, and sediment yield at LH106 is shown in table A-5. Based on the model performance criteria reported by Moriasi et al. (2007), model performance based on the RSR criterion can be evaluated as “very good” if  $0 \leq \text{RSR} \leq 0.5$ , “good” if  $0.50 < \text{RSR} \leq 0.60$ , “satisfactory” if  $0.60 < \text{RSR} \leq 0.70$ , and “unsatisfactory” if  $\text{RSR} > 0.70$ . Therefore, these rankings suggest that RHEM performance can be evaluated as “very good” for runoff volume, “good” for peak runoff, and “satisfactory” for sediment yield. However, based on Moriasi et al. (2007) PBIAS criterion, the RHEM performance can be evaluated for runoff volume and peak runoff as “very good” if  $\text{PBIAS} < \pm 10$ , “good” if  $\pm 10 \leq \text{PBIAS} \leq \pm 15$ , and “satisfactory” if  $\pm 15 \leq \text{PBIAS} \leq \pm 25$ ; and for sediment yield can be evaluated as “good” if  $\pm 15 \leq \text{PBIAS} \leq \pm 30$ . These criteria suggest that RHEM can be evaluated as “very good” for runoff volume, “satisfactory” for peak runoff, and “good” for sediment yield.

**Table A-4.** RHEM parameter values estimated using the empirical equations.

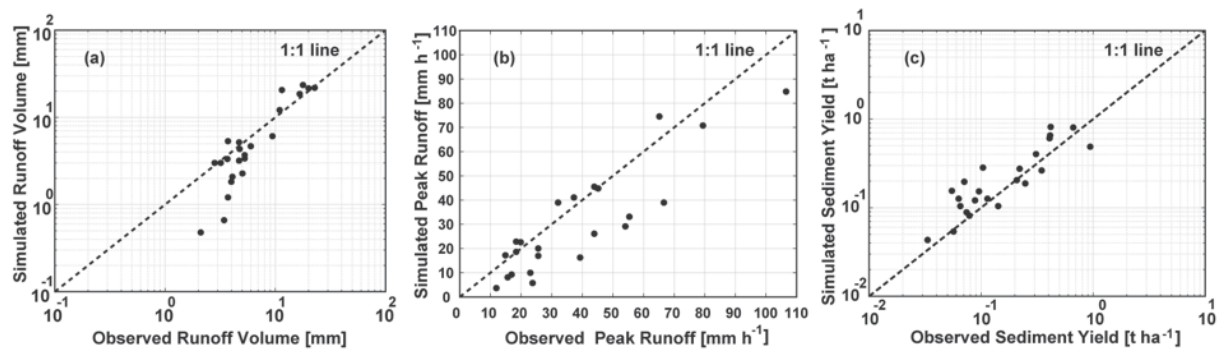
Parameters	Symbol	Units	Value
Total friction factor	$f_t$	dimensionless	5.50
Effective saturated hydraulic conductivity	$K_e$	(mm h <sup>-1</sup> )	7.29
Splash and sheet erodibility coefficient	$K_{ss}$	(kg m <sup>-3.644</sup> s <sup>0.644</sup> )	2661.22
Concentrated flow erodibility coefficient	$K_o$	(s <sup>2</sup> m <sup>-2</sup> )	$7.74 \times 10^{-6}$

**Table A-5.** Model performance statistics for Lucky Hills 106.

Evaluation criteria	Runoff Volume	Peak Runoff	Sediment Yield
RSR (dimensionless)	0.48	0.57	0.70
PBIAS (%)	2	21	-22

C. Positive PBIAS values indicate model underestimation bias, and negative values indicate overestimation bias (Gupta et al., 1999). It is apparent from figure A-6(a) that the model performance for runoff volume prediction is poor with small events and improves with large events, which is common for models (Nearing, 2000). Figure A-6(b) shows strong under-prediction of peak runoff among 14 runoff events, whereas sediment yield is in general over-predicted for the small events in figure A-6(c).

**Figure A-6.** Comparison between observed and simulated results for each rainfall-runoff event at Lucky Hills 106: (a) Runoff volume, (b) Peak runoff and (c) Sediment yield. The parameters for these simulations were based on the RHEM V2.3 parameter estimation equations.



D. In the desert southwest and central plains, rangeland vegetation has developed the ability to utilize rainfall from very small rainfall events ( $\leq 5\text{mm}$ ). Plant communities in these areas have developed mechanisms to absorb this water directly from the leaf and maintain productivity (Sala et al., 1981). This ability is an adaptive mechanism to uncertainty in precipitation in these droughty environments. Rainfall intensity is also key to understanding infiltration, runoff, and soil erosion processes. Small rainfall events result in small and dense patches of vegetation that benefit from runoff from the bare interspaces over large, more spatially separated patches. Large rainfall events benefit the larger patches to enhance runoff capture (e.g., increased soil water) over the dense vegetation patches (Magliano et al., 2015).

E. Overall, the interaction between the size, density, and connectivity of the bare interspace upslope of the vegetation patch, distance upslope, slope gradient, and rainfall intensity are the most relevant controlling factors for effectiveness of precipitation in enhancing annual net primary productivity of the vegetation patch, and thus soil erosion processes (Urgeghe et al., 2010; Urgeghe et al., 2015).

F. In rangelands it is the rare precipitation event (e.g., return period greater than 10 years) which may trigger a concentrated flow nick-point along the hillslope that can degrade the site's stability and hydrologic function by allowing water to concentrate and accelerate soil loss in concentrated flow channels and rills (Weltz et al., 2014). Since rangelands are not tilled, these flow channels and rills persist and can act to rapidly convey raindrop splash-detached sediments down the hillslope in future runoff events (Wilcox et al., 1994; Davenport et al., 1998; Urgeghe et al., 2010).

G. Protected vegetated surfaces between flow channels and rills are safe sites, resulting in minor runoff and low sediment yield from these areas (Davenport et al., 1998; Wilcox et al., 2003; Puigdefábregas 2005; Ravi et al., 2010; D'Odorinco et al., 2013; Urgeghe et al., 2015). The same landscape with uniform soil disturbance and distribution of vegetation may experience significantly more runoff and soil loss from a similar runoff event, due to increased connectivity of bare soils and formation of well-organized concentrated flow paths.

H. The RHEM V2.3 model did a good job of predicting soil erosion from the higher runoff events in comparison to RHEM V1.0. It is these high runoff and corresponding soil loss events which have the greatest impact on long-term sustainability of rangeland. RHEM V2.3 has the ability to address both undisturbed, disturbed soils, and saline and sodic soils—which is required if land managers are going to make informed decisions on how to alter current practices to enhance sustainability of rangelands. Based on the criteria for assessing goodness of fit of the model reported in table A-5 and the 1:1 line in figure A-6, it is reasonable to conclude that RHEM V2.3 worked reasonably well for the data from Lucky Hills.

### 647.14 Model calibration

A. The calibration process was carried out using PEST (section 647.10). Therefore, each calibrated parameter had a different value for different rainfall events on LH106. For most events, parameters were calibrated within eight iterations, with a maximum number of 15 iterations. NSE for cumulative runoff volume ranges from 0.85 to 0.99 with a mean of 0.96, since there are ten runoff data points and three calibrated parameters per event in the hydrology component of RHEM. The RHEM calibration produced the following average values of overland flow parameters: Total friction factor  $f_t = 3.10$  (dimensionless),  $K_e = 6.26$  (mm h<sup>-1</sup>), and net capillary drive  $C_d = 90$  (mm). The calculated parameters by the parameter estimation equations were as follows: Total friction factor  $f_t = 5.50$  (dimensionless) and  $K_e = 7.29$  (mm h<sup>-1</sup>). The calibrated net capillary drive  $C_d$  value (90 mm) was smaller than the recommended in the KINEROS2 manual (127 mm) and reported by Rawls et al. (1982) for a sandy loam soil texture class.

B. The calibration of  $K_{ss}$  for each soil erosion event using PEST was achieved as follows. Total friction factor, effective saturated hydraulic conductivity, capillary drive, and  $K_{\omega}$  remained fixed for every calibration run. For most events,  $K_{ss}$  was calibrated within three or five iterations. NSE for cumulative soil loss ranged from 0.81 to 0.96 with a mean of 0.90. The mean calibrated  $K_{ss}$  was 2,089 (m<sup>2</sup> s<sup>-2</sup>), which is lower than the value estimated by the equations proposed by Al-Hamdan et al. (2017) as reported in table A-4. The min, max, and average values for the calibrated parameters are presented in table A-6.

**Table A-6.** Minimum, maximum, and average values for the calibrated parameters.

Parameter	Min	Max	Average
$f_t$ (dimensionless)	0.96	19.62	3.10
$K_e$ (mm h <sup>-1</sup> )	1.3	12.23	6.26
$C_d$ (mm)	70	110	90
$K_{ss}$ (m <sup>2</sup> s <sup>-2</sup> )	800	6,240	2,089

### 647.15 Performance improvement from RHEM V1.0 to RHEM V2.3

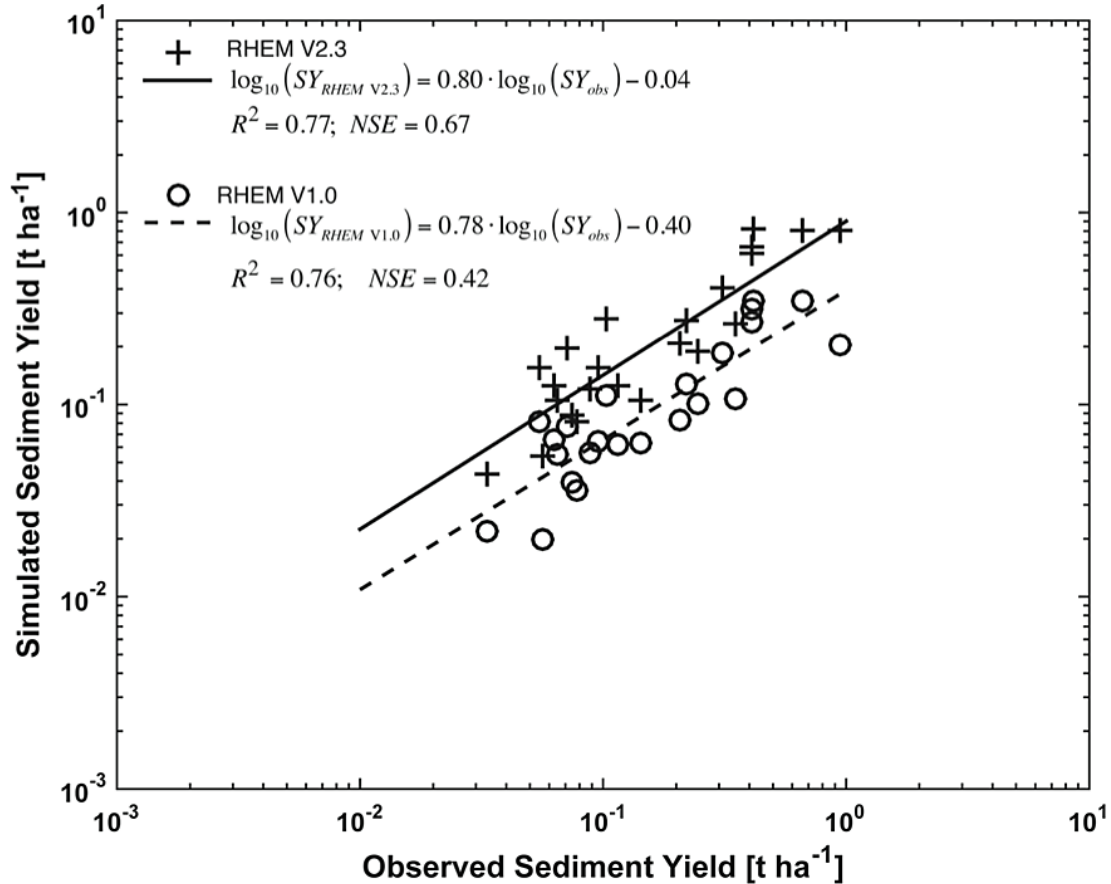
A. The improvement made in model efficiency for the Lucky Hills site was 60 percent in comparison with the previous model version, RHEM V1.0, especially with respect to low sediment yield simulation as shown in figure A-7. The system of parameter estimation equations for RHEM V1.0 was developed by Nearing et al. (2011). They used the WEPP-IRWET rangeland dataset that contains measurements of simulated rainfall, runoff, and sediment discharge and soil and plant properties on 204 plots from 49 rangeland sites distributed across 15 western states. In all studies, the rotating-boom rainfall simulator (Swanson, 1965) was used to simulate rainfall for 30 minutes at about 60 mm/hr. intensity.

B. Al-Hamdan et al. (2017) used the same WEPP-IRWET rangeland dataset for developing the new erodibility parameter equations in RHEM V2.3, but also used data for validation from independent rainfall simulation experiments conducted by the USDA-ARS Northwest Watershed Research Center, Boise, Idaho (Pierson et al., 2007, 2009, 2010, 2013; Moffet et al., 2007; Williams et al., 2014). These experiments were conducted using a Colorado State University type rainfall simulator (Holland, 1969), consisting of multiple stationary sprinklers elevated 3.05 m above the ground surface (Pierson et al., 2007, 2009, 2010, 2013).

C. As a comparison, we followed the procedure outlined in Nearing et al. (2011b) for estimating RHEM V1.0 parameter values for LH106. The computed effective saturated hydraulic conductivity and the splash and sheet erodibility coefficient are as follow:  $K_e = 4.76$  mm hr<sup>-1</sup> and  $K_{ss} = 1096$  (kg m<sup>-3.644</sup> s<sup>0.644</sup>), respectively. The RHEM V2.3 effective saturated hydraulic conductivity value is 1.5 times

greater than the RHEM V1.0. However, the RHEM V1.0  $K_{ss}$  value is 2.5 time smaller than the RHEM V2.3:  $K_{ss} = 2661 \text{ (kg m}^{-3.644} \text{ s}^{0.644}\text{)}$ .

**Figure A-7.** Performance improvement on the 23 LH106 sediment yield events by both RHEM V2.3 and RHEM V1.0 models according to the NSE criterion.



D. Al-Hamdan et al. (2017) employed piecewise (segmented) regression analysis where two continuous relationships between the log-transformed erodibility and the independent variables were fitted to improve the linear relationship. The piecewise regression analysis revealed that the best two-piece regression occurs when ground cover of 0.475 is the break point (see Eqs.19-22). That is, the value of 0.475 is in agreement with several studies which concluded that the erosion to runoff ratio (erodibility) increases substantially when bare ground exceeds 50 percent (e.g., Al-Hamdan et al., 2013; Pierson et al., 2013; Weltz et al., 1998).

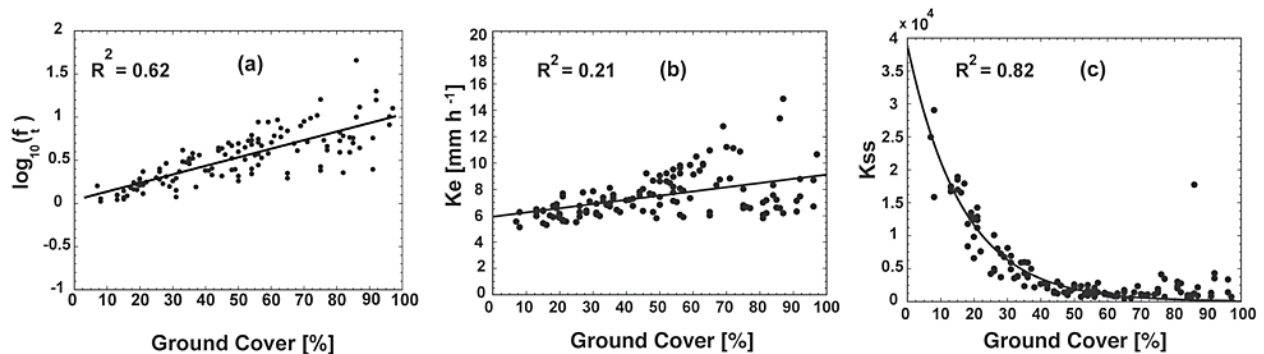
E. The reasonable performance of the RHEM V2.3 model with the new parameterization schemes shown in figure A-7 indicates that using  $K_{ss}$  alone, as the indicator of erodibility factor in RHEM, works reasonably well for this case.

### 647.16 Model application using NRI data

A. This section reports a case study of application of the model on a number of sites to assess the simulated effects of ground cover on total friction factor ( $f_t$ ), effective saturated hydraulic conductivity ( $K_e$ ), and splash and sheet erodibility factor ( $K_{ss}$ ) estimated using the parameter estimation equations, as well as the effect of foliar cover and ground cover on sediment yield.

B. To investigate these effects, we applied the model to the 124 NRI points (Hernandez et al., 2013). The RHEM V2.3 model was run for a 300-year synthetic rainfall sequence generated by CLIGEN V5.3 (Nicks et al., 1995) based on the statistics of historic rainfall at each climate station. This is the default setup for running RHEM within the user interface. The associations between ground cover and  $\log_{10}(f_t)$ ,  $K_e$ , and  $K_{ss}$  are shown in figure A-8. They provide a basis for evaluating the behavior of the parameter estimation equations. That is,  $\log_{10}(f_t)$  increased with increasing ground cover as shown in figure A-8(a), the strong positive correlation coefficient ( $r = 0.79$ ,  $p < 0.05$ ), suggesting that the parameter estimation equation to predict total friction roughness was not affected by outliers or small departures from model assumptions. For example, a slope gradient of 55 percent was reported in one NRI plot as shown in figure A-5(c). Similarly, we expected that  $K_e$  would increase with increased litter cover and basal area cover as shown in figure A-8(b). Although the spread of  $K_e$  around 80 percent ground cover, with the moderate correlation coefficient ( $r = 0.46$ ,  $p < 0.05$ ), suggests that the parameter estimation equation for predicting  $K_e$  for a sandy loam soil texture class was not affected by small departures from model assumptions.

**Figure A-8.** The association between ground cover and total friction factor ( $f_t$ ), effective saturated hydraulic conductivity ( $K_e$ ), and splash and sheet erodibility coefficient ( $K_{ss}$ ): (a) strong positive linear correlation between ground cover and  $\log_{10}(f_t)$ , (b) moderate linear correlation between ground cover and  $K_e$ , and (c) strong Spearman rank correlation coefficient between ground cover and  $K_{ss}$ .



C. The rate of rapidly increasing  $K_{ss}$  starts at about 45 percent ground cover. This threshold value is consistent with several studies that concluded that ground cover should be maintained above a critical threshold of ~50–60 percent to protect the soil surface adequately (Gifford's, 1985; and Wertz et al., 1998). A strong negative Spearman correlation coefficient ( $\rho = -0.71$ ,  $p < 0.05$ ) and a decaying exponential model ( $R^2 = 0.82$ ,  $p < 0.05$ ) fitted to the data shown in figure A-8(c) confirm the expected decreasing monotonic trend between ground cover and  $K_{ss}$ . The NRI point with 55 percent slope gradient also did not appear to cause an adverse effect on the correlation coefficient and fitted decaying exponential model.

D. Given that vegetation contributes much to the hydrologic and hydraulic properties of the surface, it is logical to account for the vegetation in the surface runoff process. To investigate the influence of litter and basal cover on percent runoff, defined as the ratio of runoff to precipitation, we found a strong negative linear correlation with litter ( $r = -0.70$ ,  $p < 0.05$ ) as depicted in figure A-9(a). Furthermore, two distinct patterns of percent runoff emerged as a function of annual rainfall amount observed at the Ganado and Willcox weather stations. That is, both weather stations' area of influence had similar average amounts of litter cover percent (Ganado: mean = 34 percent and Willcox: mean = 31 percent), but distinct annual rainfall regimes (Ganado: 268 mm and Willcox: 306 mm). Furthermore, the Ganado's area of influence is characterized by sod grasses (mean = 19 percent) and forb/annual grasses (mean = 12 percent), and the Willcox's area is characterized by a combination of shrub (mean = 19 percent), bunchgrasses (12 percent), and forb/annual grasses (mean = 11 percent). The Laveen weather station has the lowest annual rainfall amount (207mm) and the lowest litter cover

percent (16 percent), and it is mainly shrub-forb/annual grasses-dominated (mean = 9 percent and mean = 6 percent, respectively).

E. To investigate the influence of basal cover on percent runoff, we found a moderate negative relationship depicted in figure A-9(b). Although no patterns emerged in this relation, the model was able to capture the influence of basal dynamics by showing a negative trend. Transport capacity increases as flow rate and slope steepness increase. The parameter estimation equations for calculating concentrated flow width, hydraulic roughness, and splash and sheet erodibility depend on the geometry of the upland area as described by the surface slope steepness. Figure A-10 shows the graph of annual sediment yield versus slope steepness for the 124 NRI points.

**Figure A-9.** Runoff as a percent of precipitation showing the negative relationship with (a) litter cover percent and (b) basal cover percent.

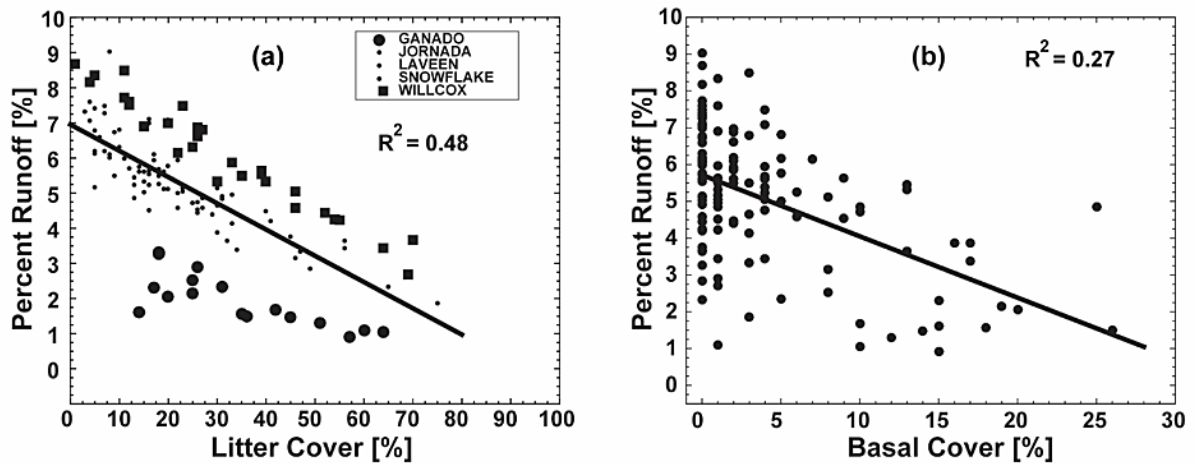
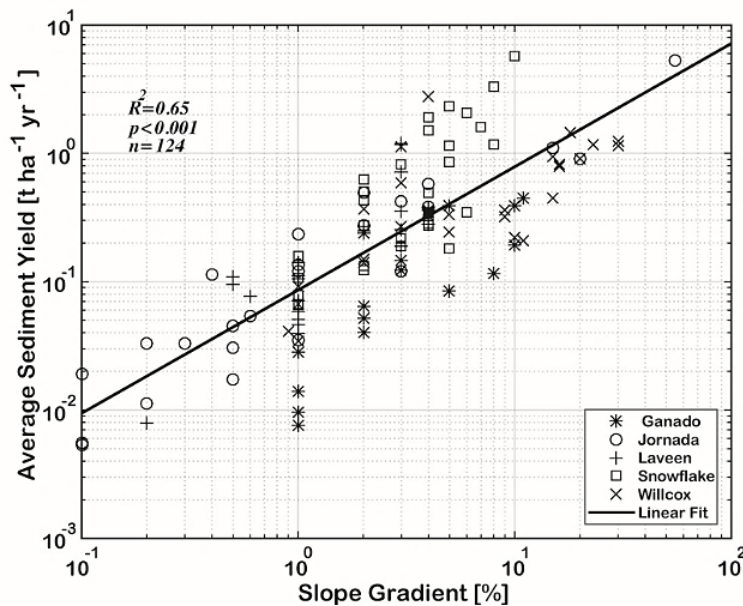


**Figure A-10.** Relationship between average annual sediment yield and slope gradient for the 124 NRI points affected by five precipitation regimes.



F. They are strongly correlated ( $R^2 = 0.65$ ;  $p < 0.001$ ) with a large variability around the 1 percent and 3 percent slope gradient interval. Sixty percent of the points fall within this percent interval. The

variability represented by the coefficient of variation (CV) in slope gradient, litter, rock, and annual sediment yield for the five rainfall regimes is reported in table A.7. The variability in rock cover on the Ganado, Jornada Experimental Range, Laveen, and Snowflake weather stations and slope gradient on the Jornada Experimental Range contribute to some extent to the large variability in annual sediment yield. Moreover, a coefficient of variation less than one is considered to be low-variance. Consequently, the variability in simulated sediment yield was less affected by the dispersion in litter cover and slope gradient, except for the Jornada Experimental Range.

**Table A-7.** Variation of mean and CV (Coefficient of Variation) in slope steepness, litter, rock and annual sediment yield for the 124 NRI points.

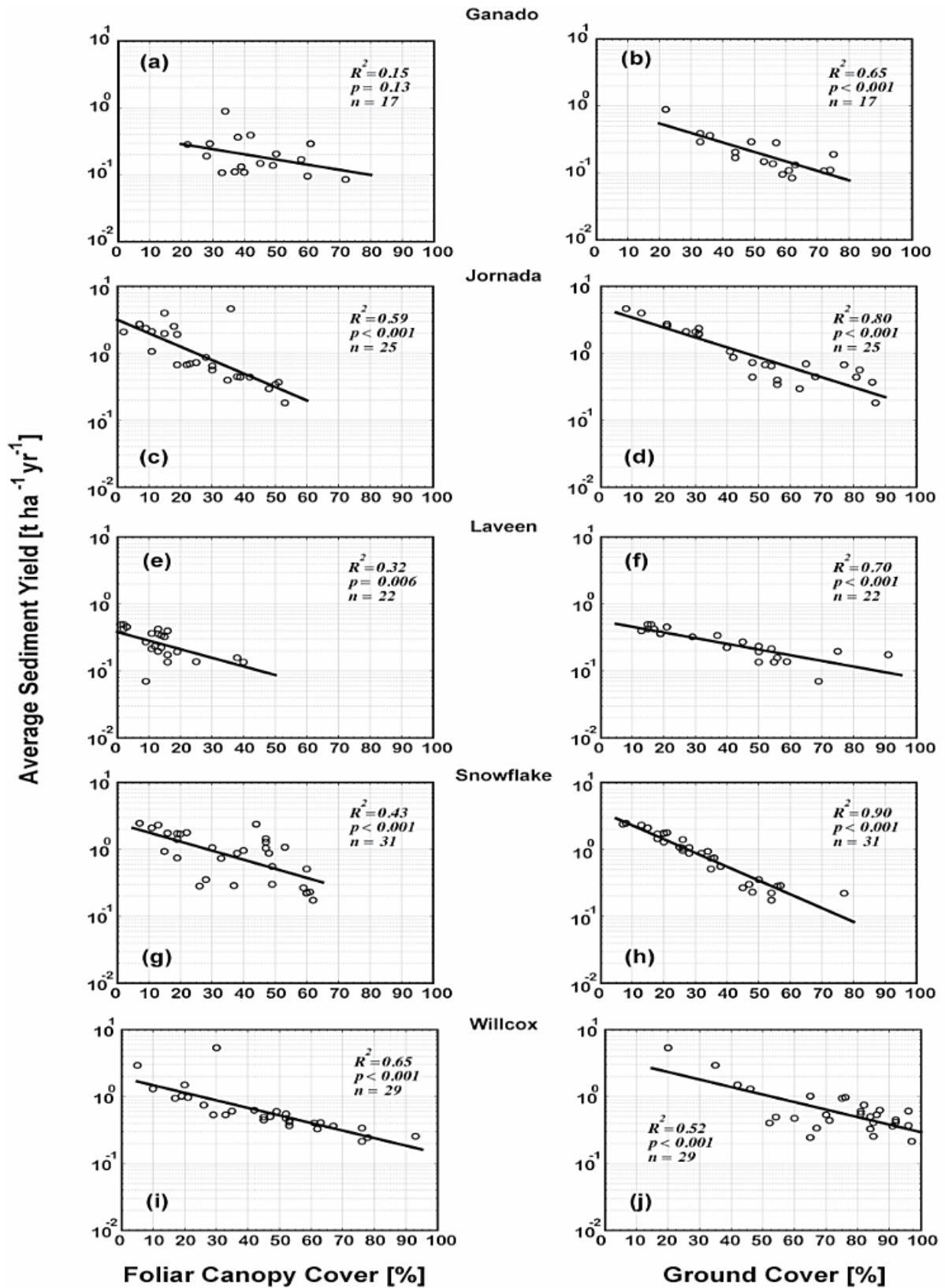
Weather Station	n	PPT (mm)	Slope: Mean (%)	Slope: CV	Litter: Mean (%)	Litter: CV	Rock: Rock: Mean (%)	Rock: CV	Annual Sediment Yield: Mean (t ha <sup>-1</sup> )	Annual Sediment Yield: CV
Ganado	17	268	4.18	0.83	34.35	0.47	3.94	2.66	0.16	0.95
Jornada Exp Range	25	262	4.64	2.48	23.96	0.73	22.64	1.06	0.42	2.51
Laveen	22	207	1.81	0.67	16.00	0.91	21.18	1.01	0.27	1.24
Snowflake	31	309	3.74	0.63	24.00	0.49	2.35	3.45	0.88	1.36
Willcox	29	306	9.10	0.96	31.45	0.62	39.97	0.73	0.59	1.01

Since the variability in sediment yield for each precipitation regime was large, sediment yield was normalized to fit a single equation to the sediment yield, foliar cover, and ground cover data from each precipitation regime. The mean slope gradient percent of NRI points within each precipitation regime represented by the five weather stations shown in table A-7 was selected for the normalization. The results are shown in figure A-11.

G. We estimated the correlation coefficient to measure the strength of association between average annual sediment yield and the foliar cover and ground cover variables, grouped by weather stations.

H. The strength of the association between average annual sediment yield and foliar and ground cover is moderate to strong. The correlation coefficient varied from -0.39 to -0.81 and -0.72 to -0.95 for foliar and ground cover, respectively. When shrub is the dominant plant form, the relationship between sediment yield and foliar cover is the strongest as shown in figures A.11(c) and A.11(i). Conversely, the weakest relationship between sediment yield and foliar cover appears to be when sod or forbs are the dominant plant forms as indicated in figures A.11(a), A.11(e), and A.11(g). The area covered by the Ganado weather station has the fewest number of NRI points (n = 17) and is dominated by forbs/annual grasses and sod grasses. The low number of NRI points and the high variability in these grasses, as shown in figures A.4(b) and A.4(d), can be attributed to the fact that only 15 percent of the variability between the annual sediment yield and foliar cover can be accounted for. When litter and rock cover are the most dominant variables, the association between average annual sediment yield and ground cover is very strong, as indicated in figures A.11(b), A.11(d), A.11(f), A.11(h), and A.11(j). These results suggest that low yearly sediment yield, in general, is not well described by foliar cover. We found that the association is stronger with ground cover than with foliar cover, which is expected (e.g., Nearing et al., 2005). The results suggest that ground cover, in general, is more highly associated with yearly sediment yield than is foliar cover.

**Figure A-11.** Association between predicted average sediment yield and foliar cover and ground cover for the five precipitation regimes.



### 647.17 Parameter estimation equations for saline and sodic soils

A. Data were collected in a broader study at nine experimental sites to develop new parameter estimation equations for RHEM V2.3 to predict soil erosion, runoff quantity and quality on the saline/sodic soils of the Upper Colorado River Basin (Cadaret et al., 2016a, b; Nouwakpo et al., 2017; McGwire et al., 2020). Six plots were selected from each experimental site for a total of 36 plots to calibrate RHEM for saline sites, ensuring that each intensity simulated at the site was represented at least once in the calibration dataset. The calibration was performed in two steps to determine best parameter sets for runoff prediction and soil loss prediction. The numerical optimization was performed using a Markov Chain Monte Carlo (MCMC) method implemented in SPOTPY (Houska et al., 2015), a model optimization tool written in the Python programming language.

B. To optimize runoff prediction, the following RHEM parameters were adjusted for each plot: soil saturation ratio (SAT), effective hydraulic conductivity ( $K_e$ , mm/hr), mean capillary drive ( $G$ , mm), variable (ALF) in the Smith-Parlange infiltration equation, and the coefficient of variability (CV) of the hydraulic conductivity. These parameters were estimated in a multi-objective optimization scheme, in which errors in both total runoff SR (L) and one-min-increment instantaneous discharges  $q_t$  (mm/hr) were minimized throughout the rainfall event. Instantaneous discharges used as observations were interpolated from observed discharges that may not systematically occur at exactly one min time increments and were compared to predicted discharges at the same time increments. This multi-objective optimization procedure allowed the estimation of parameters that adequately predicted SR while matching as closely as possible the detailed hydrograph of a rainfall event.

C. For erosion prediction, the sheet and splash erodibility  $K_{ss}$  was estimated using a separate multi-objective parameter optimization in which errors in total soil loss SL ( $K_g$ ) and one-min-increment instantaneous sediment discharge rates  $q_{st}$  (g/s) were minimized. For both runoff and soil erosion parameter estimations, the final selection of parameters was done for each calibration plot by choosing the set of parameters that simultaneously minimized the error in cumulative runoff and total soil loss (SR and SL) and belonged to the five percent best performers in matching the detailed hydrograph and sedograph. A total of 36 parameter sets were produced, corresponding to the 36 calibration events.

D. Parameter estimation equations have been developed for RHEM to translate soil biophysical characteristics into hydrology and hydraulics parameters. Currently, equations exist to estimate  $K_e$ ,  $K_{ss}$ , and the Darcy Weisbach friction factor ( $F$ ) from equations using ground and vegetation cover information as well as soil texture. For  $K_e$  and  $K_{ss}$ , current RHEM equations are:

$$K_e = a^{(b \cdot (\text{basal} + \text{litter}))} \quad (27)$$

$$K_{ss} = 10^{(c+d \cdot \text{GroundCover} + f \cdot \text{FoliarCover} + g \cdot \text{Slope})} \quad (28)$$

where coefficients  $a$  and  $b$  differ as a function of soil texture and vegetation community type (i.e., shrub, sod grass, bunchgrass and forbs, and annual grass), while coefficients  $c$ ,  $d$ ,  $f$ , and  $g$  are functions of vegetation community type and ground cover. Basal, litter, ground cover, and foliar cover are expressed as a real fraction. Basal cover represents the proportion of the soil surface that is in contact with the bases of plants. Litter cover is the proportion of the soil surface protected by detached vegetation residues. Ground cover is the sum of basal, litter, rock, and cryptogam cover. Foliar cover is the fraction of the land surface that is occupied by the projection of plant leaves onto the soil surface. As cover decreases, erosion will increase (figure A-12). Parameters  $a$ ,  $b$ ,  $c$ ,  $d$ ,  $f$ , and  $g$  were developed from a large dataset (more than 200 plots) of rainfall simulation experiments across the Western United States and represent a wide range of rangeland ecosystem types and conditions.

**Figure A-12.** Research sites near Farmington, New Mexico (left) and Moab, Utah (right) showing naturally occurring erosive conditions due to geologic formation and parent materials, steep slopes, and minimal vegetation that facilitate high salt load transport capacities. No known vegetation management practices are available to reduce soil erosion and salt transport under these naturally occurring conditions. Salt loads can be exacerbated if sites are disturbed through off road activities such as from vehicles and bikes.



E. In this study,  $K_e$  and  $K_{ss}$  values were optimized using the MCMC routine ( $K_{eOpt}$  and  $K_{ssOpt}$ ) and were compared to the values ( $K_{eRHEM}$ ,  $K_{ssRHEM}$ ) predicted by the current version of RHEM for the calibration plots. Differences ( $\Delta K_e$ ,  $\Delta K_{ss}$ ) and ratios ( $rK_e$ ,  $rK_{ss}$ ) between optimized and RHEM-predicted values were calculated and related to soil biophysical characteristics and salinity. Linear regressions were performed between  $\Delta K_e$ ,  $\Delta K_{ss}$ ,  $rK_e$  and  $rK_{ss}$  and canopy cover, fraction of bare ground, sodium adsorption ratio (SAR), electrical conductivity (EC), silt content, and slope. With a total of 36 calibration data points for this analysis, each explained variable was regressed against one explanatory variable at a time to prevent over-parameterization and maintain adequate statistical power.

F. From the linear regressions linking soil and vegetation attributes to  $K_e$  and  $K_{ss}$  differences and ratios, factors accounting for the gap between RHEM-predicted and optimized  $K_e$  and  $K_{ss}$  values were identified by selecting those exhibiting statistically significant effects on  $\Delta K_e$ ,  $rK_e$ ,  $\Delta K_{ss}$  and  $rK_{ss}$ . Factors with statistically significant effects were then evaluated against current terms used in RHEM parameter estimation equations (Eq. 29 and 30). Factors with statistically significant effects that were already present in Eq. 29 and 30 suggest a modification of coefficients applied to these terms in these equations. Factors not previously accounted for in Eq. 27 and 28 are introduced as new terms according to the nature of their relationships with RHEM-predicted parameters. In the case of statistical significance of a factor in the parameter differences  $\Delta K_e$  and  $\Delta K_{ss}$ , the new parameter  $K_n$  is calculated as:

$$K_n + K_n RHEM + (AX + B) \quad (29)$$

where X is one of the factors of canopy cover, bare ground, SAR, EC, silt content and slope, and A and B are significant coefficients of the linear regression where these factors have a significant effect.

G. Likewise, when the ratios  $rK_e$  and  $rK_{ss}$  exhibit a significant effect of a given parameter,  $K_n$  is defined as:

$$K_n = K_n RHEM + (AX + B) \quad (30)$$

H. When more than one factor was found to have a statistically significant effect on a parameter  $K_n$ , the final correction equation retained was sequentially developed by first incorporating the factor with

the highest  $R^2$  and then re-computing  $\Delta K_n$  or  $rK_n$  values and relating these values to the subsequent factors to verify that any statistically significant effect remained. For example, if bare ground has a statistically significant effect on  $\Delta K_e$ , and EC has a significant effect on  $rK_e$  with  $R^2$  bare ground >  $R^2$  EC, then  $K_e$  would be corrected for bare ground first,  $K_{e,bare} = K_e RHEM + (A \times Bare + B)$ . Then  $rK_e$  would be recalculated as  $K_{e,Opt}/K_{e,bare}$ , and this new variable re-evaluated against EC to see if the initial statistical significance remains.

### 647.18 Performance evaluation for salinity adjustments

A. The performance of the adjusted parameter estimation equations (Eq. 29 and 30) was assessed by comparing erosion and runoff predictions with the amended parameters  $K_n$  to those obtained with Eq. 27 and 28. Model performance metrics used for this comparison are the coefficient of determination  $R^2$ , the Nash- Sutcliffe Efficiency, NSE, and the percent bias, pbias.

$$R^2 = 1 - \frac{\sum_{i=1}^n (Y_{lm,i} - Y_{o,i})^2}{\sum_{i=1}^n (Y_{o,i} - \bar{Y}_o)^2} \quad (31)$$

$$NSE = 1 - \frac{\sum_{i=1}^n (Y_{p,i} - Y_{o,i})^2}{\sum_{i=1}^n (Y_{o,i} - \bar{Y}_o)^2} \quad (32)$$

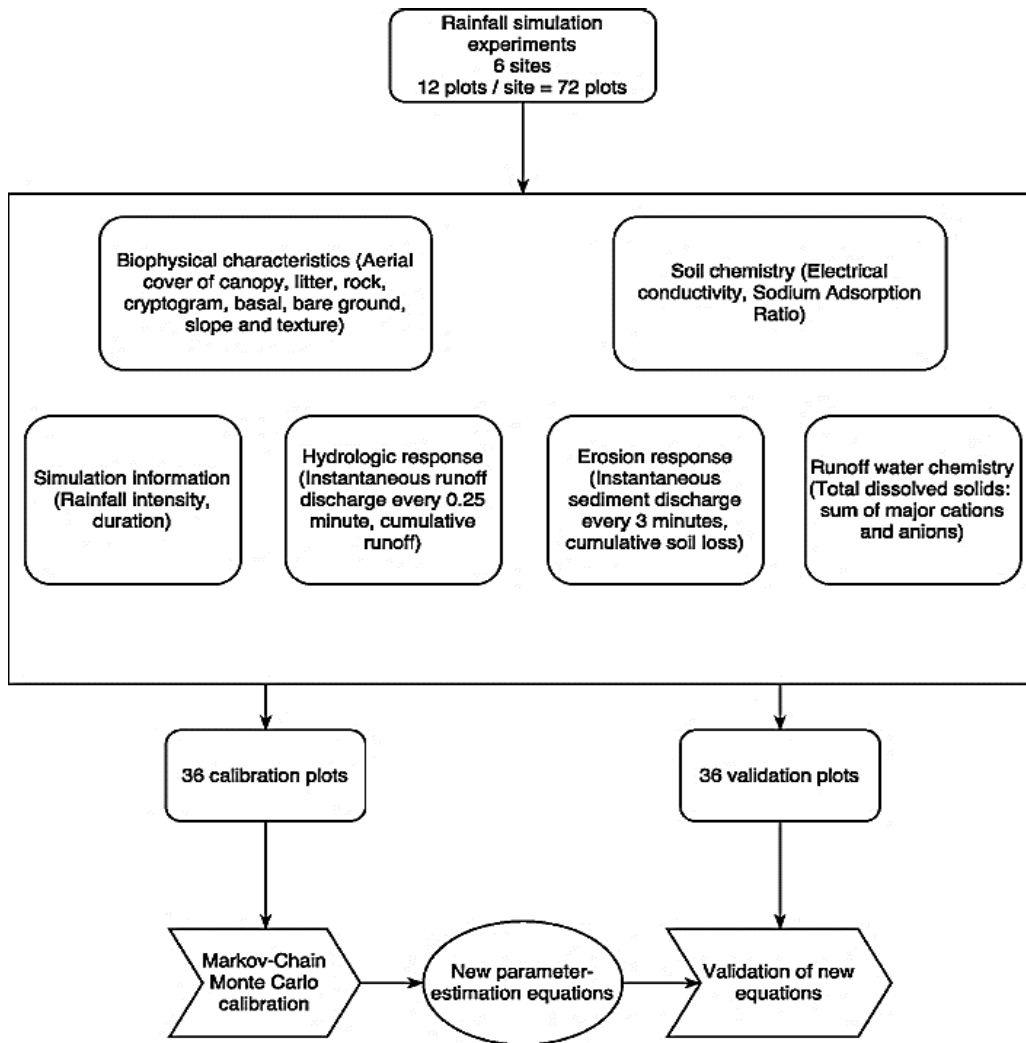
$$pbias = \left[ \frac{\sum_{i=1}^n (Y_{p,i} - Y_{o,i}) \times 100}{\sum_{i=1}^n Y_{o,i}} \right] \quad (33)$$

where  $Y_o$ ,  $Y_p$ , and  $Y_{lm}$  are respectively the observed, RHEM-predicted, and linear model prediction between  $Y_o$  and  $Y_p$  for runoff or soil loss, while  $\bar{Y}_o$  is the average of all observations.

B. These performance metrics were calculated for the 36 calibration data points and the 36 validation data points. The linear model for salt load prediction was also evaluated with these performance metrics.

C. Figure A-13 shows a flowchart diagram of the experimental data, describes its content, and graphically illustrates how it was used to develop and test the new parameter-estimation equations. Additionally, Welch's t-test was used to compare validation and calibration data to ensure equal means of input parameters between these two populations. Statistical analyses were conducted in R (R Core Team 2018), and a probability of 0.05 was used as the threshold of statistical significance.

**Figure A-13.** Flowchart diagram of the experimental data utilized for the development and validation of new parameter-estimation equations on saline sites.



### 647.19 Results of salinity adjustments

A. Figures A-14 and A-15 show the results of the runoff and soil loss prediction on the 36 calibration data points, using Eq. 27 and 28 to estimate  $K_e$  and  $K_{ss}$ . NSE and  $R^2$  for runoff were respectively 0.56 and 0.68, suggesting that relationships between soil biophysical properties and  $K_e$  represented in Eq. 27 were roughly consistent with observed patterns in runoff and infiltration at the experimental sites. Eq. 34 under-predicted  $K_e$ , resulting in a positive bias in predicted cumulative runoff depths (predicted runoff > observed runoff, PBIAS = 32.03 percent). Soil loss was predicted with an NSE of 0.81 and an  $R^2$  of 0.85, with a negative bias (PBIAS = -6.47 percent). This negative bias in soil loss prediction contrasts with the positive bias in runoff noted in figure A-14, which indicates an under-prediction of soil erodibility.

**Figure A-14.** Observed vs. predicted runoff on 36 rainfall simulation calibration plots using current RHEM parameter estimation equations.

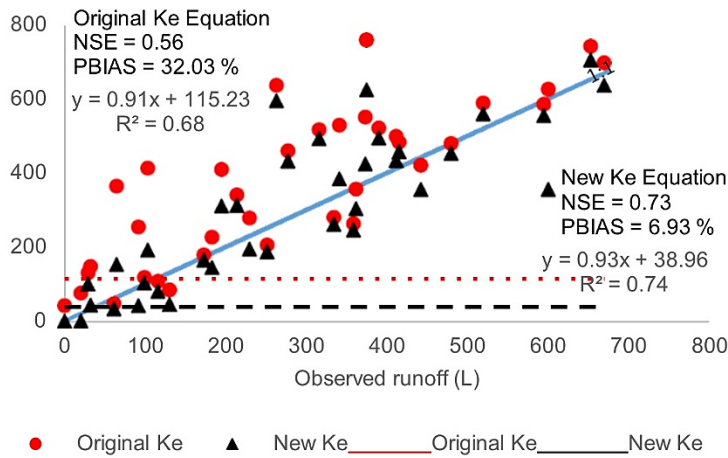
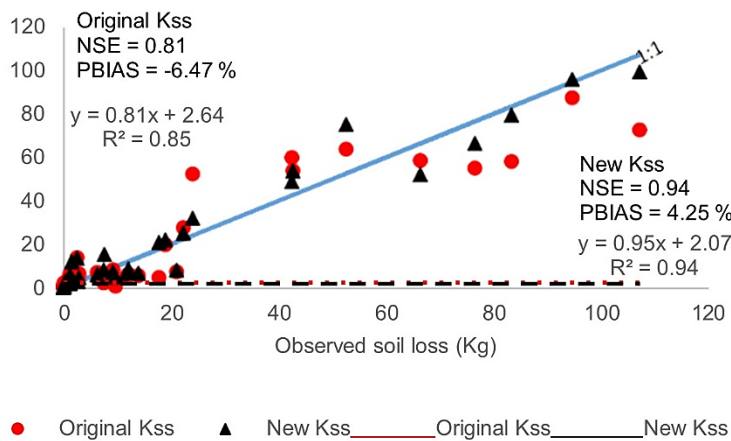


**Figure A-15.** Observed vs. predicted soil loss on 36 rainfall simulation calibration plots using current RHEM parameter estimation equations.



B. The new equation for  $K_e$  developed from this dataset for saline sites was:

$$K_e = a^{(1.554b(\text{basal} + \text{litter}))} \tag{34}$$

Performance of Eq. 34 on the calibration data was better overall than that of the additive correction model for bare ground with  $NSE = 0.73$ ,  $PBIAS = 6.93$  percent and  $R^2 = 0.74$ .

C. Differences and ratios between optimized and RHEM-predicted  $K_{ss}$  values show significant effects of only SAR.  $\Delta K_{ss}$  and SAR are related through a positive relationship ( $R^2 = 0.26$ ,  $p = 0.002$ ), while  $rK_{ss}$  relates to SAR with much less predictability ( $R^2 = 0.13$ ,  $p = 0.042$ ). Correcting RHEM  $K_{ss}$  values for SAR with both additive (Eq. 29) and multiplicative (Eq. 30) models resulted in an improvement of NSE (0.94 and 0.89 vs 0.81) and  $R^2$  (0.94 and 0.93 vs. 0.85) of soil loss prediction compared to the current RHEM  $K_{ss}$  estimation equation. While the bias achieved with the additive model ( $PBIAS = 4.25$  percent) matched that achieved with Eq. 28, a greater bias was noted when the multiplicative model was used for the  $K_{ss}$  correction ( $PBIAS = 17.18$  percent). The additive model was then retained to adjust  $K_{ss}$  for SAR.

D. Figures A-16 and A-17 show the result of the runoff and soil loss prediction with the new  $K_e$  and  $K_{ss}$  equations on the 36 validation plots.  $K_e$  values estimated with equation 34 predicted runoff on the

36 validation plots with slightly improved NSE (0.88) and  $R^2$  (0.89) over the original RHEM equation Eq. 27 (NSE = 0.83 and  $R^2 = 0.85$ ). The runoff prediction bias was substantially improved on these validation plots, dropping from PBIAS = 12.05 percent with Eq. 27 to PBIAS = 5.41 percent when the newly developed Eq. 34 was used.

**Figure A-16.** Observed vs. predicted runoff on the 36 validation data points using the current and the newly developed estimation equation for the hydraulic conductivity  $K_c$ .

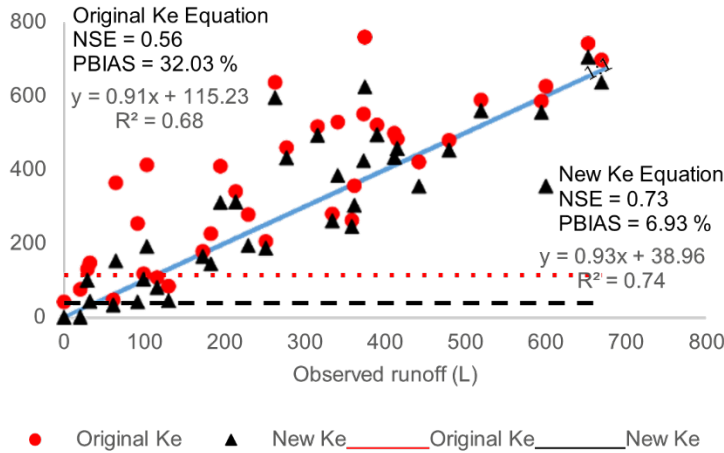
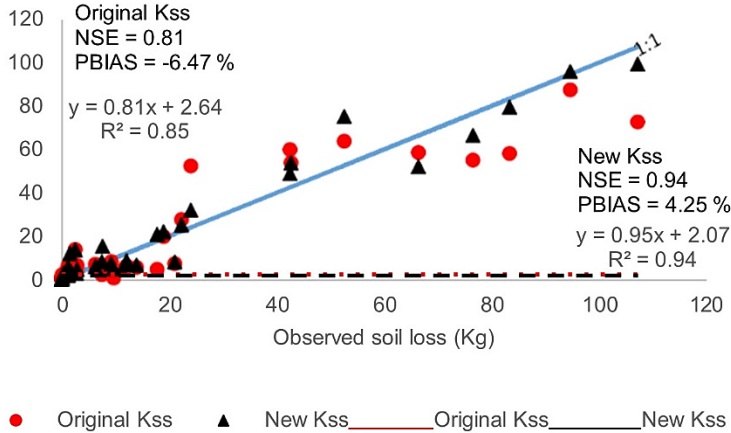


**Figure A-17.** Observed vs. predicted soil loss on the 36 validation data points using the current and the newly developed estimation equation for the sheet and splash erodibility  $K_{ss}$ .



E. The sheet and splash erodibility  $K_{ss}$  were reasonably predicted on the validation data when SAR was added to the  $K_{ss}$  prediction. Compared to the original  $K_{ss}$  equation, the use of the SAR-adjusted  $K_{ss}$  equation improved soil loss prediction from NSE = 0.38,  $R^2 = 0.6$  and PBIAS = -24.25 to NSE = 0.69,  $R^2 = 0.73$  and PBIAS = -3.82 percent. Nevertheless, validation NSE (0.69) and  $R^2$  (0.73) declined compared to the calibration performance (NSE = 0.94 and  $R^2 = 0.94$ ) due to increased error propagation from runoff prediction to soil loss estimates in the validation data. In effect, calibrated  $K_c$  values were used in the estimation of soil loss for evaluating  $K_{ss}$  on the calibration data, while estimates of  $K_c$  from Eq. 34 were used for the validation data. The percent bias of the additive  $K_{ss}$  model was maintained within the same order of magnitude across calibration and validation data (PBIAS = 4.25 percent for the calibration data and -3.82 percent for the validation).

F. The relationship between soil loss and total dissolved solids is shown in figure A-18. The linear model was adequate to predict runoff chemistry from its sediment concentration ( $R^2 = 0.94$ ). TDS was related to SL through a positive relationship. Based on the equation of the linear model in figure A-18, a 1 Kg change in total soil loss results in a 2.36 g change in TDS ( $p = 0.00$ ). In other words, the average salt to sediment mass ratio of the runoff was  $2.36 \times 10^{-3}$  g/g, or 0.24 percent. The non-zero intercept of the linear model was not statistically significant. The equation used for predicting TDS from soil loss was therefore:

$$TDS = 2.36 \times SL + 0.99 \quad (35)$$

G. Figure A-18 shows that Eq. 35 performed well at predicting TDS when RHEM-predicted SL values were used on the calibration data (figure A-19a) and the validation data (figure A-19b). The improvement in soil loss prediction gained with the use of newly developed saline equations was reflected on TDS predictions as well. On the calibration data, NSE and  $R^2$  improved from 0.75 and 0.83 with the original  $K_e$  and  $K_{ss}$  equations to 0.90 and 0.91 with the saline equations developed from this work (figure A-18). PBIAS on the calibration was overall low but showed a mild improvement from -6.34 percent to 4.16 percent. On the validation data, a more dramatic improvement was noted on the NSE which increased from 0.43 with the original  $K_e$  and  $K_{ss}$  equations to 0.83 with the saline equations.  $R^2$  improved from 0.51 to 0.61 while PBIAS degraded from -6.29 percent to 23.18 percent. Soil loss predicted with the new  $K_e$  and  $K_{ss}$  equations underestimated observed SL values, especially in the high SL range. These findings contrast with the overestimation of TDS observed in figure A-19b when the new  $K_e$  and  $K_{ss}$  equations were used on the validation data, suggesting that this overprediction might be the result of the inherent variability in the runoff chemistry data.

**Figure A-18.** Relationship between cumulative soil loss and cumulative dissolved solids measured in runoff.

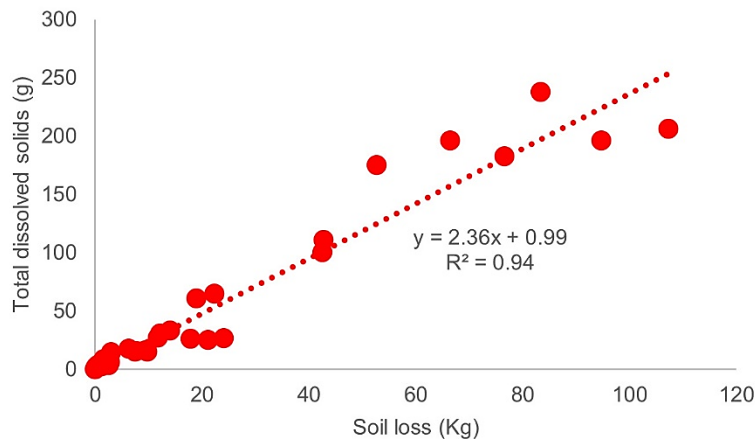
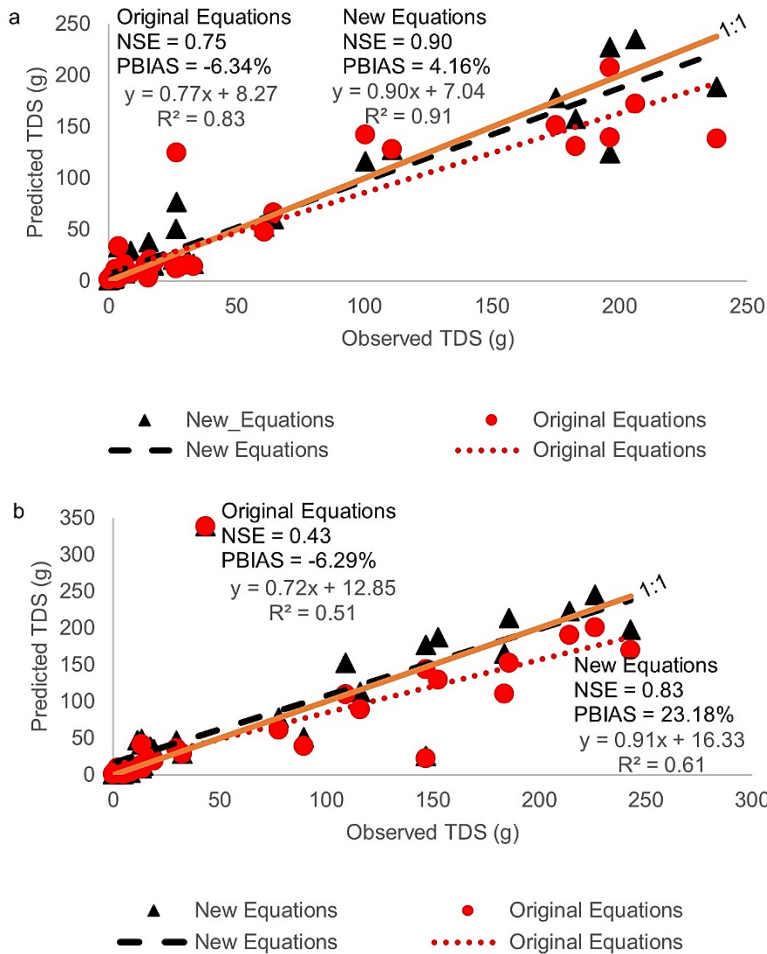


**Figure A-19.** Observed vs. predicted total dissolved solids (TDS) on the 36 calibration (a) and 36 validation (b) data points using the current and the newly developed estimation equations for  $K_e$  and  $K_{ss}$ .



## 647.20 Conclusions

A. We presented an improved version of the RHEM model in this handbook. This model was developed to fill the need for a process-based rangeland erosion model that can function as a practical tool for quantifying runoff and erosion rates specific to western U.S. rangelands to provide reasonable runoff and soil loss prediction capacity for rangeland management and research.

B. The capability of RHEM V2.3 for simulating flow and soil erosion processes was tested on a small watershed in Arizona and on 124 NRI plots placed in Arizona and New Mexico. In particular, we were interested in evaluating the parameter estimation equations of the RHEM V1.0 and RHEM V2.3 models for predicting total friction factor ( $f_t$ ), effective saturated hydraulic conductivity ( $K_e$ ), splash and sheet erodibility coefficient ( $K_{ss}$ ), concentrated flow erodibility coefficient ( $K_\omega$ ) (Hernandez et al., 2013), and improvements to address saline and sodic soils (Cadaret et al., 2016a,b; Nouwakpo et al., 2017; McGwire et al., 2020).

C. The improvements made in model efficiency is significant in comparison with the original version RHEM V1.0 when the new equations for estimating  $K_{ss}$  are used, especially with respect to low-sediment yield simulation. In developing RHEM, we were aware that the model would evolve in the

future to further improve its reliability as progress was made in conducting new rainfall simulator experiments and exploring new model structure for defining parameter estimation equations. The evaluation of the new erodibility equations conducted by Al-Hamdan et al. (2017) showed the ability of the RHEM V2.3 model to predict erosion at the plot scale with a satisfactory range of error. The test that we conducted here of the RHEM V2.3 model at the hillslope scale showed that, compared to the RHEM V1.0 model, its results for this site were statistically robust.

D. The parameter values calculated with the parameter estimation equations fell within the lowest and highest calibrated values of each parameter. The ability of the parameter estimation equations to adequately produce parameter values for the application of RHEM V2.3 on a small watershed suggest that the model is suited for small sub-watersheds, provided that gully erosion and side-wall sloughing are not the main active soil erosion processes in the watershed.

E. The analysis of the 124 NRI points in Arizona and New Mexico suggests that the parameter estimation equations conveyed coherent information to the model. That is, moderate and strong negative correlation coefficients between ground cover percent and total friction factor, effective hydraulic conductivity, and splash and sheet erodibility coefficient were achieved. Likewise, moderate and strong negative correlation coefficients were found between litter cover and basal cover percent and percent runoff. Similarly, moderate and strong negative correlation coefficients were found between foliar cover, ground cover, and sediment yield. In general, the model results are more sensitive to ground cover than to foliar cover, which is a product of the structure of the parameter estimation equations. This is consistent with our understanding of the basic processes of soil erosion, largely because of shear stress partitioning (Foster, 1982), and of most soil erosion models (Nearing et al., 2005; Nouwakpo et al., 2016).

F. Evaluation of the model predictions undertaken in this study demonstrates that RHEM V2.3 produces results of satisfactory quality, when simulating large flows and soil erosion events; but a greater degree of uncertainty is associated with predictions of small runoff and soil erosion events. The reasonable performance of the model with the new parameterization equations indicates that using  $K_{ss}$  alone works reasonably well, as long as concentrated flow paths function only for transport of the splash and sheet-generated sediment, as opposed to functioning also as a significant sediment source. Our test of the model was conducted on an undisturbed hillslope with a mild slope gradient (8 percent). Therefore, the concentrated flow erodibility was negligible, and the estimation of the concentrated flow erodibility coefficient ( $K_{ss}$ ) was not needed. For concentrated flow paths on rangelands to generate sediment detachment, they need to have high erodibility values (i.e., high availability of erodible sediments) and high erosivity (i.e., stream power, which increases with slope steepness). Further research needs to be carried out at the hillslope scale to study the special case of abrupt disturbance, such as post-fire, with steep slope gradients whereby both  $K_e$  and  $K_{ss}$  erodibility parameters might be needed (figure A-20).

**Figure A-20.** Rill erosion in western Nevada where the site has been burned, and the annual invasive grass has revegetated the site.



## Subpart B – Rangeland Hydrology and Erosion Model Tutorial Guide

**Figure B-1.** Rill erosion western Colorado



**Figure B-2.** Gully erosion central Utah



**Figure B-3.** Sagebrush plant community in Central Nevada near reference condition.



**Figure B-4.** Mixed grass prairie in North Dakota near reference conditions.



## Contents

<b>Subpart B – Rangeland Hydrology and Erosion Model Tutorial Guide .....</b>	<b>B.1</b>
647.21 Introduction .....	B.3
647.22 Description of the Ecological Site .....	B.5
647.23 Soil.....	B.6
647.24 Plant Communities.....	B.8

### List of Figures

Figure B-1. Rill erosion western Colorado.....	B.1
------------------------------------------------	-----

Figure B-2. Gully erosion central Utah ..... B.1  
 Figure B-3. Sagebrush plant community in Central Nevada near reference condition..... B.2  
 Figure B-4. Mixed grass prairie in North Dakota near reference conditions ..... B.2  
 Figure B-5. Map of rainfall simulation experiments sites from which RHEM was developed shown on Omernik Level IV Ecoregions..... B.4  
 Figure B-6. Limy Slopes 12–16” PZ Ecological Site within the Walnut Gulch Experimental Watershed in Tombstone, Arizona. .... B.6  
 Figure B-7. Web Soil Survey area of interest with map unit legend. .... B.7  
 Figure B-8. Historic Plant Community (HPC). .... B.8  
 Figure B-9. The State and Transition Model diagram for the Limy Slopes 12–16” PZ Ecological Site. Site Type: Rangeland; Site Id: R041XC308AZ; Major Land Resource Area (MLRA) 041- Southern Arizona Basin and Range. CAER = false mesquite (*Calliandra conferta*); KRER = ratany (*Krameria erecta*); BOER = black grama (*Bouteloua eriopoda*); BOSCU = sidecoats grama (*Bouteloua curtipendula*). .... B.10  
 Figure B-10. Exotic perennial grass. .... B.10  
 Figure B-11. Shrub Invaded State..... B.11  
 Figure B-12. Eroded rangeland..... B.11

**List of Tables**

Table B-1. Description of community transitions..... B.8  
 Table B-2. Summary of input parameters for various represented states. .... B.9

**647.20 Contributors:**

- Mark A. Weltz, Research Leader, Rangeland Hydrologist; USDA-ARS, Reno, NV
- Mariano Hernandez, Hydrologist, University of Arizona, Tucson, AZ
- Mark A. Nearing, Research Agricultural Engineer, USDA-ARS, Tucson, AZ
- Ken E. Spaeth, Rangeland Management Specialist, USDA-NRCS, Fort Worth, TX
- Fred B. Pierson, Research Leader, USDA-ARS, Boise, ID
- C. Jason Williams, Research Hydrologist, USDA-ARS, Tucson, AZ
- Osama Z. Al-Hamdan, Assistant Professor, Texas A&M Kingsville, Kingsville, TX
- S. Kossi, Nouwakpo, Soil Scientist, USDA-ARS, Kimberly, ID
- Gerardo Armendariz, IT Specialist, USDA-ARS, Tucson, AZ
- Haiyan Wei, Hydrologist, University of Arizona, Tucson, AZ
- Dave C. Goodrich, Research Hydraulic Engineer, USDA-ARS, Tucson, AZ
- Phillip Guertin, Hydrologist, University of Arizona, Tucson, AZ
- Carl Unkrich, Hydrologist, USDA-ARS, Tucson, AZ
- Viktor Polyakov, Soil Scientist, USDA-ARS, Tucson, AZ
- Kenneth McGwire, Physical Scientist, Desert Research Institute, Reno, NV.
- Jason Nesbit, IT Specialist, USDA-ARS, Reno, NV
- Gary Frazier, retired USDA-ARS, Loveland, CO
- Leonard Jolley, retired NRCS, Napa, CA
- Jeff Stone, retired ARS, Tucson, AZ

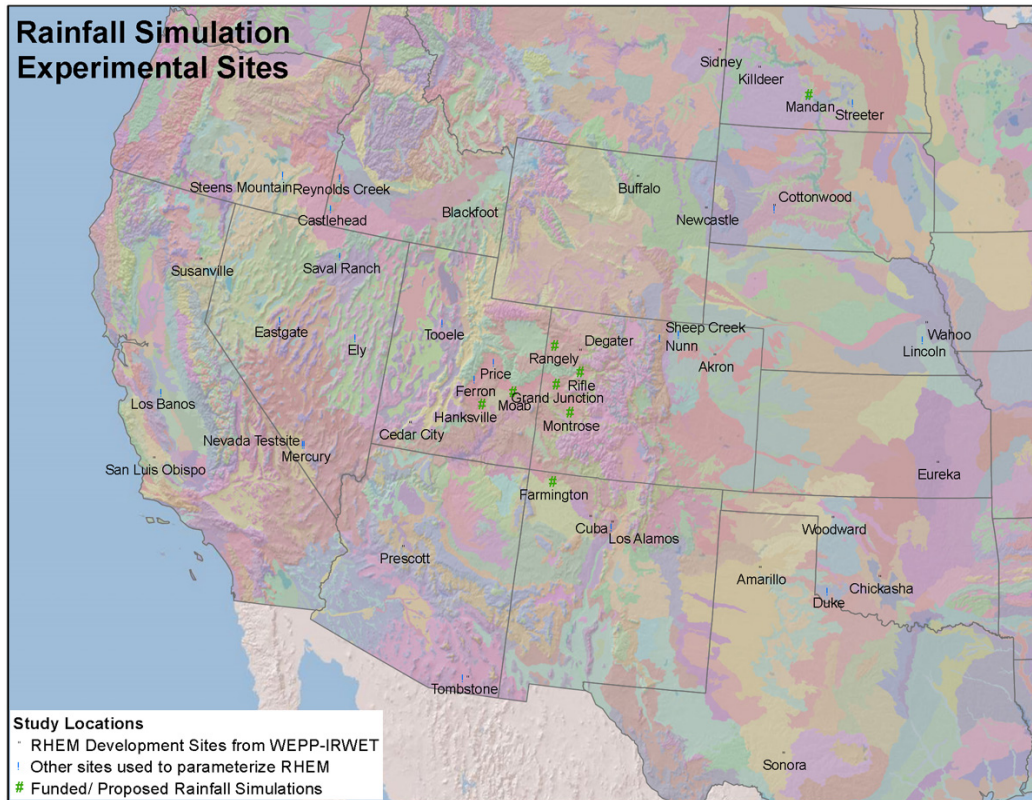
**647.21 Introduction**

A. Soil erosion is a natural process. The erosion potential of a site is the result of complex interactions among soil, vegetation, topographic position, land use and management, and climate. Soil erosion occurs when climatic processes (wind, rainfall, and runoff) exceed the soil’s inherent resistance to these forces. Splash, sheet, and concentrated flow erosion (i.e., rill) are important erosion processes to measure and predict because they are the dominant types of soil erosion occurring on rangelands.

B. A new physically based model has been developed by the Agricultural Research Service (ARS) and Natural Resources Conservation Service (NRCS) for assessing soil loss rates on rangelands that

specifically assess the risk of soil loss at national, regional, and local scales. The Rangeland Hydrology and Erosion Model (RHEM) was developed exclusively from rangeland data from across the western United States (figure B-5). Measured field data from 49 Ecological Sites in 15 states addressing all major ecological regions was used to develop the RHEM erosion equations.

**Figure B-5.** Map of rainfall simulation experiments sites from which RHEM was developed shown on Omernik Level IV Ecoregions.



C. The ecological site concept is the primary means of grouping landscape-level rangeland units in the U.S. and provides a basis for evaluating ecosystem health, targeting conservation practices, and communicating ecosystem responses to management (Williams et al., 2016). An ecological site unit is classified based on site-specific physical attributes (climate, soils, landscape position, and topography) that separate the respective unit from other units in its ability to produce characteristic vegetation and to respond to management and disturbances (USDA 2013). Plant community dynamics and ecosystem responses to management and disturbances are conceptualized within Ecological Site Descriptions (ESD) primarily using a State-and-Transition Model (STM).

D. Hydrologic function is well-recognized as an indicator of rangeland health, but hydrologic data and information on fundamental ecohydrologic feedbacks that govern state resilience are often missing in ESDs. Hydrologic vulnerability for a particular state is a function of climate (i.e., precipitation regime) and the susceptibility of the ground surface to runoff generation and erosion (Williams et al., 2016). Vegetation, litter, and ground cover dampen the erosive energy of rainfall and overland flow and delay and reduce runoff and erosion by trapping water input, stabilizing sediment, and promoting infiltration. Sparsely vegetated or bare patches (source areas) on sloping terrain exhibit high evaporative losses and low soil water storage, promote runoff and erosion, and facilitate transfer of water and soil resources to areas with ample surface protection (sink areas). Accumulation of soil water and nutrients in sink areas stimulates below-ground biological activity, plant growth, and reproduction that further sustain the vegetative community and the overall source-sink structure.

Alteration of a plant community structure that promotes water and soil retention can have major ramifications on hydrologic function and state resilience. Climate and its interactions with management provide the means of maintaining a state or in guiding change to a desired state through alteration of vegetation.

E. The current structure for ESDs includes a section for hydrologic function, but guidance is limited, and actual information is often missing regarding the hydrology content. Upon completion of this tutorial, you will be able to assess how plant community transitions in a STM affect hydrologic function of the site as a function of changes in plant lifeform, plant canopy, and ground cover. Additional information on rangeland hydrologic processes and the Rangeland Hydrology and Erosion Model (RHEM) tool can be found in the scientific publications listed in the Appendix.

(1) Capabilities

RHEM estimates runoff, soil loss, and sediment delivery rates and volumes at the hillslope spatial scale and the temporal scale of a single rainfall event (Nearing et al., 2011; Hernandez et al., 2017).

(2) Limitations

The RHEM model is a single event prediction tool and therefore does not predict daily and seasonal changes in plant growth and associated changes in standing biomass, foliar canopy cover, or ground cover. RHEM does not address channel, gully, side-bank sloughing, head cutting, rain-on-snow, or seep-induced soil erosion processes.

(3) Objectives

- (i) Use the RHEM model output for various ecological states to characterize how changes in percent of foliar canopy cover and ground cover affect runoff and erosion.
- (ii) Use the Risk Assessment Tool (within RHEM) for illustrating how STM and probability of occurrence of yearly soil losses between ecological states can be used to define different soil erosion severity levels.

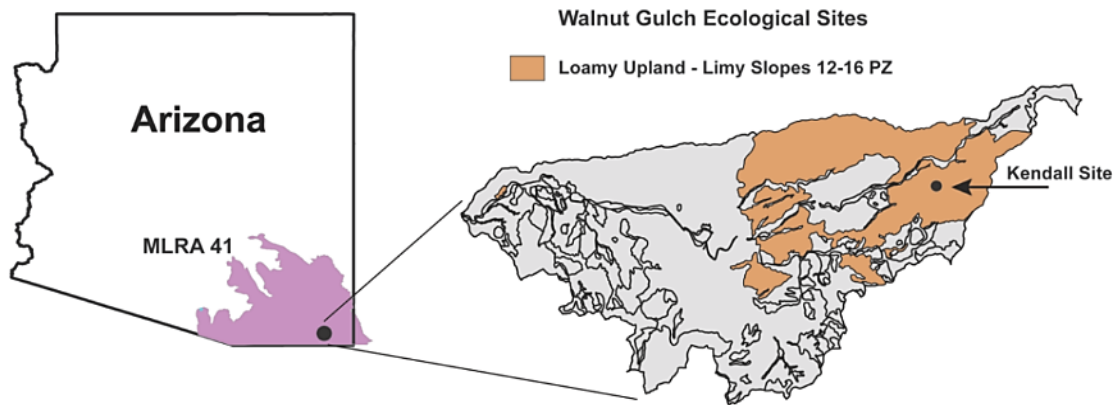
## 647.22 Description of the Ecological Site

A. Example 1: This exercise will illustrate the use of the Rangeland Hydrology and Erosion Model – RHEM V2.3 and the RHEM Web-based interface at the Kendall Grassland site (109°56'28"W, 31°44'10"N, 1526 m asl), located in the Walnut Gulch Experimental Watershed (WGEW), ca. 11 km east of Tombstone, AZ (figure B-6). The Soil Map Unit is a complex of Elgin and similar soils, 50 percent; and Stronghold and similar soils, 40 percent. The area of interest is the Elgin soil, which is correlated with the Limy Slopes 12–16" PZ ecological site (Site ID: R041XC308AZ, Major land resource area (MLRA): 041-Southeastern Arizona Basin and Range).

### Climatic Features

The climate of the area is semiarid with annual precipitation of approximately 345 mm (13.6 in) and a highly spatially and temporally varying precipitation pattern dominated by the North American Monsoon. Summer rainfall occurs in July–September. The precipitation originates in the Gulf of Mexico or Pacific Ocean (from the southwest) and occurs as brief convective, intense thunderstorms. Cool season moisture tends to be frontal, originates in the Pacific or Gulf of California, and falls in widespread storms with long duration and low intensity. Snow rarely lasts more than one day. May and June are the driest months of the year. Humidity is generally very low. Mean annual temperature is 18°C.

**Figure B-6.** Limy Slopes 12–16” PZ Ecological Site within the Walnut Gulch Experimental Watershed in Tombstone, Arizona.



## 647.23 Soil

### A. Soil Features

Using Web Soil Survey (<http://websoilsurvey.sc.egov.usda.gov/App/HomePage.htm>), the soil mapped in this example is an Elgin-Stronghold complex, 3 to 20 percent slopes, Cochise County, Arizona, Douglas-Tombstone Part (AZ671) (figure B-7)

### B. Map Unit Composition

Elgin and similar soils, 50 percent; and Stronghold and similar soils, 40 percent

### C. Description of Elgin Soil

#### (1) Setting

- (i) Landform: Fan terraces
- (ii) Landform position (two-dimensional): Summit
- (iii) Landform position (three-dimensional): Tread
- (iv) Down-slope shape: Convex
- (v) Across-slope shape: Convex
- (vi) Parent material: Mixed fan alluvium

#### (2) Typical profile

- (i) 1:0 to 2.54 cm (0 to 1 inches), very gravelly fine sandy loam
- (ii) Bt: 2.54 to 38.1 cm (1 to 15 inches), clay
- (iii) Btk: 38.1 to 53.3 cm (15 to 21 inches), gravelly sandy clay loam
- (iv) Bk1: 53.3 to 68.6 cm (21 to 27 inches), gravelly sandy loam
- (v) Bk2: 68.6 to 152.4 cm (27 to 60 inches), very gravelly sandy loam

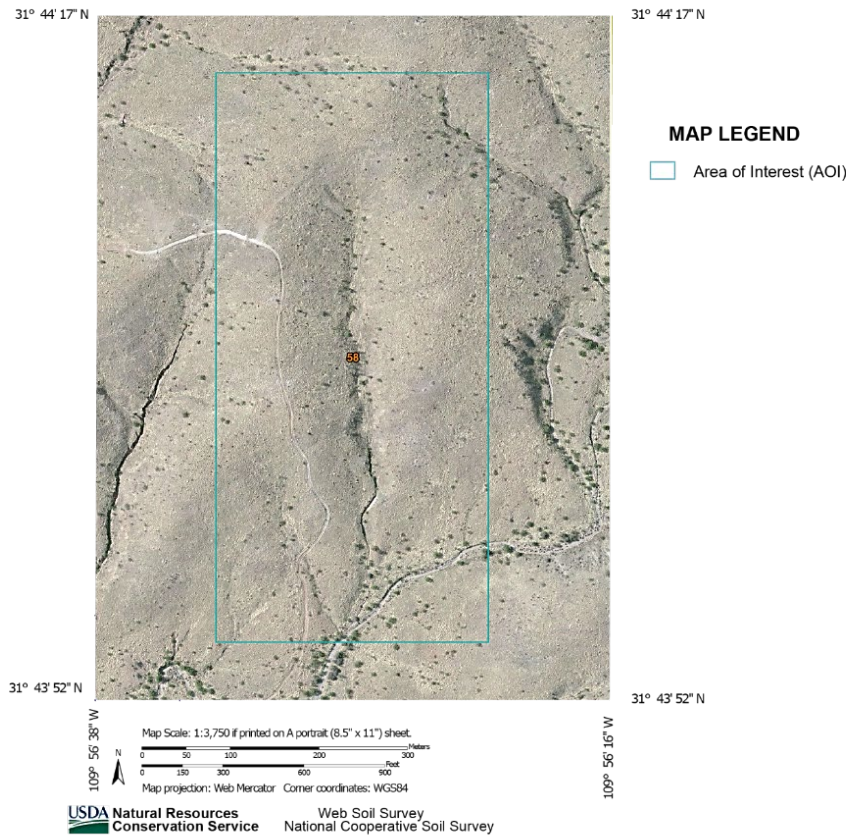
#### (3) Properties and qualities

- (i) Slope: 3 to 20 percent
- (ii) Depth to restrictive feature: More than 2.03 m (80 inches)
- (iii) Natural drainage class: Well drained

- (iv) Runoff class: High
- (v) Capacity of the most limiting layer to transmit water (Ksat): Moderately low to moderately high, 1.52 to 5.08 mm/hr (0.06 to 0.20 in/hr)
- (vi) Depth to water table: More than 2.03 m (80 inches)
- (vii) Frequency of flooding: None
- (viii) Frequency of ponding: None
- (ix) Calcium carbonate, maximum in profile: 25 percent
- (x) Available water storage in profile: Low (about 0.15 m) (5.7 inches)

**Figure B-7.** Web Soil Survey area of interest with map unit legend.

**Soil Map - Cochise County, Arizona, Douglas-Tombstone Part**  
**(RHEM Tutorial Guide: Desert Southwest Grassland Limy Slopes 12-16" PZ Ecological Site)**



**Map Unit Legend**

Cochise County, Arizona, Douglas-Tombstone Part (AZ671)			
Map Unit Symbol	Map Unit Name	Acres in AOI	Percent of AOI
58	Elgin-Stronghold complex, 3 to 20 percent slopes	48.8	100.0%
<b>Totals for Area of Interest</b>		<b>48.8</b>	<b>100.0%</b>

D. Figure B-7 shows the STM for the Limy Slopes 12–16” PZ ecological site. The model for this site includes four ecological states. The ecological states are outlined by bold black rectangles. Plant community phases are shown by light gray rectangles. Based on the ESD within the Historic Plant Community (HPC) or reference plant community state (concept established by the NRCS), fire and drought could cause temporary shifts between the two plant communities shown. According to the STM, the Eroded to Limy Upland state (hereinafter called Eroded) is considered so degraded by soil

erosion that it has crossed a threshold, and now has a different, less productive, potential plant community.

E. By 2006, seed sources for both shrub and Lehmann lovegrass (*Eragrostis lehmanniana*) (see Transition 1a in table B-1) had appeared in the upland areas around the Kendall study area (Heilman et al., 2010). The vegetation was beginning to transition from the HPC state toward the Lehmann state as small shrubs were getting established. Prolonged drought resulted in high perennial grass mortality prior to the 2006 summer monsoon (Robinett, 1992), and 2006 saw a significant shift toward the exotic grass and the shrub-invaded states, which impacted the hydrological and sediment response of the system for a period of time (Polyakov et al., 2010).

**Table B-1.** Description of community transitions.

Transition	Description
1a.	Continuous Heavy Grazing (CHG), introduction of a seed source, or direct seeding of Lehmann lovegrass.
1b.	Unknown. Possible herbicide treatment of exotic species and seeding of native grasses.
2a.	CHG with drought, fire interaction. Invasion by creosote bush and whitethorn acacia. Other shrubs and succulents can also increase. Lack of fine fuel for fire. Remnant perennial grasses cannot re-colonize areas with shrub competition.
2b.	Prescribed Grazing/No Grazing (PG/NG) with herbicide shrub control. Possible seeding of native grasses, maintenance treatments for shrubs (fire, herbicide).
3.	CHG, trailing and soil surface compaction, accelerated sheet and rill erosion. Over time (50-100 years); loss of dark colored (mollic) soil.

## 647.24 Plant Communities

A. The Historic Plant Community is dominated by warm season perennial grasses (figure B-8). Perennial forbs are well represented on the site, as well as a few species of half shrubs. Most of the major perennial grasses on the site are well dispersed throughout the plant community. Black gramma occurs in patches of various sizes, and these patches appear to be well dispersed over large areas of the site. The aspect is open grassland.

B. With continuous heavy grazing, the potential dominant grasses are replaced by increases in species like red threeawn (*Aristida purpurea*). Low shrubs that can increase on the site include snakeweed (*Gutierrezia sarothrae*). Large shrubs such as creosote-bush (*Larrea tridentata*), whitethorn (*Acacia constricta*), and paloverde (*Parkinsonia florida*) can invade this site from adjacent areas of Limy Upland. Natural fire may have been a factor in the development of the potential plant community. Gravel size cover may be inadequate in preventing water erosion on steep slopes. Lehmann lovegrass can invade and become dominant on areas of this site where perennial grass cover has been lost due to the interactions of drought, fire, and continuous grazing.

C. When the native perennial grass cover is depleted due to the combination of continuous grazing and drought or fire, Lehmann lovegrass can invade areas of this site, as long as seed source is present (figure B-10). Over time Lehmann can dominate the grass and forb component of the plant community. The dominant half shrubs seem to be able to persist under these circumstances.

D. Table B-2 shows the inputs for the model. Figure B-9 shows the State and Transition Model diagram for the site.

**Figure B-8.** Historic Plant Community (HPC).



**Table B-2.** Summary of input parameters for various represented states.

Input Parameters	Baseline Scenario: HPC	Scenario 1: Eroded	Scenario 2: Shrub invaded	Scenario 3: Exotic Grass
State ID	AZ	AZ	AZ	AZ
Climate Station	Tombstone	Tombstone	Tombstone	Tombstone
Soil Texture	Sandy Loam	Sandy Loam	Sandy Loam	Sandy Loam
Soil Water Saturation (%)	25	25	25	25
Slope Length (m)	50	50	50	50
Slope Shape	S-Shaped	S-Shaped	S-Shaped	S-Shaped
Slope Steepness (%)	12.5	12.5	12.5	12.5
Bunchgrass Foliar Cover (%)	50	0	1	26
Forbs and/or Annual Grasses	1	0	2	2
Shrub Foliar Cover (%)	10	35	35	10
Sod Grass Foliar Cover (%)	10	35	35	10
Total Foliar Cover (%)	61	35	38	38
Basal Cover (%)	8	0	3	3
Rock Cover (%)	16	16	16	16
Litter Cover (%)	1	0	0	0
Total Ground Cover (%)	70	25	29	54

**Figure B-9.** The State and Transition Model diagram for the Limy Slopes 12–16” PZ Ecological Site. Site Type: Rangeland; Site Id: R041XC308AZ; Major Land Resource Area (MLRA) 041-Southern Arizona Basin and Range. CAER = false mesquite (*Calliandra conferta*); KRER = ratany (*Krameria erecta*); BOER = black grama (*Bouteloua eriopoda*); BOSCU = sidecoats grama (*Bouteloua curtipendula*).

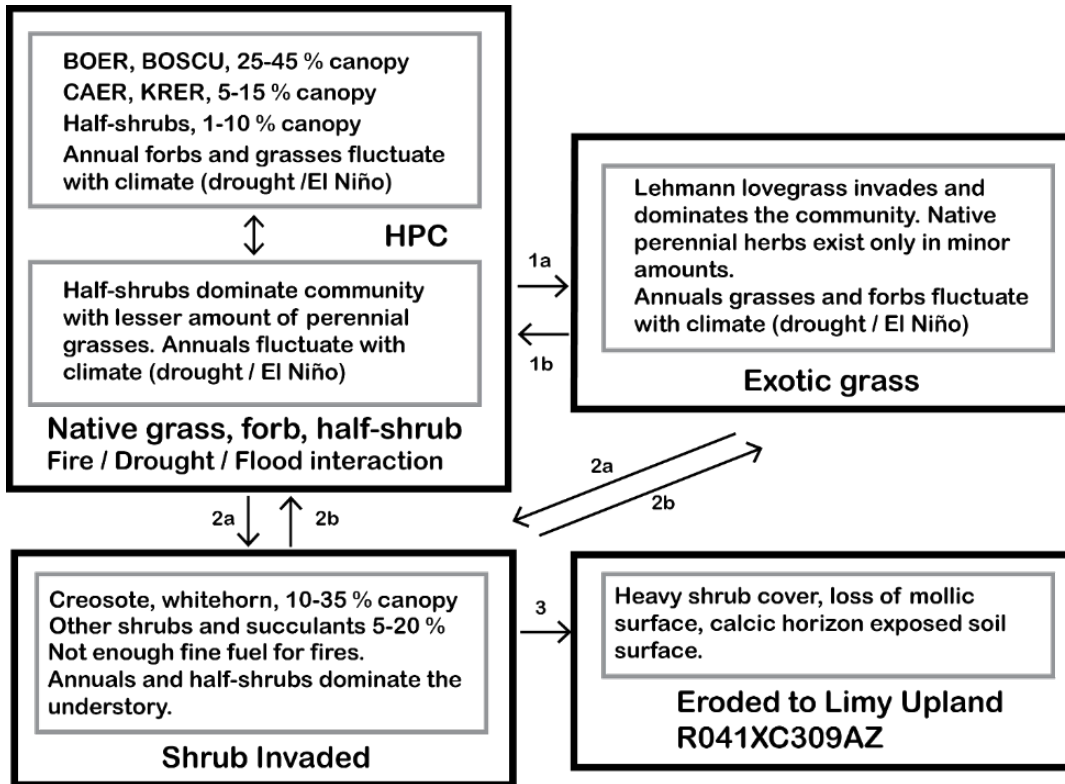


**Figure B-10.** Exotic perennial grass.



E. In the absence of fire for long periods and with the interaction of drought, fire, and continuous grazing, shrubs like creosote-bush and whitethorn can invade and increase to dominate the site (figure

B-11). In some areas other shrubs like mesquite can also increase. As woody plants increase, the herbaceous part of the plant community diminishes until there is no longer enough fine fuel produced to carry fire.

**Figure B-11.** Shrub Invaded State.



F. The interaction of continuous heavy grazing with drought or fire over time (50-100 years) can lead to accelerated sheet and rill erosion and loss of the entire A (mollic) horizon (figure B-12). This state has heavy shrub cover, and the calcic horizon is exposed at the soil surface. Its potential to grow perennial grasses is greatly reduced. Shrub control with herbicides will be short lived as the new site potential is shrubland. Shrubs like creosote dominate the plant community.

**Figure B-12.** Eroded rangeland.



## Subpart C – Part I: Developing and Analyzing RHEM Scenarios

### Contents

647.31 Data Available for Analysis.....	C.1
647.32 Modeling Results.....	C.6
647.33 Discussion.....	C.9

#### List of Figures

Figure C-1. RHEM initial screen Web-based system.....	C.2
Figure C-2. Define scenario for RHEM analysis.....	C.3
Figure C-3. Define units for analysis.....	C.3
Figure C-4. Define climate station for analysis. ....	C.2
Figure C-5. Define soil texture of the site.....	C.3
Figure C-6. Define slope of the site.....	C.4
Figure C-7. Define vegetation type, canopy cover and ground cover.....	C.5
Figure C-8. Diagram of ground surface cover classes as used by RHEM. ....	C.5
Figure C-9. Run the scenario.....	C.5
Figure C-10. Select scenario to review output.....	C.6
Figure C-11. Average annual results for rain, runoff, sediment yield, and soil loss.....	C.6
Figure C-12. Annual averages for precipitation, runoff, sediment yield, and soil loss for scenarios. ....	C.7
Figure C-13. Return frequency graphs for rain, runoff, sediment yield, and soil loss based on yearly summation values.....	C.7

#### List of Tables

Table C-1. Estimated rain, runoff, sediment yield, and soil loss for the 5-year return frequency year.....	C.8
Table C-2. Estimated rain, runoff, sediment yield, and soil loss for the 25-year return frequency year.....	C.8
Table C-3. Estimated rain, runoff, sediment yield, and soil loss for the 50-year return frequency year.....	C.8
Table C-4. Estimated rain, runoff, sediment yield, and soil loss for the 100-year return frequency year.....	C.8

### 647.31 Data Available for Analysis

A. Getting Started. Figure C-1 illustrates the sequence of steps performed within RHEM. The numbers on the left of the input parameter window show the order in which they are performed. First, the user accesses the application through an internet browser interface ([dss.tucson.ars.ag.gov/rhem/](https://dss.tucson.ars.ag.gov/rhem/)) and must register to use the application. The user is notified of any major updates and provided disk space to save and edit scenarios that the user has created.

Figure C-1. RHEM initial screen Web-based system

B. The following steps describe the sequence of actions to run the model:

- (1) create a new scenario
- (2) select units for input and output
- (3) select a climate weather station
- (4) select a soil texture class
- (5) provide a description of slope and topography characteristics
- (6) provide estimates of foliar canopy cover and ground cover characteristics
- (7) run new scenario
- (8) perform a comparison of scenarios
- (9) risk assessment and analysis of soil loss.

C. Detailed steps in running the RHEM model.

- (1) **Step 1- Define scenario:** Start RHEM with a new scenario by typing a name that identifies the new scenario and provide a short description of the project on the Name and Description dialog boxes, respectively (figure C-2).
- (2) **Step 2- Select Metric or English Units** (figure C-3)

**Figure C-2.** Define scenario for RHEM analysis

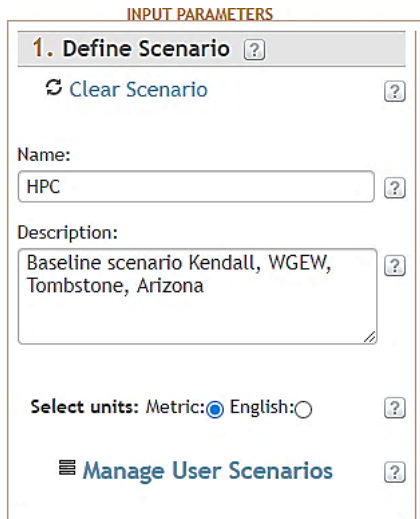
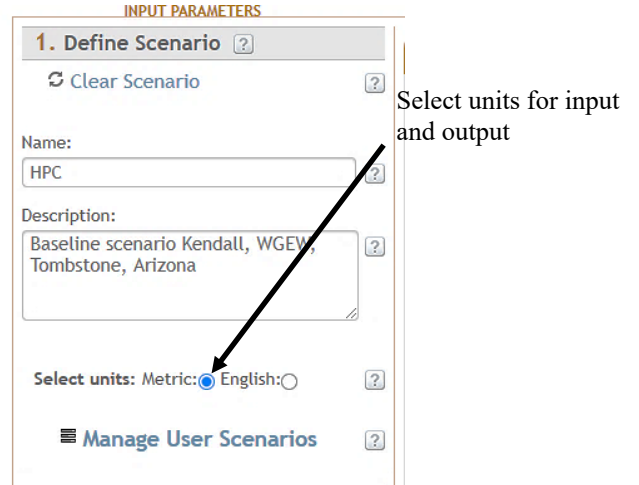


**Figure C-3.** Define units for analysis



A scenario is defined as a unique set of input parameters needed to run RHEM. It can be saved to view results, compared with other scenarios, or modified to create a new scenario. The user can select the units to be used for the current scenario’s input and output values.

(3) **Step 3- Climate station**

- (i) The second step involves entering the climate data to parameterize the simulation model. See figure C-4. In the Climate Station Panel two dialog boxes are available. In the State dialog box, select the state of the project location, and in the Station dialog box select the name of the climate station that is closest to the location being analyzed, or a station with similar elevation to the study area.
- (ii) Climate data is obtained via the CLIGEN (Version 5.3) climate generator. RHEM uses the CLIGEN model to generate daily rainfall statistics for a 300-year weather sequence that is representative of a time-stationary climate and used by the rainfall disaggregation component of RHEM. The disaggregation component uses rainfall amount, duration, ratio of time of peak intensity to duration, and the ratio of peak intensity to average intensity to compute a time-intensity distribution of a rainfall event. The CLIGEN database consists of 2,600 weather stations across the continental U.S. and limited international locations.

Figure C-4. Define climate station for analysis.

The screenshot displays the RHEM Web Tool interface. On the left, the '2. Climate Station' panel is active, showing 'National' selected, 'State: Arizona', and 'Station: Tombstone'. A 'Show Map' button is visible. The main area is titled 'RESULTS' and contains a 'CLIMATE STATIONS MAP'. A popup window for 'TOMBSTONE' provides the following data:

- Name: TOMBSTONE
- ID: 028619
- Elevation: 1383.79 m (4540 ft)
- Lat: 31.72 Long: -110.07
- Avg. Precipitation: 335.33 mm (13.20 in)
- Monthly Precipitation (mm):

Month	Precipitation (mm)
Jan	18.5
Feb	18.1
Mar	15.3
Apr	6.3
May	4.6
Jun	13
Jul	87
Aug	80.8
Sep	37
Oct	19.3
Nov	14.7
Dec	20.8

The popup also notes 'Currently using this station!' and includes a close button (X). The map shows the location of Tombstone in southern Arizona, with various cities and geographical features labeled.

(4) Step 4- Soil texture class

In the Soil Texture Class panel, the user defines the soil texture of the upper 4 cm (1.57 in.) of the soil profile. It is input as a class name from the USDA soil textural triangle. The RHEM database contains a list of soil hydraulic properties to parameterize the Smith-Parlange infiltration equation and look-up tables with percent of sand, silt, and clay to estimate the Darcy-Weisbach friction factor, and the maximum initial

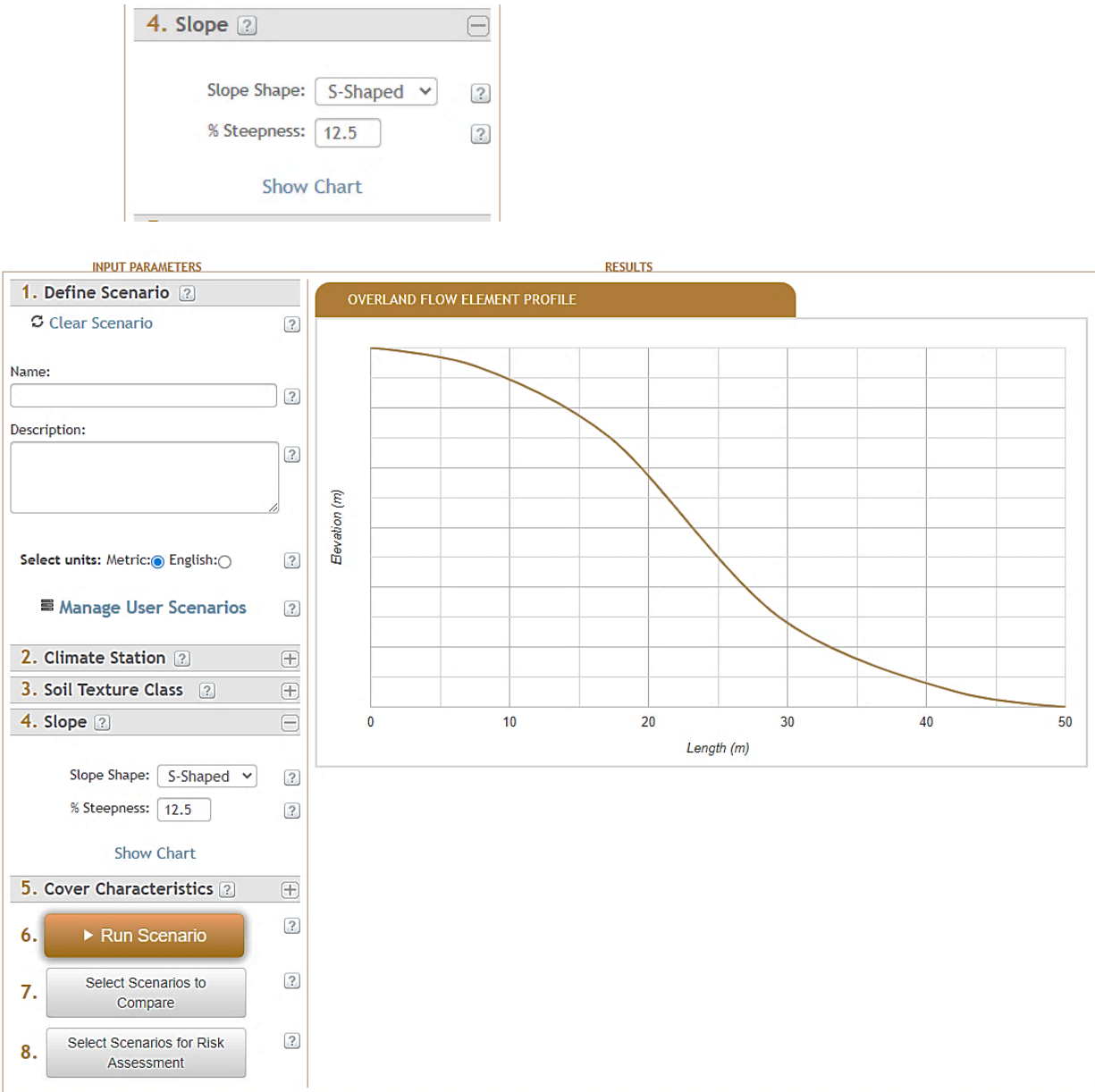
concentrated flow erodibility coefficient. If soil is saline or sodic, then check the saline option and enter the Sodium Adsorption Ratio (figure C-5).

**Figure C-5.** Define soil texture of the site.

### (5) Step 5- Slope

To characterize the topography of the hillslope profile, the slope profile panel presents three dialog boxes to enter the slope length, slope shape, and slope steepness. In RHEM we define slope length as the length of the path that water flows down a slope as sheet and rill flow, until it reaches an area where flow begins to concentrate in a channel, or to the point where the slope flattens out, causing deposition of the sediment load. Slope lengths up to 120 m (394 ft.) are supported. A distance greater than 120 m (394 ft.) is considered to be a very long slope length. We suggest using a slope length of 50 m for consistency and comparability. In addition, RHEM provides four hillslope shapes for different topographic scenarios as follows: uniform, convex, concave, and S-shaped. In order to assess sediment delivery from a hillslope to a channel, the user must designate the shape of the hillslope either as concave or S-shaped. See figure C-6. These are the slope shapes that will experience toe-slope deposition. The slope steepness is the slope of the hillslope area rather than the average land slope.

**Figure C-6.** Define slope of the site.

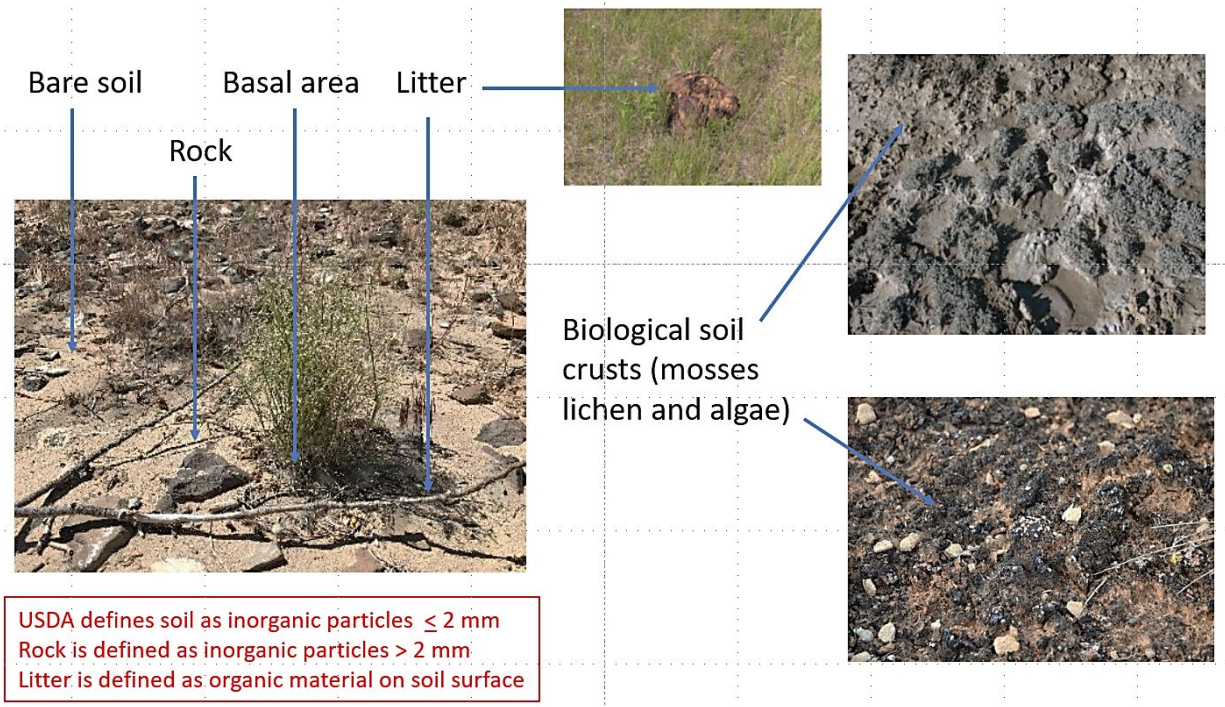


**(6) Step 6- Cover characteristics**

The Cover Characteristics panel (figures C-7 and C-8) presents eight dialog boxes to enter information on vegetative foliar canopy cover and surface ground cover. RHEM’s system of parameter estimation equations and procedures reflects the concept that hydrology and erosion processes are affected by plant growth forms and surface ground cover. Thus, the user can enter percent foliar canopy for four rangeland plant community groups: bunchgrass, shrub, sod grass, and annual grass/forbs. RHEM was designed to require minimal inputs for surface ground cover that are readily available for most rangeland ecological sites. Percent ground cover by component is defined as follows: rocks, plant litter, plant basal area, and biological soil crust.

**Figure C-7.** Define vegetation type, canopy cover and ground cover.

**Figure C-8.** Diagram of ground surface cover classes as used by RHEM.



**(7) Step 7- Run scenario**

- (i) The Run Scenario panel is used to generate output from a new scenario, an edited scenario, and a re-named scenario. See figure C-9. The web-based interface generates a summary report, input parameter file, and the storm file.

**Figure C-9.** Run the scenario



- (ii) Repeat Step 1 through Step 6 for Exotic Grass, Shrub Invaded, and Eroded states

**(8) Step 8- Select scenarios to compare**

The Select Scenario to Compare panel allows the user to compare up to five existing scenarios. See figure C-10.

**Figure C-10.** Select scenario to review output.



(9) Step 9- Risk assessment and analysis of soil loss (See Subpart D).

### 647.32 Modeling Results

A. Soil loss on many rangelands is not uniformly distributed spatially or temporally across the landscape. Average annual soil loss rates cannot explain all soil loss in arid and semiarid rangelands because most soil loss occurs during high-intensity rainfall events that generate large amounts of runoff and that may occur only a few times in a decade. The RHEM return frequency output is based on yearly summations of runoff and erosion which will take into account the occurrence of years that have these large events.

B. For many arid and semiarid western rangelands soils, the sustainable soil loss rate is estimated to be  $\leq 2.2$  tons  $\text{ha}^{-1}$  year $^{-1}$  due to their shallow depth, low organic matter content, and the slow rate of soil formation in erratic and dry climates (DeBano and Wood, 1990). Weltz et al. (2014) proposed that soil loss rates of 2.2 to 4.5 tons  $\text{ha}^{-1}$  year $^{-1}$  put the long-term sustainability of these rangelands at risk and that soil loss rates  $> 4.5$  tons  $\text{ha}^{-1}$  year $^{-1}$  be considered unsustainable. The output screens shown in tables C-1, C-2, C-3, and C-4 provide a summary of soil loss rates for the 5, 25, 50, and 100-year recurrence interval. Based on the soil loss thresholds proposed by Weltz et al. (2014), the Eroded state becomes unsustainable for soil loss years with 25, 50, and 100-year return intervals.

C. The application of the RHEM V2.3 yields the following results for this ecological site, displayed in figures C-11, C-12, and C-13. Tabular results for the 5, 25, 50, and 100-year storm return intervals are shown in tables C-1 through C-4.

**Figure C-11.** Average annual results for rain, runoff, sediment yield, and soil loss.

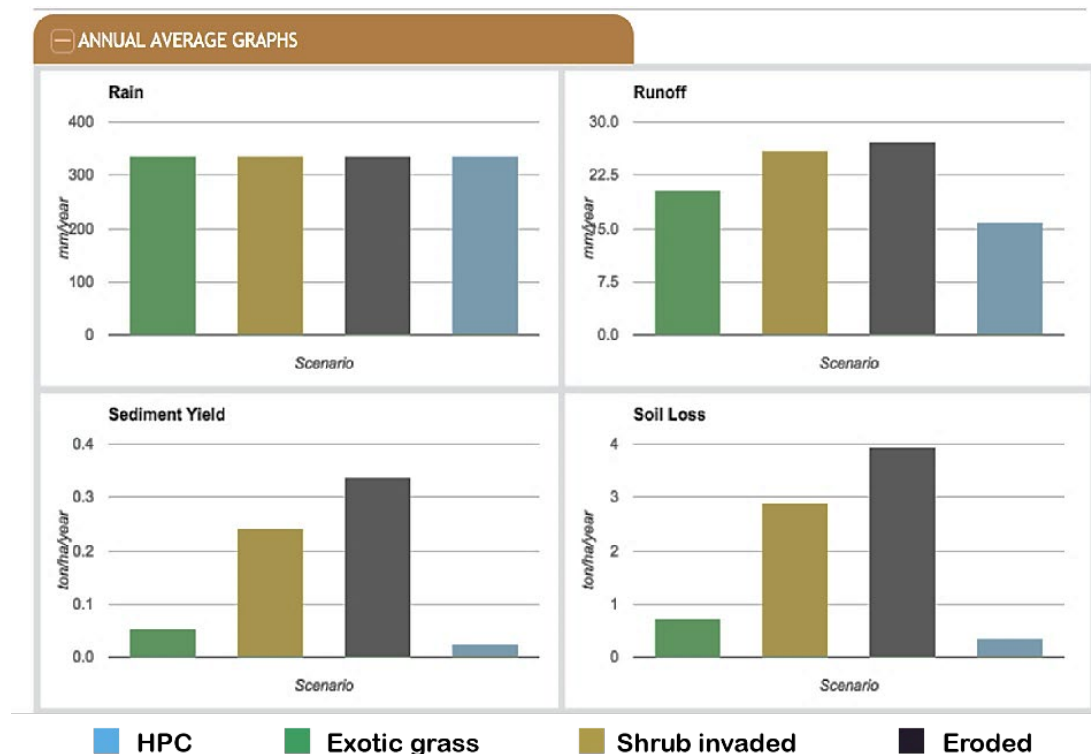


**Figure C-12.** Annual averages for precipitation, runoff, sediment yield, and soil loss for scenarios.

ANNUAL AVERAGES				
	EXOTIC GRASS	SHRUB INVADED	ERODED	HPC
Avg. Precipitation (mm/year)	335.330	335.330	335.330	335.330
Avg. Runoff (mm/year)	20.288	26.035	27.187	15.839
Avg. Sediment Yield (ton/ha/year)	0.054	0.243	0.339	0.025
Avg. Soil Loss (ton/ha/year)	0.725	2.898	3.949	0.360

**Figure C-13.** Return frequency graphs for rain, runoff, sediment yield, and soil loss based on yearly summation values.

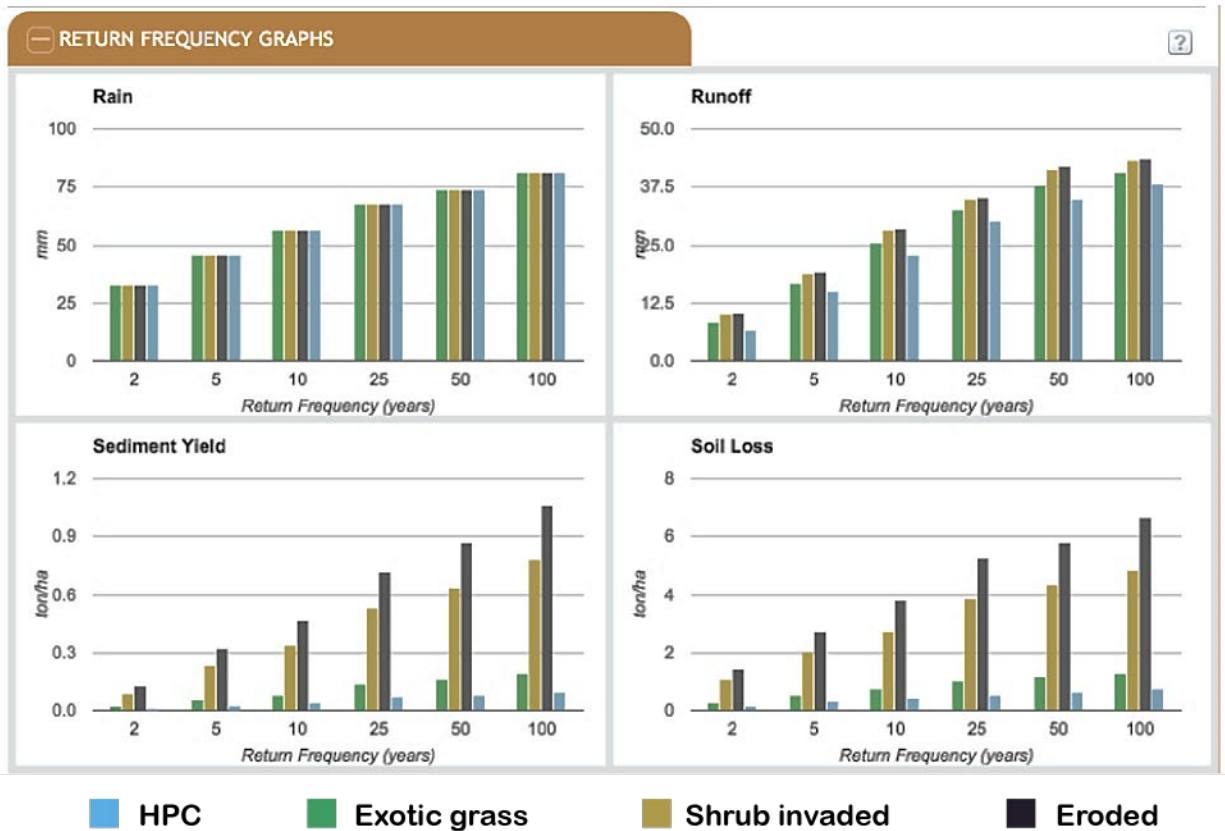


**Table C-1.** Estimated rain, runoff, sediment yield, and soil loss for the 5-year return frequency year.

5 YEAR RETURN FREQUENCY RESULTS				
	EXOTIC GRASS	SHRUB INVADED	ERODED	HPC
Rain (mm)	45.600	45.600	45.600	45.600
Runoff (mm)	16.899	18.690	19.162	14.981
Sediment Yield (ton/ha)	0.055	0.233	0.323	0.027
Soil Loss (ton/ha)	0.546	2.041	2.753	0.297

**Table C-2.** Estimated rain, runoff, sediment yield, and soil loss for the 25-year return frequency year.

25 YEAR RETURN FREQUENCY RESULTS				
	EXOTIC GRASS	SHRUB INVADED	ERODED	HPC
Rain (mm)	68.000	68.000	68.000	68.000
Runoff (mm)	32.446	34.883	35.364	30.086
Sediment Yield (ton/ha)	0.134	0.528	0.720	0.070
Soil Loss (ton/ha)	1.010	3.873	5.238	0.562

**Table C-3.** Estimated rain, runoff, sediment yield, and soil loss for the 50-year return frequency year.

50 YEAR RETURN FREQUENCY RESULTS				
	EXOTIC GRASS	SHRUB INVADED	ERODED	HPC
Rain (mm)	73.600	73.600	73.600	73.600
Runoff (mm)	37.931	41.172	41.788	34.808
Sediment Yield (ton/ha)	0.161	0.637	0.871	0.084
Soil Loss (ton/ha)	1.156	4.342	5.825	0.639

**Table C-4.** Estimated rain, runoff, sediment yield, and soil loss for the 100-year return frequency year.

100 YEAR RETURN FREQUENCY RESULTS				
	EXOTIC GRASS	SHRUB INVADED	ERODED	HPC
Rain (mm)	81.400	81.400	81.400	81.400
Runoff (mm)	40.697	43.283	43.710	38.206
Sediment Yield (ton/ha)	0.194	0.778	1.061	0.101
Soil Loss (ton/ha)	1.313	4.847	6.659	0.727

### 647.33 Discussion

A. Soil loss on many rangelands is not uniformly distributed, spatially or temporally, across the landscape. Average annual soil loss rates cannot explain all soil loss in arid and semiarid rangelands because most soil loss occurs during high-intensity rainfall events that generate large amounts of runoff and that may occur only a few times in a decade. The RHEM return frequency output is based on yearly summations of runoff and erosion, which will take into account the occurrence of years that have these large events.

B. For many arid and semiarid western rangelands soils, the sustainable soil loss rate is estimated to be  $\leq 2.2$  tons  $\text{ha}^{-1}$  year $^{-1}$  due to their shallow depth, low organic matter content, and the slow rate of soil formation in erratic and dry climates (DeBano and Wood, 1990). Weltz et al., 2014 proposed that soil loss rates of 2.2 to 4.5 tons  $\text{ha}^{-1}$  year $^{-1}$  put the long-term sustainability of these rangelands at risk and that soil loss rates  $> 4.5$  tons  $\text{ha}^{-1}$  year $^{-1}$  should be considered unsustainable. The output screens shown in Tables C-1, C-2, C-3, and C-4 provide a summary of soil loss rates for the 5, 25, 50, and 100- year recurrence intervals. Based on the soil loss thresholds proposed by Weltz et al., 2014, the Eroded state becomes unsustainable for soil loss years with 25, 50, and 100-year return intervals.

## Subpart D – Part II: Developing and Analyzing a Risk Assessment

### Contents

647.41 Example.....	D.1
647.42 Risk Assessment Modeling Results.....	D.3
647.43 Risk Assessment Discussion.....	D.4
647.44 Summary.....	D.5

#### List of Figures

Figure D-1. Select scenario for risk assessment from completed model runs. ....	D.1
Figure D-2. Select Account button. ....	D.1
Figure D-3. Screenshot illustrating how to enable the detailed output option. ....	D.2
Figure D-4. Screenshot illustrating scenarios with detailed output previously generated in Part I. The green button indicates the baseline scenario.....	D.3
Figure D-5. Probability of occurrence for yearly soil loss for all scenarios. ....	D.4
Figure D-6. Rotating boom simulator used to collect data for development of the Rangeland Hydrology and Erosion Model (RHEM). Plots were 3 m (10 ft.) wide by 10.7 m (35 ft.) long.....	D.6
Figure D-7. Walnut Gulch rainfall simulator used to collect data near Moab, Utah for development of the Rangeland Hydrology and Erosion Model (RHEM). Plots were 2m (6ft) wide by 6m (20ft) long. ....	D.7

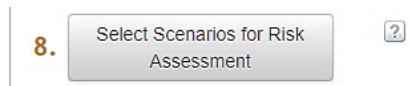
#### List of Tables

Table D-1. Percent probability of occurrence of yearly soil losses and soil loss severity. ....	D.3
-------------------------------------------------------------------------------------------------	-----

### 647.41 Example

A. **Step 9- Select Scenarios for Risk Assessment.** In this section you will use the Risk Assessment Tool for exploring how STM and probability of occurrence of yearly soil losses between ecological states can be used to define different soil erosion severity levels. The Risk Assessment Tool estimates probability of occurrence of yearly soil losses using the output generated from simulation runs discussed earlier. Only scenarios with detailed output and that were run with version 2.3 of RHEM will be available for running the risk assessment analysis. To run scenarios with detailed output, please be sure to enable this in your “Account” section (top right corner). Figures D-1, D-2, and D-3 show how to enable this option.

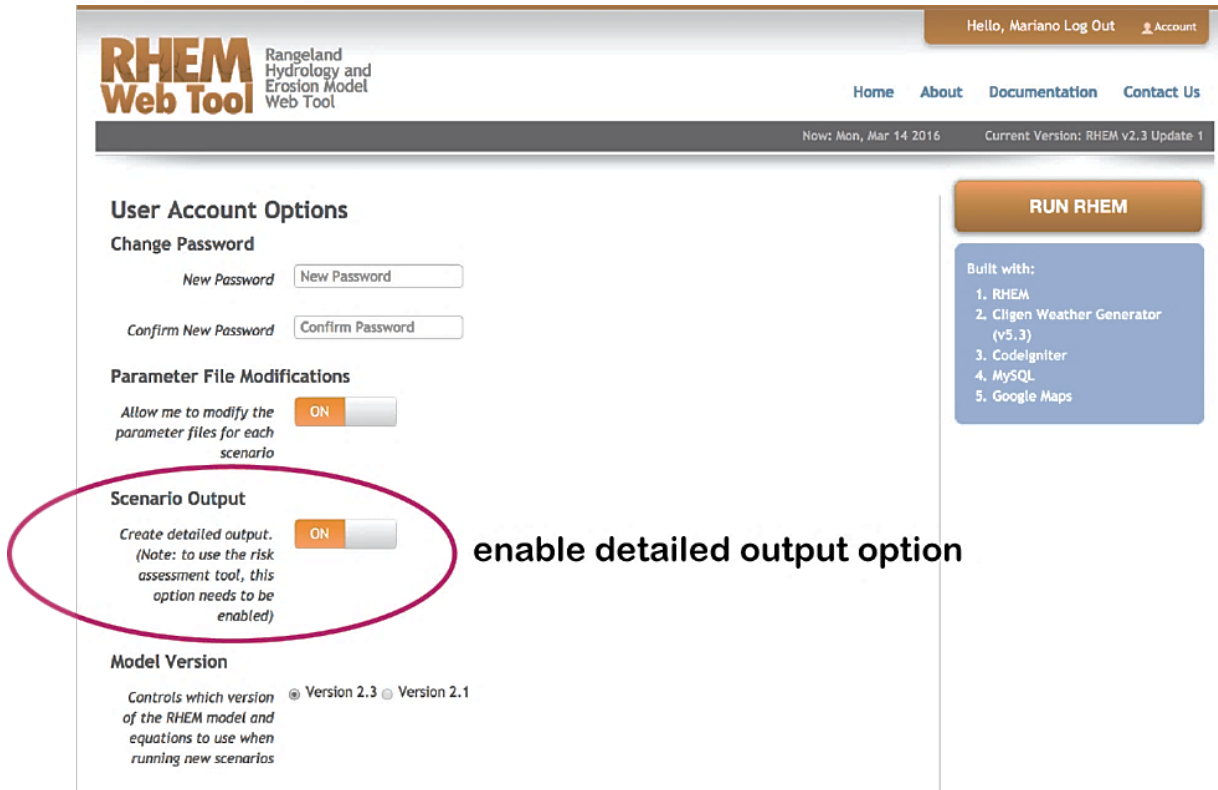
**Figure D-1.** Select scenario for risk assessment from completed model runs.



**Figure D-2.** Select Account button.



**Figure D-3.** Screenshot illustrating how to enable the detailed output option.



B. To run the Risk Assessment Tool, check off on the list of scenarios displayed on the dialog window the four scenarios generated from simulation runs discussed earlier in Part I (table B-2). By default, the Risk Assessment Tool assigns the first scenario checked off as the reference or baseline state. See figure D-4.

C. For this exercise, the HPC state, which is described in the STM (figure B-5), is used as a reference state. The assumption is that partitioning the probability distribution by specifying the 50<sup>th</sup>, 80<sup>th</sup>, and 95<sup>th</sup> percentiles of the reference state enables comparison of yearly soil losses of alternative states for different severity levels. They represent four soil erosion severity levels: low, medium, high, and very high. The literature provides no consensus on the level at which events should be considered as extremes, so our thresholds are established for practical applications as discussed below.

**Figure D-4.** Screenshot illustrating scenarios with detailed output previously generated in Part I. The green button indicates the baseline scenario.

**RESULTS**

**Note** ×

Only scenarios with detailed output and ran with verion 2.3 of RHEM will be displayed here. To run scenarios with detailed output, please enable this in your Account section (top right corner).

SCENARIO NAME	DATE RAN	VERSION	STATE	CLIMATE STATION	UNITS	SOIL LOSS (TON/AC OR HA/YEAR)	ALTERNATIVE	BASILINE
Exotic grass	03/14/16 19:15:02	2.3	AZ	Tombstone	metric	0.72453	<input checked="" type="checkbox"/>	<input type="checkbox"/>
Shrub invaded	03/14/16 19:13:54	2.3	AZ	Tombstone	metric	2.89842	<input checked="" type="checkbox"/>	<input type="checkbox"/>
ERODED	03/14/16 19:12:35	2.3	AZ	Tombstone	metric	3.94891	<input checked="" type="checkbox"/>	<input type="checkbox"/>
HPC	03/10/16 10:27:39	2.3	AZ	Tombstone	metric	0.36039	<input checked="" type="checkbox"/>	<input type="checkbox"/>
Test Prob in Risk Baseli...	02/26/16 17:12:49	2.3	NM	Beaverhead Rs	metric	0.07201	<input type="checkbox"/>	<input type="checkbox"/>
Test Prob in Risk Alter...	02/26/16 17:11:42	2.3	NM	Beaverhead	metric	0.81889	<input type="checkbox"/>	<input type="checkbox"/>
Test Prob in Risk Alter	02/26/16	2.3	NM		metric	1.92387	<input type="checkbox"/>	<input type="checkbox"/>

Run Risk Assessment

### 647.42 Risk Assessment Modeling Results

A. Results of running the model for risk assessment are shown in table D-1 and figure D-5.

**Table D-1.** Percent probability of occurrence of yearly soil losses and soil loss severity.

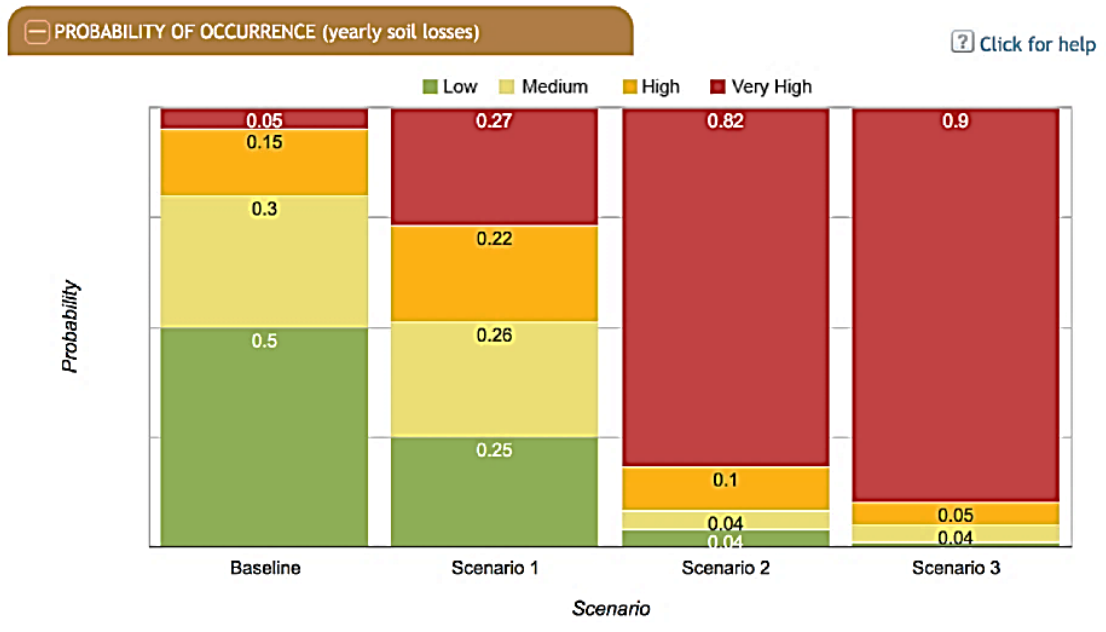
PROBABILITY OF OCCURRENCE TABLE (yearly soil losses)					
SOIL LOSS SEVERITY CLASS	RANGE OF ANNUAL SOIL LOSS (TON/HA)	BASILINE SCENARIO	SCENARIO 1	SCENARIO 2	SCENARIO 3
		HPC	GRASS	SHRUB	ERODED
	Low $X < 0.367$	0.5	0.25	0.04	0.01
	Medium $0.367 \leq X < 0.655$	0.3	0.26	0.04	0.04
	High $0.655 \leq X < 1.049$	0.15	0.22	0.1	0.05
	Very High $X \geq 1.049$	0.05	0.27	0.82	0.9

**HPC**  
Low soil loss severity  
50% probability of < 0.367 ton/ha

**GRASS**  
Very High soil loss severity  
27% probability of  $\geq 1.049$  ton/ha

**ERODED**  
Very High soil loss severity  
90% probability of  $\geq 1.049$  ton/ha

**Figure D-5.** Probability of occurrence for yearly soil loss for all scenarios.



### 647.43 Risk Assessment Discussion

A. In table D-1, the 50<sup>th</sup>, 80<sup>th</sup>, and 95<sup>th</sup> percentiles for yearly soil loss were determined:  $\beta_1 = 0.367$  ton/ha,  $\beta_2 = 0.655$  ton/ha, and  $\beta_3 = 1.049$  ton/ha, respectively, from the HPC (designated baseline in this case) empirical cumulative distribution of yearly soil loss values. The mean annual soil losses for the HPC, Grass, Shrub, and Eroded states are 0.360 ton/ha, 0.725 ton/ha, 2.898 ton/ha, and 3.949 ton/ha, respectively (figure C-12, Annual averages for precipitation, runoff, sediment yield, and soil loss for scenarios). The probabilities (percent probability) of occurrence of yearly average soil loss for each state are presented in table D-1 (note: each of the columns for HPC, Grass, Shrub, Eroded sums equal 100 percent).

B. Figure D-5 represents the probability of occurrence of soil loss for any year for the Low, Medium, High, or Very High categories to occur. Low, Medium, High, and Very High thresholds are based on the 50<sup>th</sup>, 80<sup>th</sup>, and 95<sup>th</sup> percentiles for probability of occurrence of yearly soil loss for the baseline condition.

C. For example, in every baseline case it is considered that five percent of the years (in red) for the baseline scenario are categorized as “Very High.” The red parts of the bars in the other scenarios represent the fraction of years for those scenarios that also fall in that same range of yearly soil losses as defined by the greatest five percent of the baseline condition.

D. Note that the output is reporting soil losses and not sediment yields, which are different. Soil loss is defined as soil detached and moved by raindrop splash, sheetflow, and concentrated flow. Sediment yield is calculated as the amount of soil that is detached and transported off the slope. For uniform slopes, all soils that are detached are considered mobile and transported off site. Therefore, soil loss and sediment are equal. When using S-shape or concave slope shapes, the slope gradient is reduced at the toe of the slope, allowing for potential deposition to occur. Therefore, sediment yield should be less than soil loss on S-shaped or concaved slopes. Deposition can be calculated as the difference between soil loss and sediment yield.

E. Interpretive Examples from table D-1 and figure D-5 indicate:

- (1) For HPC, there is a 50 percent annual probability of soil loss being equal to or lower than 0.367 tons/ha. Likewise, there is a five percent chance of Very High erosion  $\geq 1.049$  tons/ha soil loss for any given year. The mean annual soil loss for the HPC state (0.36 tons/ha) falls in the Low soil loss severity class ( $< 0.367$  tons/ha).
- (2) For the Exotic grass state, there is a 25 percent chance that erosion will be Low ( $< 0.367$  tons/ha). Likewise, there is a 27 percent chance of Very High erosion being  $\geq 1.049$  tons/ha for any given year. The mean annual soil loss of the Grass state (0.725 ton/ha) falls in the High soil loss severity class (0.655 to 1.049 tons/ha).
- (3) For the Shrub invaded state, there is a four percent chance that erosion will be Low ( $< 0.367$  tons/ha). Likewise, there is an 82 percent chance of Very High erosion  $\geq 1.049$  tons/ha. The mean annual soil loss of the Shrub invaded state (2.898 tons/ha) falls in the Very High soil loss severity class ( $\geq 1.049$  tons/ha).
- (4) For the Eroded state, there is a one percent chance that erosion will be Low,  $< 0.367$  tons/ha. Likewise, there is a 90 percent chance of Very High erosion,  $\geq 1.049$  tons/ha soil loss for any given year. The mean annual soil loss of the Eroded state (3.949 tons/ha) falls in the Very High soil loss severity class ( $\geq 1.049$  tons/ha). Thus, the Eroded site would be evaluated as unsustainable in reference to the baseline HPC site. RHEM results indicate that this state has significantly more years that fall within the Very High soil erosion severity class, relative to the HPC condition for the ecological site.

#### 647.44 Summary

A. Analysis of the RHEM simulation runs on the “Limy Slopes 12–16 PZ Ecological Site” provides a basis for interpreting the impacts of vegetative canopy cover, surface ground cover, and topography on dominant processes in controlling infiltration and runoff as well as sediment detachment, transport, and deposition in overland flow at each state. Our results suggest that RHEM can predict runoff and erosion as a function of vegetation structure and behavior of different plant community phases and amount of cover for the different states.

B. Numerous studies (Castillo et al., 1997; Cerdá, 1999; Chartier and Rostagno, 2006; and Barthès and Roose, 2002) have shown that soil erosion decreases as canopy cover increases, and that runoff decreases as canopy cover increases. Weltz’s (et al., 1998) extensive review of the literature on rangeland cover concluded that ground cover should be maintained above a critical threshold of ~50–60 percent to adequately protect the soil surface from erosion. Johansen et al. (2001) compiled data from the literature on burned grassland, shrublands, and forest ecosystems and found that sediment yield increased non-linearly as the percentage of bare ground exceeded 60–70 percent. Pierson et al. (2009, 2011, and 2013) conducted rainfall simulator experiments on small and large plots on burned sagebrush sites. They reported that the small plot data suggest that the soil on burned sagebrush is relatively protected from high-intensity storm events when ground cover is near 40 percent (60 percent bare ground).

C. The large plot rainfall and concentrated flow data, however, suggest that burned sagebrush sites may remain more susceptible to increased erosion from high intensity or long duration storm events until ground cover is as high as 60 percent (40 percent bare ground). The explanation for the difference in runoff and erosion between the HPC and Exotic grass states can be related to differences in cover, but also to the increased water storage associated with native bunchgrasses due to the formation of litter dams, intact soil A horizon, greater soil surface horizon depth, and greater soil organic matter content. The grass cover and litter on the baseline state cause water to pond behind small litter and debris dams as it moves downslope, which has the effect of backing up water and allowing more time for infiltration and increased tortuosity of the flow paths. This results in reduced

overland flow velocities as the water moves around the bunchgrasses (Mitchel and Humphreys, 1987; Puigdefábregas, 2005; Nearing et al., 2007).

D. According to Polyakov et al. (2010) before the Lehmann lovegrass invasion, the microtopography was characteristic of small terraces formed from of large clumps of upslope vegetation. With die-out of native grasses and greater spread of Lehmann lovegrass, there were fewer obstructions, which allowed water to move down the slope more rapidly, increasing flow connectivity, runoff, and sediment yield.

E. The difference in estimated soil erosion rate between the Shrub invaded and Eroded scenarios is about one ton/ha, table D-1. The explanation for the difference in soil erosion rates can be related to the additional foliar canopy and ground cover protection present in the Shrub invaded state as shown in table B-2.

F. The results from the risk assessment suggest that a shift from the High to Medium soil erosion severity class may be possible if management practices are implemented to promote litter production and reduce runoff and erosion. In contrast, based on the STM, the Eroded and Shrub Invaded states are considered to be so degraded by soil erosion that they have crossed a threshold and now have a different, less productive, potential plant community. These states are within the Very High soil erosion severity class, and the probability of bringing them back to the reference state is impossible due to loss of surface soil horizons that control water holding capacity and nutrient availability. Furthermore, once in the Eroded state, the concentrated flow/rill network is well established resulting in increased runoff and sediment yield. This is self-reinforcing and results in the concentrated flow channels transitioning into rills and eventually gullies if no conservation activities are applied.

**Figure D-6.** Rotating boom simulator used to collect data for development of the Rangeland Hydrology and Erosion Model (RHEM). Plots were 3 m (10 ft.) wide by 10.7 m (35 ft.) long.



**Figure D-7.** Walnut Gulch rainfall simulator used to collect data near Moab, Utah for development of the Rangeland Hydrology and Erosion Model (RHEM). Plots were 2m (6ft) wide by 6m (20ft) long.



## Subpart E – References

### Contents

647.51 Conversion Factors.....	E-1
647.52 Vegetation and ground cover definitions and photographs.....	E-1
647.53 Hydrologic Terms.....	E-5
647.54 References .....	E-5
Appendices: RHEM Guide Sheets (see Title 190, Part 647 in eDirectives to access Appendices).....	E-11

#### 647.51 Conversion Factors

Multiply	By	To obtain
degree Celsius (°C)	33.8	degree Fahrenheit (°F)
millimeter (mm)	$3.94 \times 10^{-2}$	inch (in)
centimeter (cm)	$3.94 \times 10^{-1}$	inch (in)
meter (m)	3.28	feet (ft)
kilometer (km)	$6.21 \times 10^{-1}$	mile (mi)
gram (g)	$3.53 \times 10^{-2}$	ounce (oz)
kilogram (kg)	2.205	pound (lb)
square meter (m <sup>2</sup> )	10.76	square foot (ft <sup>2</sup> )
square meter (m <sup>2</sup> )	$2.47 \times 10^{-4}$	acre (ac)
hectare (ha)	2.47	acre (ac)
square kilometer (km <sup>2</sup> )	$3.86 \times 10^{-1}$	square mile (mi <sup>2</sup> )
square kilometer (km <sup>2</sup> )	247	acre (ac)
cubic meter (m <sup>3</sup> )	35.3	cubic foot (ft <sup>3</sup> )
liter (L)	$3.53 \times 10^{-2}$	cubic foot (ft <sup>3</sup> )
millimeter per hour (mm h <sup>-1</sup> )	$3.94 \times 10^{-2}$	inch per hour (in h <sup>-1</sup> )
liter per second (L s <sup>-1</sup> )	$3.53 \times 10^{-2}$	cubic foot per second (ft <sup>3</sup> s <sup>-1</sup> )
cubic meter per second (m <sup>3</sup> s <sup>-1</sup> )	35.3	cubic foot per second (ft <sup>3</sup> s <sup>-1</sup> )
gram per square meter (g m <sup>-2</sup> )	$4.46 \times 10^{-3}$	ton per acre (t ac <sup>-1</sup> )

#### 647.52 Vegetation and ground cover definitions and photographs



Biological and salt crust



Biological soil crust



Salt crusts and biological soil crust



Micro shrub coppice dune and bare soil



Sod grass with bare interspace



Sod grass with manure (e.g., litter)



Rock, bare interspace and trace litter



Rock, bare interspace and trace litter



Shrub with forbs in foreground



Bunchgrass with woody agave



Litter and bare soil



Bunchgrass, annual grass, rock, litter and bare soil



Juniper trees invading bunchgrass



Savanna with tallgrass and scattered trees



Shrubland with open interspace and encroachment by juniper trees



Shrubland with bunchgrass interspace



Shrub, rock and bare soil



Shrub, cacti, rock and bare soil



Forb in bunchgrass



Forb in bunchgrass



Forb



Forb in litter



Wind erosion showing bare soil and burned basal stumps of shrubs



Forbs in mixed grass prairie

### 647.53 Hydrologic Terms



Raindrop splash erosion



Sheet flow erosion



Concentrated flow path/rill



Concentrated flow path/rill



Flash flood/stream flow



Gully erosion

### 647.54 References

- A. Al-Hamdan O.Z, Pierson Jr., F.B., Nearing, M.A., Stone, J.J., Williams, C.J., Moffet, C.A., Kormos, P.R., Boll, J., Weltz, M.A. (2012a). Characteristics of concentrated flow hydraulics for rangeland ecosystems: Implications for hydrologic modeling. *Earth Surface Processes and Landforms*, 37:157–168.
- B. Al-Hamdan, O.Z., Pierson, F.B., Nearing, M.A., Williams, C.J., Hernandez, M., Boll, J., Nouwakpo, S.K., Weltz, M.A., Spaeth, K. (2017). Developing a parameterization approach for soil erodibility for the rangeland

- hydrology and erosion model (RHEM). Transactions of the American Society of Agricultural and Biological Engineers, 60:85–94.
- C. Al-Hamdan, O.Z., Pierson, F.B., Nearing, M.A., Williams, C.J., Stone, J.J., Kormos, P.R., Boll, J., Weltz, M.A. (2012b). Concentrated flow erodibility for physically based erosion models: Temporal variability in disturbed and undisturbed rangelands. *Water Resources Research*, 48:W07504.1.
- D. Al-Hamdan, O.Z., Pierson, F.B., Nearing, M.A., Williams, C.J., Stone, J.J., Kormos, P.R., Boll, J., Weltz, M.A. (2013). Risk assessment of erosion from concentrated flow on rangelands using overland flow distribution and shear stress partitioning. *Transactions of the American Society of Agricultural and Biological Engineers*, 56:539–548.
- E. Al-Hamdan, O.Z., Pierson, F.B., Nearing, M.A., Williams, C.J., Hernandez, M., Boll, J., Nouwakpo, S.K., Weltz, M.A., Spaeth, K. (2017). Developing a parameterization approach for soil erodibility for the rangeland hydrology and erosion model (RHEM). *Transactions of the American Society of Agricultural and Biological Engineers*, 60:85–94.
- F. Al-Hamdan, O.Z., Pierson, F.B., Nearing, M.A., Williams, C.J., Stone, J.J., Kormos, P.R., Boll, J., Weltz, M.A. (2012b). Concentrated flow erodibility for physically based erosion models: Temporal variability in disturbed and undisturbed rangelands. *Water Resources Research*, 48:W07504.1.
- G. Al-Hamdan, O., F. Pierson, M. Nearing, C. Williams, M. Hernandez, K. Spaeth, J. Boll, and M. Weltz (2015). Use of RHEM to assess runoff and erosion following disturbance on rangelands *in* Society for Range Management Meeting Abstracts.
- H. Barthès, B., and E. Roose (2002). Aggregate stability as an indicator of soil susceptibility to runoff and erosion: validation at several levels. *Catena*, 47:133–149.
- I. Bennett, J.P. (1974). Concepts of mathematical modeling of sediment yield. *Water Resources Research*, 10:485–492.
- J. Castillo, V.M., Martinez-Mena, M., Albaladejo, J. (1997). Runoff and soil loss response to vegetation removal in a semiarid environment. *Soil Science Society of America Journal*, 61:1116–1121.
- K. Cerdà, A. (1999). Parent material and vegetation affect soil erosion in Eastern Spain. *Soil Science Society America Journal*, 63:362–368.
- L. Cerdà, A. (1998). Changes in overland flow and infiltration after a rangeland fire in a Mediterranean scrubland. *Hydrological Processes*, 12:1031–1042.
- M. Chartier, M.P., Rostagno, C.M. (2006). Soil erosion thresholds and alternative states in Northeastern Patagonian rangelands. *Rangeland Ecology & Management*, 59:616–624.
- N. D’Odorico P., Bhattachan A., Davis K.F., Ravi S., Rumyan C.W., 2013, Global desertification drivers and feedbacks, *Advances in Water Resources*. 51. 326–344.
- O. Dahlstrom, D.J. (2015). Calibration and uncertainty analysis for complex environmental models. *Ground Water*, 53:673–674.
- P. Davenport, D.W., D.D. Breshears, B.P. Wilcox, and C.D. Allen. (1998). Viewpoint: Sustainability of pinion-juniper ecosystems—a unifying perspective of soil erosion thresholds. *Journal of Range Management*, 51:231–240.
- Q. DeBano, L.F., Wood, M.K. (1990). Soil loss tolerance as related to rangeland productivity. In: *Proceedings of Soil Quality Standards Symposium*, 15–27.
- R. Doherty, J. (1994). PEST: a unique computer program for model-independent parameter optimization. *Water Down Under 94: Groundwater/Surface Hydrology Common Interest Papers; Preprints of Papers*, 551.
- S. Dortignac, E.J., Love, L.D. (1961). Infiltration studies on ponderosa pine ranges of Colorado. *Infiltration studies on ponderosa pine ranges of Colorado*.
- T. Fair, G.M., Geyer, J.C. (1954). Water supply and wastewater disposal. In: *Water supply and waste water disposal*. John Wiley.
- U. Foltz, R.B., Rhee, H., Elliot, W.J. (2008). Modeling changes in rill erodibility and critical shear stress on native surface roads. *Hydrologic Processes*, 22:4783–4788.

- V. Foster, G.R. (1982). Modeling the erosion process. In: Hydrologic Modeling of Small Watersheds, Haan, C.T., Johnson, H.P., Brakensiek, D.L. (eds.). American Society of Agricultural Engineers Monograph, 5:297–360.
- W. Gifford, G.F. (1985). Cover allocation in rangeland watershed management. In: Watershed Management in the Eighties. Jones, E.B., Ward, T.J. (eds.). American Society of Civil Engineers, 23–31.
- X. Goebel, J.J. (1998). The national resources inventory and its role in U.S. agriculture, Agricultural Statistics 2000: An International Conference on Agricultural Statistics, International Statistical Institute, 181–192.
- Y. Green, W.H., Ampt, G.A. (1911). Studies on soil physics, part I, the flow of air and water through soils. *Journal of Agricultural Science*, 4:11–24.
- Z. Gupta, H.V., Sorooshian, S., Yapo, P.O. (1999). Status of automatic calibration for hydrologic models: Comparison with multilevel expert calibration. *Journal of Hydrologic Engineering*, 4:135–143.
- AA. Havstad, K.M., Peters, D., B., Allen-Diaz, B., Bestelmeyer, B., Briske, D., Brown, J.R., Brunson, M., Herrick, J.E., Johnson, P., Joyce, L., Pieper, R., Svejcar, A.J., Yao, J., Bartolome, J., Huntsinger, L. (2009). The western United States rangelands, a major resource. In: Grassland, Quietness and Strength for a New American Agriculture, Chapter 5:75–93.
- AB. Heilman, P., Stone, J.J., Robinett, D. (2010). Ecological sites of the Walnut Gulch Experimental Watershed. In: American Water Resources Association Summer Specialty Conference, Orlando, FL, 29–31.
- AC. Hernandez, M., M.A. Nearing, O.Z. Al-Hamdan, F.B. Pierson, G. Armendariz, M.A. Wertz, K.E. Spaeth, C.J. Williams, S.K. Nouwakpo, and D.C. Goodrich. (2017). The Rangeland Hydrology and Erosion Model: A dynamic approach for predicting soil loss on rangelands. *Water Resources Research* **53**:9368–9391.
- AD. Hernandez, M., Nearing, M.A., Stone, J.J., Pierson, F.B., Wei, H., Spaeth, K.E., Heilman, P., Wertz, M.A., Goodrich, D.C. (2013). Application of a rangeland soil erosion model using National Resources Inventory data in southeastern Arizona. *Journal of Soil and Water Conservation*, 68:512–525.
- AE. Herrick, J.E., Wills, S., Karl, J., Pyke, D. (2010). Terrestrial indicators and measurements: Selection process and recommendations. U.S. Department of Agriculture.
- AF. Holland, M.E. (1969). Design and testing of rainfall system. Colorado State University Experimental Station, CER 69–70, MEH21, Fort Collins, Colorado.
- AG. Holland, M.E. (1969). Design and testing of rainfall system. Colorado State University Experimental Station, CER 69–70, MEH21, Fort Collins, Colorado.
- AH. Houska, T., P. Kraft, A. Chamorro-Chavez, and L. Breuer. (2015). SPOTting model parameters.
- AI. Johansen, M.P., Hakonson, T.E., Breshears, D.D. (2001). Post-fire runoff and erosion from rainfall simulation: Contrasting forest with shrublands and grasslands. *Hydrological Processes*, 15:2953–2965.
- AJ. Keefer, T.O., Renard, K.G., Goodrich, D.C., Heilman, P., Unkrich, C.L. (2015). Quantifying extreme rainfall events and their hydrologic response in southeastern Arizona. *Journal of Hydrologic Engineering*, 21:1–10.
- AK. Lane, L.J., Hernandez, M., Nichols, M.H. (1997). Dominant processes controlling sediment yield as functions of watershed scale. In: Proceedings of the International Conference on Modelling and Simulation, Hobart, Tasmania, McDonald, A.D., McAleer, M. (eds.). 1:5.
- AL. Ludwig, J.A., Wilcox, B.P., Breshears, D.D., Tongway, D.J., Imeson, A.C. (2005). Vegetation patches and runoff-erosion as interacting ecohydrological processes in semiarid landscapes. *Ecology*, 86:288–297.
- AM. Magliano, P.N., D.D. Breshear, R.J. Fernandez, and E.G. Jobbagy, 2015. Rainfall intensity switches ecohydrological runoff/runon redistribution patterns in dryland vegetation patches. *Ecological Applications*. 8:2094–2100. <https://doi.org/10.1890/15-0550.1>.
- AN. Meeuwig, R.O. (1970). Infiltration and soil erosion as influenced by vegetation and soil in northern Utah. *Journal of Range Management*, 23:185–188.
- AO. Mitchell, P.B., Humphreys, G.S. (1987). Litter dams and microterraces formed on hillslopes subject to rainwash in the Sydney Basin, Australia. *Geoderma*, 39:331–357.
- AP. Moffet, C.A., Pierson, F.B., Robichaud, P.R., Spaeth, K.E., Hardegree, S.P. (2007). Modeling soil erosion on steep sagebrush rangeland before and after prescribed fire. *Catena*, 71:218–228.

- AQ. Moriasi, D.N., Arnold, J.G., Van Liew, M.W., Bingner, R.L., Harmel, R.D., Veith, T.L., (2007). Model evaluation guidelines for systematic quantification of accuracy in watershed simulations. *Transactions of the American Society of Agricultural and Biological Engineers*, 50:885–900.
- AR. Morris, S.E., Moses, T.A. (1987). Forest fire and the natural soil erosion regime in the Colorado Front Range. *Annals of the Association of American Geographers*, 77:245 – 254.
- AS. Nash, J.E., Sutcliffe, J.V. (1970). River flow forecasting through conceptual models part I - A discussion of principles. *Journal of Hydrology*, 10:282–290.
- AT. Nearing M.A., Norton, L.D., Bulgakov, D.A., Larionov, G.A., West, L.T., Dontsova, K.M. (1997). Hydraulics and erosion in eroding rills. *Water Resources Research*, 33:865–876.
- AU. Nearing, M.A. (2000). Evaluating soil erosion models using measured plot data: Accounting for variability in the data. *Earth Surface Processes and Landforms*, 25:1035–1043.
- AV. Nearing, M.A., Hairsine, P.B. (2011a). The Future of Soil Erosion Modelling. Ch. 20 In: Morgan, R.P., Nearing, M.A. (eds.). Wiley-Blackwell Publishers, Chichester, West Sussex, UK., 387–397.
- AW. Nearing, M.A., Jetten, V., Baffaut, C., Cerdan, O., Couturier, A., Hernandez, M., Le Bissonnais, Y., Nichols, M.H., Nunes, J.P., Renschler, C.S., Souchère, V., van Oost, K. (2005). Modeling response of soil erosion and runoff to changes in precipitation and cover. *Catena*, 61:131–154.
- AX. Nearing, M.A., Nichols, M.H., Stone, J.J., Renard, K.G., Simanton, J.R. (2007). Sediment yields from unit-source semiarid watersheds at Walnut Gulch. *Water Resources Research* 43:W06426.
- AY. Nearing, M.A., Pruski, F.F., O'Neal, M.R. (2004). Expected climate change impacts on soil erosion rates: A review. *Journal of Soil and Water Conservation*, 59:43–50.
- AZ. Nearing, M.A., Unkrich, C.L., Goodrich, D., Nichols, M.H., Keefer, T.O. (2015). Temporal and elevation trends in rainfall erosivity on a 149km<sup>2</sup> watershed in a semi-arid region of the American Southwest. *International Soil and Water Conservation Research*, 3:77–85.
- BA. Nearing, M.A., Wei, H., Stone, J.J., Pierson, F.B., Spaeth, K.E., Weltz, M.A., Flanagan, D.C., Hernandez, M. (2011b). A rangeland hydrology and erosion model. *Transactions of the American Society of Agricultural and Biological Engineers*, 54:901–908.
- BB. Nichols, M.H., Nearing, M.A., Polyakov, V.O., Stone, J.J. (2012). A sediment budget for a small semiarid watershed in southeastern Arizona, USA. *Geomorphology*, 180–181:137–145.
- BC. Nicks, A.D., Lane, L.J., Gander, G.A. (1995). Weather generator. In: USDA-Water Erosion Prediction Project: Hillslope Profile and Watershed Model Documentation, Flanagan, D.C., Nearing, M.A. (eds.). NSERL Report 10:2–1.
- BD. Nielsen, D.R., Biggar, J.W., Erh, K.T. (1973). Spatial variability of field-measured soil-water properties. *Hilgardia*, 42:215–259.
- BE. Nouwakpo, S.K., M.A. Weltz, A. Arslan, C.H. Green, and O.Z. Al-Hamdan. (2018). Process-based Modeling of Infiltration, Soil Loss and Dissolved Solids on Saline and Sodic Soils. *Transactions of the American Society of Agricultural and Biological Engineers* 61:1–16. <https://doi.org/10.13031/trans.12705>.
- BF. Nouwakpo, S.K., M.A. Weltz, K.C. McGwire, J.C. Williams, A.H. Osama, and C.H. Green. (2017). Insight into sediment transport processes on saline rangeland hillslopes using three-dimensional soil microtopography changes. *Earth Surface Processes and Landforms* 42:681–696.
- BG. Parlange, J.Y., Lisle, I., Braddock, R.D., Smith, R.E. (1982). The three-parameter infiltration equation. *Soil Science*, 133:337–341.
- BH. Peters, D.P.C., Bestelmeyer, B.T., Turner, M.G. (2007). Cross-scale interactions and changing pattern-process relationships: Consequences for system dynamics. *Ecosystems*, 10:790–796.
- BI. Petersen, S.L., Stringham, T.K., Roundy, B.A. (2009). A process-based application of state-and-transition models: A case study of western juniper (*Juniperus occidentalis*) encroachment. *Rangeland Ecology & Management*, 62:186–192.
- BJ. Pierson, F.B., Bates, J.D., Svejcar, T.J., Hardegree, S.P. (2007). Runoff and erosion after cutting western juniper, *Rangeland Ecology & Management*, 60:285–292.

- BK. Pierson, F.B., Carlson, D.H., Spaeth, K.E. (2002). Impacts of wildfire on soil hydrological properties of steep sagebrush-steppe rangeland. *International Journal of Wildland Fire*, 11:145 – 151.
- BL. Pierson, F.B., Moffet, C.A., Williams, C.J., Hardegee, S.P., Clark, P.E. (2009). Prescribed-fire effects on rill and interrill runoff and erosion in a mountainous sagebrush landscape. *Earth Surface Processes and Landforms*, 34:193–203.
- BM. Pierson, F.B., Robichaud, P.R., Moffet, C.A., Spaeth, K.E., Hardegee, S.P., Clark, P.E., Williams, C.J. (2008). Fire effects on rangeland hydrology and erosion in a steep sagebrush-dominated landscape. *Hydrological Processes*, 22:2916–2929.
- BN. Pierson, F.B., Williams, C.J., Hardegee, S.P., Clark, P.E., Kormos, P.R., Al-Hamdan, O.Z. (2013). Hydrologic and erosion responses of sagebrush steppe following juniper encroachment, wildfire, and tree cutting. *Rangeland Ecology & Management*, 66:274–289.
- BO. Pierson, F.B., Williams, C.J., Hardegee, S.P., Clark, P.E., Kormos, P.R., Al-Hamdan, O.Z. (2013). Hydrologic and erosion responses of sagebrush steppe following juniper encroachment, wildfire, and tree cutting. *Rangeland Ecology and Management*, 66:274–289.
- BP. Pierson, F.B., Williams, C.J., Hardegee, S.P., Weltz, M.A., Stone, J.J., Clark, P.E. (2011). Fire, plant invasions, and erosion events on western rangelands. *Rangeland Ecology & Management*, 64:439–449.
- BQ. Pierson, F.B., Williams, C.J., Kormos, P.R., Hardegee, S.P., Clark, P.E., Rau, B.M. (2010). Hydrologic vulnerability of sagebrush steppe following pinyon and juniper encroachment. *Rangeland Ecology & Management*, 63:614–629.
- BR. Polyakov, V.O., Nearing, M.A., Stone, J.J., Hamerlynck, E.P., Nichols, M.H., Holifield Collins, C.D., Scott, R.L. (2010). Runoff and erosional responses to a drought-induced shift in a desert grassland community composition. *Journal of Geophysical Research: Biogeosciences*, 115:G04027.
- BS. Puigdefábregas, J. (2005). The role of vegetation patterns in structuring runoff and sediment fluxes in drylands. *Earth Surface Processes and Landforms*, 30:133–147.
- BT. R Core Team (2018). R: A language and environment for statistical computing. R Foundation for Statistical Computing, Vienna, Austria. <https://www.R-project.org/>.
- BU. Ravi S., D.D. Breshears, T.E. Huxman, P. D’Odorical. (2010). Land degradation in drylands: interactions among hydrologic-aeolian erosion and vegetation dynamics. *Geomorphology*. 216:236–245.
- BV. Rawls, W.J., Brakensiek, D.L., Saxton, K.E. (1982). Estimation of soil water properties. *Transactions of the American Society of Agricultural and Biological Engineers*, 81–2510.
- BW. Rawls, W.J., Brakensiek, D.L., Simanton, J.R., Kho, K.D. (1990). Development of a crust factor for a Green Ampt model. *Transactions of the American Society of Agricultural and Biological Engineers*, 33:1224–1228.
- BX. Rawls, W.J., Gimenez, D., Grossman, R. (1998). Use of soil texture, bulk density, and slope of the water retention curve to predict saturated hydraulic conductivity. *Transactions of the American Society of Agricultural and Biological Engineers*, 41:983–988.
- BY. Renard, K.G. (1980). Estimating erosion and sediment yield from rangeland. In: *Proceedings of ASCE Symposium on Watershed Management*, Boise, ID, 164–175.
- BZ. Robichaud, P.R., Ashmun, L.E., Sims, B.D. (2010). Post-fire treatment effectiveness for hillslope stabilization. U.S. Department of Agriculture, Forest Service, Rocky Mountain Research Station, General Technical Report RMRS-GTR-240. DIANE Publishing.
- CA. Robinett, D. (1992). Lehmann lovegrass and drought in southern Arizona. *Rangelands Archives*, 14:100–103.
- CB. Sala, O.E., Lauenroth, W.K., Parton, W.J., & Trlica, M.J. (1981). Water status of soil and vegetation in a shortgrass steppe. *Oecologia*, 48(3), 327–331.
- CC. Scott, D.F., van Wyk, D.B. (1992). The effects of fire on soil water repellency, catchment sediment yields and stream flow. In: *Fire in South African Mountains Fynbos*. Springer Berlin Heidelberg, 93:216–239.
- CD. Shakesby, R.A., Coelho, C.D.A., Ferreira, A.D., Terry, J.P., Walsh, R.P.D. (1993). Wildfire impacts on soil-erosion and hydrology in wet Mediterranean Forest, Portugal. *International Journal of Wildland Fire*, 3:95–110.

- CE. Simanton, J.R., Osterkamp, W.R., Renard, K.G. (1993). Sediment yield in a semiarid basin: Sampling equipment impacts. IAHS publication, 3–3.
- CF. Smith, R.E., Corradini, C., Melone, F. (1993). Modeling infiltration for multi-storm runoff event. *Water Resources Research*, 29:133–44.
- CG. Smith, R.E., Goodrich, D.C. (2000). Model for rainfall excess patterns on randomly heterogeneous areas. *Journal of Hydrology Engineering*, 5:355–362.
- CH. Smith, R.E., Goodrich, D.C., Woolhiser, D.A., Unkrich, C.L. (1995). KINEROS - a kinematic runoff and erosion model. In: *Computer Models of Watershed Hydrology*, V.P. Singh (eds.). Water Resources Publications, 20:697–732.
- CI. Smith, R.E., Parlange, J.Y. (1978). A parameter-efficient hydrologic infiltration model. *Water Resources Research*, 14:533–538.
- CJ. Spaeth, K.E., Pierson, F.B., Weltz, M.A., Awang, J.B. (1996). Gradient analysis of infiltration and environmental variables as related to rangeland vegetation. *Transactions of the American Society of Agricultural and Biological Engineers*, 39:67-77.
- CK. Stone, J.J., Lane, L.J., Shirley, E.D. (1992). Infiltration and runoff simulation on a plane. *Transactions of the American Society of Agricultural and Biological Engineers*, 35:161–170.
- CL. Swanson, N.P. (1965). Rotating-boom rainfall simulator. *Transactions of the American Society of Agricultural and Biological Engineers*, 8:71–72.
- CM. Thompson, S.E., Harman, C.J., Heine, P., Katul, G.G. (2010). Vegetation-infiltration relationships across climatic and soil type gradient. *Journal of Geophysical Research*, 115:G02023.
- CN. Tromble, J.M., Renard, K.G., Thatcher, A.P. (1974). Infiltration for three rangeland soil-vegetation complexes. *Journal of Range Management*, 27:318–321.
- CO. Turnbull, L., Wainwright, J., Brazier, R.E. (2008). A conceptual framework for understanding semi-arid land degradation: Ecohydrological interactions across multiple-space and time scales. *Ecohydrology*, 1:23–34.
- CP. Turnbull, L., Wilcox, B.P., Belnap, J., Ravi, S., D'Odorico, P., Childers, D., Gwenzi, W., Okin, G., Wainwright, J., Caylor, K.K., Sankey, T. (2012). Understanding the role of ecohydrological feedbacks in ecosystem state change in drylands. *Ecohydrology*, 5:174–183.
- CQ. UNCCD. (1994). United Nations convention to combat desertification in countries experiencing serious drought and/or desertification, particularly in Africa. Homepage UNCCD: [www.unccd.int](http://www.unccd.int).
- CR. Urgeghe, A.M., & Bautista, S. (2015). Size and connectivity of upslope runoff-source areas modulate the performance of woody plants in Mediterranean drylands. *Ecohydrology*, 8(7), 1292–1303. doi:10.1002/eco.1582
- CS. Urgeghe, A., Breshears, D., Martens, S., & Beeson, P. (2010). Redistribution of Runoff Among Vegetation Patch Types: On Ecohydrological Optimality of Herbaceous Capture of Run-On. *Rangeland Ecology & Management*, 63(5), 497–504.
- CT. USDA United States Department of Agriculture. 2013. Interagency Ecological Site Description handbook for rangelands. Washington DC, USA: United States Department of Agriculture. 109 p. using a ready-made python package. Plos One 10:e0145180
- CU. USDA-NRCS (2018). 2018 National Resources Inventory Rangeland Resource Assessment. <https://www.nrcs.usda.gov/wps/portal/nrcs/detail/national/technical/nra/nri/results/?cid=nrcseprd1343027>.
- CV. Wainwright, J., Parsons, A.J., Abrahams, A.D. (2000). Plot-scale studies of vegetation, overland flow and erosion interactions: Case studies from Arizona and New Mexico. *Hydrological Processes*, 14:2921–2943.
- CW. Wei, H., Nearing, M.A., Stone, J.J., Guertin, D.P., Spaeth, K.E., Pierson, F.B., Nichols, M.H., Moffett, C.A. (2009). A new splash and sheet erosion equation for rangelands. *Soil Science Society of America Journal*, 73:1386–1392.
- CX. Weltz, M.A., Joelly, L., Hernandez, M., Spaeth, K.E., Rossi, C., Talbot, C., Nearing, M.A., Stone, J.J., Goodrich, D.C., Pierson, F.B., Wei, H., Morris, C. (2014a). Estimating conservation needs for rangelands using

- USDA National Resources Inventory assessments. American Society of Agricultural and Biological Engineers, 57:1559–1570.
- CY. Weltz, M.A., Kidwell, M.R., Fox, H.D. (1998). Influence of abiotic and biotic factors in measuring and modeling soil erosion on rangelands: State of knowledge. *Journal of Range Management*, 51:482–495.
- CZ. Weltz, M.A., Speath, K.E., Taylor, M.H., Rollins, K., Pierson, F.B., Jolley, L.W., Nearing, M.A., Goodrich, D.C., Hernandez, M., Nouwakpo, S., Rossi, C. (2014). Cheatgrass invasion and woody species encroachment in the Great Basin: Benefits of conservation. *Journal of Soil and Water Conservation*, 69:39A–44A.
- DA. Wilcox, B.P. (1994). Runoff and erosion in intercanopy zones of pinyon-juniper woodlands. *Journal of Range Management*, 285–295.
- DB. Wilcox, B.P., Breshears, D.D., & Allen, C.D. (2003). Ecohydrology of a resource-conserving semiarid woodland: Effects of scale and disturbance. *Ecological Monographs*, 73(2), 223–239.
- DC. Wilcox, B.P., Seyfried, M.S., Breshears, D.D., McDonnell, J.J. (2012). Ecohydrologic connections and complexities in drylands: New perspectives for understanding transformative landscape change. *Ecohydrology*, 5:143–144.
- DD. Williams, C.J., Pierson, F.B., Robichaud, P.R., Boll, J. (2014). Hydrologic and erosion responses to wildfire along the rangeland-xeric forest continuum in the western U.S.: A review and model of hydrologic vulnerability. *International Journal of Wildland Fire*, 23:155–172.
- DE. Williams, C.J., Pierson, F.B., Spaeth, K.E., Brown, J.R., Al-Hamdan, O.Z., Weltz, M.A., Nearing, M.A., Herrick, J.E., Boll, J., Robichaud, P.R., Goodrich, D.C., Heilman, P., Guertin, D.P., Hernandez, M., Wei, H., Hardegree, S.P., Strand, E.K., Bates, J.D., Metz, L.J., Nichols, M.H. (2016). Incorporating hydrologic data and ecohydrologic relationships into ecological site descriptions. *Rangeland Ecology & Management*, 69:4–19.
- DF. Williams, C.J., Pierson, F.B., Spaeth, K.E., Brown, J.R., Al-Hamdan, O.Z., Weltz, M.A., Nearing, M.A., Herrick, J.E., Boll, J., Robichaud, P.R., Goodrich, D.C., Heilman, P., Guertin, D.P., Hernandez, M., Wei, H., Hardegree, S.P., Strand, E.K., Bates, J.D. (2016a). Incorporating hydrologic data and ecohydrologic relationships in ecological site descriptions. *Rangeland Ecology & Management*, 69:4–19.
- DG. Williams, C.J., Pierson, F.B., Spaeth, K.E., Brown, J.R., Al-Hamdan, O.Z., Weltz, M.A., Nearing, M.A., Herrick, J.E., Boll, J., Robichaud, P.R., Goodrich, D.C., Heilman, P., Guertin, D.P., Hernandez, M., Wei, H., Hardegree, S.P., Strand, E.K., Bates, J.D., Metz, L.J., Nichols, M.H. (2016b). Incorporating hydrologic data and ecohydrologic relationships into ecological site descriptions. *Rangeland Ecology & Management*, 69:4–19.
- DH. Woolhiser, D.A., Smith, R.E., Goodrich, D.C. (1990). KINEROS, a kinematic runoff and erosion model: Documentation and user manual. U. S. Department of Agriculture, Agricultural Research Service, p. 5.
- DI. Zhang, X.C., Nearing, M.A., Risse, L.M. (1995). Estimation of green-ampt conductivity parameters: Part I. row crops. *Transactions of the American Society of Agricultural and Biological Engineers*, 38:1069–1077.

**Appendices: RHEM Guide Sheets** (see Title 190, Part 647 in eDirectives to access Appendices)